

# HETEROGENEOUS REACTIONS OF NO<sub>3</sub> AND OTHER OXIDANTS WITH ORGANIC FILMS AND SUBSTRATES OF ATMOSPHERIC RELEVANCE

by

SIMONE GROSS

A THESIS SUBMITTED IN PARTIAL FULFILLMENT OF  
THE REQUIREMENTS FOR THE DEGREE OF

DOCTOR OF PHILOSOPHY

in

The Faculty of Graduate Studies  
(Chemistry)

THE UNIVERSITY OF BRITISH COLUMBIA  
(Vancouver)

APRIL 2009

© Simone Gross, 2009

## ABSTRACT

Knowledge of atmospheric heterogeneous reactions between gas-phase species and aerosol particles is limited. The goal of this thesis was to contribute to the understanding of these reactions, in particular to the reactions of gas-phase oxidants ( $\text{NO}_3$ ,  $\text{N}_2\text{O}_5$ ,  $\text{NO}_2$ ,  $\text{HNO}_3$ , and  $\text{O}_3$ ) with a variety of organic substrates that served as proxies for aerosol surfaces. Organics chosen for this study represent classes of compounds found in field studies.

A cylindrical flow tube reactor coupled to a chemical ionization mass spectrometer was employed to study the reactive uptake of the different gas-phase oxidants on organic substrates. These studies showed fast reaction of polycyclic aromatic hydrocarbons (PAHs) with  $\text{NO}_3$  (uptake coefficient  $\gamma \geq 0.059$ ), while reactions of the different PAHs with the other gas-phase species ( $\text{N}_2\text{O}_5$ ,  $\text{NO}_2$ ,  $\text{HNO}_3$ , and  $\text{O}_3$ ) were at or below the detection limit ( $\gamma \leq 6.6 \times 10^{-5}$ ).  $\text{NO}_2$  and  $\text{HNO}_3$  were identified as gas-phase products in the reactions of  $\text{NO}_3$  with PAHs. The results show that  $\text{NO}_3$  may be a more important sink for tropospheric PAHs than  $\text{NO}_2$ ,  $\text{N}_2\text{O}_5$ ,  $\text{HNO}_3$ , or  $\text{O}_3$ .

The uptake of  $\text{NO}_3$  and  $\text{N}_2\text{O}_5$  on liquid and solid films of an alkenoic acid, an alkanoate, and a polyalcohol was measured. Uptake of  $\text{NO}_3$  on the alkenoic acid was fast ( $\gamma > 0.07$  for the liquid), approximately two orders of magnitude faster than for the other two compounds. Uptake of  $\text{N}_2\text{O}_5$  was slower than  $\text{NO}_3$  reaction for all three compounds. The polyalcohol had the highest uptake coefficient with  $\text{N}_2\text{O}_5$  ( $\gamma = (4 - 8) \times 10^{-4}$ ). Based on these results, the presence of  $\text{NO}_3$  and  $\text{N}_2\text{O}_5$  may decrease the atmospheric lifetimes of alkenoic acids and alcohols, respectively.

The flow reactor enabled quantitative exposures of self assembled monolayers to controlled amounts of  $\text{NO}_3$  in order to mimic atmospheric exposures of aerosol surfaces. These  $\text{NO}_3$  exposed monolayers (an alkane and a terminal alkene) were subsequently analyzed with different surface-analytical tools in order to determine condensed phase reaction products and deduce reaction mechanisms. Hydroxyl, carbonyl, carboxylic acid, and N-containing functional groups were confirmed. Additionally, the atmospheric lifetime of alkenes in the presence of  $\text{NO}_3$  was shown to be short.

# TABLE OF CONTENTS

ABSTRACT.....	ii
TABLE OF CONTENTS .....	iii
LIST OF TABLES.....	vii
LIST OF FIGURES .....	ix
ACKNOWLEDGEMENTS.....	xv
<b>1 AEROSOL PARTICLES IN THE LOWER TROPOSPHERE.....</b>	<b>1</b>
1.1 Introduction and Importance.....	1
1.2 Sources and Composition .....	2
1.2.1 Sources of Aerosol Particles .....	2
1.2.2 Composition of Aerosol Particles .....	3
<b>2 ATMOSPHERIC CHEMISTRY .....</b>	<b>8</b>
2.1 Homogeneous Reactions in the Atmosphere .....	8
2.2 Heterogeneous Atmospheric Chemistry .....	9
<b>3 THESIS OVERVIEW .....</b>	<b>13</b>
<b>4 BACKGROUND INFORMATION ON GAS-PHASE SPECIES .....</b>	<b>16</b>
4.1 NO <sub>3</sub> Chemistry in the Troposphere.....	16
4.2 NO <sub>2</sub> , N <sub>2</sub> O <sub>5</sub> , HNO <sub>3</sub> , and O <sub>3</sub> Chemistry in the Troposphere .....	17
4.2.1 Nitrogen Dioxide (NO <sub>2</sub> ).....	17
4.2.2 Dinitrogen Pentoxide (N <sub>2</sub> O <sub>5</sub> ) .....	19
4.2.3 Nitric Acid (HNO <sub>3</sub> ).....	19
4.2.4 Ozone (O <sub>3</sub> ) .....	20
<b>5 GENERAL OVERVIEW OF EXPERIMENTAL TECHNIQUES USED IN THIS THESIS.....</b>	<b>21</b>
5.1 Chemical Ionization Mass Spectrometry (CIMS).....	21

5.2 Coated Wall Flow Reactor.....	22
5.3 X-Ray Photoelectron Spectroscopy (XPS).....	24
5.4 Time-of-Flight Secondary Ion Mass Spectrometry (ToF-SIMS) .....	26
<b>6 REACTIVE UPTAKE OF NO<sub>3</sub>, N<sub>2</sub>O<sub>5</sub>, NO<sub>2</sub>, HNO<sub>3</sub>, AND O<sub>3</sub> ON THREE TYPES OF POLYCYCLIC AROMATIC HYDROCARBON SURFACES .....</b>	<b>28</b>
6.1 Introduction.....	28
6.2 Experimental.....	31
6.2.1 Experimental Setup and Procedure.....	31
6.2.2 Chemicals.....	32
6.2.3 Preparation and Characterization of the PAH Films.....	33
6.3 Results and Discussion .....	33
6.3.1 Surface Properties of PAH Films.....	33
6.3.2 Measurements of the Initial Reactive Uptake Coefficients for NO <sub>3</sub> .....	35
6.3.3 Measurements of the Initial Reactive Uptake Coefficients for N <sub>2</sub> O <sub>5</sub> .....	41
6.3.4 Measurements of the Initial Reactive Uptake Coefficients for O <sub>3</sub> .....	42
6.3.5 Measurements of the Initial Reactive Uptake Coefficients for NO <sub>2</sub> .....	43
6.3.6 Measurements of the Initial Reactive Uptake Coefficients for HNO <sub>3</sub> .....	44
6.3.7 Processing Studies of NO <sub>3</sub> (i.e. Uptake of NO <sub>3</sub> as a Function of Exposure)...	46
6.3.8 Gas-Phase Product Studies for the Reaction of NO <sub>3</sub> with Pyrene .....	49
6.3.9 Proposed Reaction Mechanism for the Reaction of NO <sub>3</sub> on Pyrene .....	51
6.4 Atmospheric Implications.....	52
6.4.1 Comparison of the Different Oxidants.....	52
6.4.2 Lifetime ( $\tau_{\text{atm}}$ ) of Surface-Adsorbed PAHs with Respect to the Different Oxidants .....	53
6.4.3 Direct Acting Mutagenicity of Wood Smoke and NO <sub>3</sub> Heterogeneous Chemistry .....	53
6.5 Summary and Conclusions .....	53
<b>7 REACTIVE UPTAKE COEFFICIENT MEASUREMENTS OF NO<sub>3</sub> AND N<sub>2</sub>O<sub>5</sub> ON A LIQUID AND FROZEN ALKENOIC ACID, ALKANOATE, AND POLYALCOHOL .....</b>	<b>56</b>

7.1 Introduction.....	56
7.2 Experimental.....	58
7.2.1 Experimental Setup and Procedure.....	58
7.2.2 Chemicals.....	60
7.3 Results and Discussion .....	60
7.3.1 Reactive Uptake of NO <sub>3</sub> on Oleic Acid (an Alkenoic Acid) .....	61
7.3.2 Reactive Uptake of NO <sub>3</sub> on Glycerol (a Polyalcohol).....	63
7.3.3 Reactive Uptake of NO <sub>3</sub> on DES (an Alkanoate) .....	64
7.3.4 Overall Trend in NO <sub>3</sub> Reactivity .....	65
7.3.5 Reactive Uptake of N <sub>2</sub> O <sub>5</sub> on Glycerol .....	66
7.3.6 Reactive Uptake of N <sub>2</sub> O <sub>5</sub> on Oleic Acid.....	68
7.3.7 Reactive Uptake of N <sub>2</sub> O <sub>5</sub> on DES.....	68
7.3.8 Overall Trend in N <sub>2</sub> O <sub>5</sub> Reactivity .....	70
7.4 Atmospheric Implications.....	70
7.4.1 Oxidation Timescale for Liquid Organic Particles .....	70
7.4.2 Importance of these Heterogeneous Reactions to Secondary Organic Aerosol (SOA) Studies .....	74
7.4.3 Oxidation Timescale for Surface Organics.....	75
7.5 Summary and Conclusions .....	76
 <b>8 PRODUCTS OF THE REACTIONS OF AN ALKANE MONOLAYER WITH NO<sub>3</sub> RADICALS. 78</b>	
8.1 Introduction.....	78
8.2 Experimental.....	81
8.2.1 Chemicals.....	81
8.2.2 Monolayer Preparation.....	81
8.2.3 Product Studies as a Function of Exposure.....	81
8.2.4 XPS, IR, ToF-SIMS, and Contact Angle Measurements.....	82
8.3 Results and Discussion .....	82
8.3.1 X-ray Photoelectron Spectroscopy .....	82
8.3.2 IR-Spectroscopy.....	86
8.3.3 ToF-SIMS Measurements.....	90

8.3.4 Contact Angle Measurements .....	91
8.3.5 Proposed Reaction Mechanism.....	93
8.4 Summary and Conclusions .....	96
<b>9 PRODUCTS AND KINETICS OF THE REACTIONS OF A TERMINAL ALKENE MONOLAYER WITH NO<sub>3</sub> RADICALS .....</b>	<b>98</b>
9.1 Introduction.....	98
9.2 Experimental.....	99
9.2.1 Chemicals.....	99
9.2.2 Monolayer Preparation.....	99
9.2.3 Measurements of the Reactive Uptake Coefficient .....	100
9.2.4 Product Studies as a Function of Exposure.....	100
9.2.5 XPS, IR, ToF-SIMS, and Contact Angle Measurements.....	100
9.3 Results and Discussion .....	100
9.3.1 Reactive Uptake Coefficient of NO <sub>3</sub> on an Unoxidized UDT SAM .....	100
9.3.2 Measurements of the Reactive Uptake of NO <sub>3</sub> as a Function of Exposure Time .....	102
9.3.3 X-Ray Photoelectron Spectroscopy .....	104
9.3.4 IR-Spectroscopy.....	108
9.3.5 ToF-SIMS Measurements.....	109
9.3.6 Contact Angle Measurements .....	110
9.3.7 Proposed Reaction Mechanism.....	111
9.4 Conclusions and Atmospheric Implications .....	114
<b>10 CONCLUDING REMARKS.....</b>	<b>115</b>
10.1 Conclusions.....	115
10.2 Considerations for Future Work .....	117
<b>REFERENCES.....</b>	<b>120</b>
<b>APPENDIX.....</b>	<b>136</b>

## LIST OF TABLES

Table 6.1: Polycyclic aromatic hydrocarbons studied, their molecular structures, molecular weights, melting points, vapour pressures, and typical tropospheric concentrations. ....	30
Table 6.2: Results of the uptake experiments at 273 K. Uptake coefficients of $\text{N}_2\text{O}_5$ , $\text{NO}_2$ , $\text{HNO}_3$ , and $\text{O}_3$ are reported as upper limits. Uptake coefficients of $\text{NO}_3$ on PAHs reported with upper limit of 1 indicate that these experiments were diffusion limited. ....	38
Table 6.3: Results of the uptake experiments at 293 – 297 K. See Table 2 for explanations. n.d.= not determined. ....	38
Table 6.4: Summary of measurements of $\text{O}_3$ uptake on PAH surfaces. For calculations of lifetimes ( $\tau_{\text{atm}}$ ), $\text{O}_3$ concentrations of 100 ppb were used for all studies for comparison purposes. ....	43
Table 7.1: Comparison of the reactive uptake coefficient $\gamma$ for $\text{NO}_3$ reactions with unsaturated organics between this study and results by Moise et al. ....	62
Table 7.2: $\gamma$ comparison of $\text{NO}_3$ reactions with saturated organics between this study and results by Moise et al. ....	64
Table 7.3: Atmospheric lifetimes ( $\tau$ ) of solid surfaces with respect to oxidation by $\text{NO}_3$ , $\text{N}_2\text{O}_5$ , or $\text{OH}$ at 0 °C. It is assumed that the whole surface consists only of the corresponding organic (oleic acid or DES). The number of organic molecules at the surface is assumed to be $1 \times 10^{14}$ molecule $\text{cm}^{-2}$ . The uptake coefficients used in the calculations are given in parenthesis under the calculated lifetimes. Uptake coefficients for $\text{NO}_3$ and $\text{N}_2\text{O}_5$ are from this study, $\gamma_{\text{OH}}$ with oleic acid and DES are from Bertram et al. <sup>67</sup> Their values reported for a vinyl-terminated	

and a methyl-terminated monolayer were used as  $\gamma_{OH}$  with oleic acid and DES, respectively..... 76

Table 8.1: Peak assignment for IR spectroscopy of different nitrogen containing species (R = alkyl chain, PAN = peroxyacetylnitrate). Typical ranges of wavenumbers [ $cm^{-1}$ ] and references are provided. .... 88

Table 9.1: Reactive uptake coefficients ( $\gamma$ ) of different gas-phase oxidants on terminal alkene monolayers, average atmospheric concentrations of the gas-phase species ([oxidant] / molecule  $cm^{-3}$ ) and calculated oxidative powers ( $\gamma \times$  [oxidant]). For  $NO_3$  radicals, calculations have been performed for both high  $NO_3$  concentrations (50 ppt) and low concentrations (5 ppt) to represent approximately a range of concentrations encountered in the atmosphere due to spatial and seasonal fluctuations..... 102



# LIST OF FIGURES

Figure 1.1: Composition of aerosol particles in A) an urban air mass (Los Angeles) and B) a rural setting in Hungary. A) adapted from Rogge et al. <sup>18</sup> B) adapted from Krivacsy et al. <sup>19</sup> .....	3
Figure 1.2: Model of a surface active organic film coating an aqueous aerosol core.....	4
Figure 1.3: Composition of the resolvable elutable organics in aerosol particles in Los Angeles, adapted from Rogge et al. <sup>18</sup> .....	5
Figure 2.1: Schematic illustration of diffusion, uptake, and reaction of gas-phase species on and in liquid aerosol particles, adapted from Finlayson-Pitts and Pitts. <sup>1</sup> .....	12
Figure 4.1: Lewis structures of inorganic gas-phase species used in this thesis.....	16
Figure 4.2: Reaction mechanism for the OH initiated oxidation of alkanes in the troposphere and simultaneous formation of NO <sub>2</sub> . Adapted from Finlayson-Pitts and Pitts. <sup>1</sup> .....	18
Figure 5.1: Schematic drawing of the quadrupole mass spectrometer with chemical ionization region at the left-hand side. ....	22
Figure 5.2: Experimental setup for N <sub>2</sub> O <sub>5</sub> and NO <sub>3</sub> experiments. Flow tube reactor with movable injector, N <sub>2</sub> O <sub>5</sub> glass trap, and oven for thermal conversion of N <sub>2</sub> O <sub>5</sub> to NO <sub>3</sub> . ....	23
Figure 6.1: Scanning electron microscope images of solid PAH surfaces (A: benz[a]anthracene, B: fluoranthene, C: pyrene). ....	34
Figure 6.2: NO <sub>3</sub> signal as a function of time for a typical uptake experiment of NO <sub>3</sub> on fluoranthene at 273 K. Each step down corresponds to an increase of the reactive surface (i.e. the injector is pulled back in 1 cm increments). At the	

end, the signal recovers as the injector is pushed back to its original position (“0” position, no exposure). Scale within the graph corresponds to the positions of the NO<sub>3</sub> injector during the different steps of the experiment. .. 36

Figure 6.3: Plot of the natural logarithm of the CIMS signals vs. the injector position for NO<sub>3</sub> and N<sub>2</sub>O<sub>5</sub> during typical experiments on pyrene solid surfaces at 273 K. .... 37

Figure 6.4: HNO<sub>3</sub> signal as a function of time for a typical uptake experiment of HNO<sub>3</sub> on fluoranthene at 273 K. Within the first 10 minutes the injector is pulled back in 1 cm increments, 6 cm total. At the end (at approx. 10 min), the signal increases compared to its original intensity as the injector is pushed back to its original position (“0”, no exposure) and finally decreases to the original intensity. Scale within the graph corresponds to the positions of the injector during the different steps of the experiment. .... 45

Figure 6.5: Relative changes of the NO<sub>3</sub> signal during exposure of PAH surfaces (27.5 cm<sup>2</sup>) to NO<sub>3</sub> for 60 min. NO<sub>3</sub> exposure corresponds to the product of NO<sub>3</sub> concentration and exposure time. Panels A and B: pyrene. Panels C and D: fluoranthene. Panels E and F: benz[a]anthracene. Left-hand side (A, C, E): 263 ± 2 K. Right-hand side (B, D, F): 297 ± 3 K. The shaded region in Panel A corresponds to the area integrated to determine the number of NO<sub>3</sub> radicals lost during the whole exposure experiment. .... 47

Figure 6.6: Changes in concentrations of HNO<sub>3</sub> (panel A), and NO<sub>2</sub> (panel B) during exposure of pyrene surfaces (27.5 cm<sup>2</sup>) to NO<sub>3</sub> for 60 min at 297 ± 1 K. NO<sub>3</sub> concentrations exposed to the surfaces were approximately 2.5 × 10<sup>11</sup> molecule cm<sup>-3</sup> ..... 50

Figure 6.7: Suggested mechanism for the surface reaction of pyrene with NO<sub>3</sub> based on gas-phase chemistry of PAHs with NO<sub>3</sub>. Note that other isomers may be formed as well..... 52

Figure 7.1: Molecular structures of the three different organic compounds investigated in this study.....	58
Figure 7.2: Plot of the natural logarithm of the CIMS signals of NO <sub>3</sub> vs. reaction time during typical experiments on liquid surfaces of glycerol (squares), oleic acid (triangles), and DES (open diamonds) at 288 K (for oleic acid and DES) and at 293 K (for glycerol). .....	59
Figure 7.3: Measured reactive uptake coefficients $\gamma$ vs. temperature for NO <sub>3</sub> reactions on different solid and liquid organics. OA = oleic acid, DES = diethyl sebacate, Gly = glycerol. mp denotes melting points of the different compounds. ....	61
Figure 7.4: Measured reactive uptake coefficients $\gamma$ vs. temperature for N <sub>2</sub> O <sub>5</sub> reactions on different solid and liquid organics. OA = oleic acid, DES = diethyl sebacate, Gly = glycerol. mp denotes melting points of the different compounds. ....	67
Figure 7.5: Reaction mechanism of N <sub>2</sub> O <sub>5</sub> with a saturated alcohol based on the gas-phase mechanism of methanol and N <sub>2</sub> O <sub>5</sub> suggested by Langer and Ljungström. <sup>156</sup> .....	68
Figure 7.6: Atmospheric lifetimes $\tau$ of liquid droplets as a function of particle diameter with respect to oxidation by NO <sub>3</sub> , N <sub>2</sub> O <sub>5</sub> or OH at 25 °C. It is assumed that the whole particle consists of oleic acid (panel a), DES (panel b) or glycerol (panel c). Grey horizontal lines indicate lifetimes of 5 and 15 days. ....	72
Figure 8.1: Panel (a) shows XPS spectra of the C(1s) region for an ODT monolayer exposed to NO <sub>3</sub> concentrations of 0 - $9.3 \times 10^{-5}$ atm sec. Also included are the Gaussian-Lorentzian peaks from the fitting procedure. The spectra are shifted vertically for better visibility. Panel (b) shows an enlarged view of the best fit of the C(1s) region for an ODT monolayer exposed to NO <sub>3</sub> concentrations of $9.3 \times 10^{-5}$ atm sec. Numbers in panels represent exposure levels in $10^{-5}$ atm sec.....	83

Figure 8.2: A summary of the XPS results. Panel (A): the atomic ratio of the total carbon,  $C_{\text{total}}$ , to total gold, Au. The solid line is a linear fit to the data, and the dashed lines correspond to the 95% confidence limit. Panel (B): the atomic ratio of total oxygen, O, to  $C_{\text{total}}$  as a function of  $\text{NO}_3$  exposure. Panel (C): the atomic ratio of oxidized carbon,  $C_{\text{ox}}$ , to  $C_{\text{total}}$  determined by fitting the C(1s) spectrum with Gaussian-Lorentzian peaks (see text for further details). ..... 85

Figure 8.3: ODT IR spectrum calculated from an ODT sample exposed to  $3.6 \times 10^{-5}$  atm sec of  $\text{NO}_3$  and an unoxidized ODT SAM as reference sample (see text). Negative peaks correspond to features only present or more prominent in the unexposed ODT SAM, positive peaks show features only present or more prominent in the exposed ODT SAM. .... 89

Figure 8.4: Negative ion ToF-SIMS spectra of ODT on gold in the  $m/z$  1 – 700 region. Spectrum (a) was obtained on an ODT sample without  $\text{NO}_3$  exposure, spectrum (b) was obtained after an  $\text{NO}_3$  exposure of  $5.4 \times 10^{-5}$  atm sec (equivalent to 50 ppt  $\text{NO}_3$  for 12.6 days). .... 90

Figure 8.5: Millipore grade  $\text{H}_2\text{O}$  droplets on ODT monolayers before (image A) and after  $\text{NO}_3$  exposure (equivalent to 50 ppt for 3 weeks, image B). .... 92

Figure 8.6: Proposed reaction mechanism for an alkane surface with  $\text{NO}_3$  in the presence of  $\text{NO}_2$  and  $\text{O}_2$  based on gas-phase chemistry. .... 93

Figure 9.1: Changes in the reactive uptake coefficient  $\gamma$  with increasing  $\text{NO}_3$  exposure of a UDT SAM. Bottom x-axis corresponds to actual time of the experiment [min] (at an  $\text{NO}_3$  concentration of  $1.0 \times 10^{11}$  molecule  $\text{cm}^{-3}$ ), top x-axis shows the corresponding total  $\text{NO}_3$  exposure time [h] of the SAM at an atmospheric concentration of 50 ppt. .... 103

Figure 9.2: XPS spectra of the C(1s) region for a UDT monolayer before exposure to  $\text{NO}_3$  (0 atm sec, top panel) and after exposures of  $1.2 \times 10^{-6}$  atm sec

(equivalent to 50 ppt for 6.7 h, centre panel) and  $9.1 \times 10^{-5}$  atm sec (equivalent to 50 ppt for 50 h, bottom panel). ..... 105

Figure 9.3: Summary of processing study and XPS results for UDT. Panel (a) shows the changes in  $\gamma$  with increasing  $\text{NO}_3$  exposure. Panels (b)-(d) show changes in atomic ratios obtained in XPS as a function of  $\text{NO}_3$  exposure. (b) Atomic ratio of total oxygen, O, to total carbon, C. (c) Atomic ratio of oxidized carbon,  $\text{C}_{\text{ox}}$ , to total carbon,  $\text{C}_{\text{total}}$ . (d) Atomic ratio of total carbon,  $\text{C}_{\text{total}}$ , to total gold, Au. The two scales on the top and bottom x-axes are valid for all four panels and provide information on  $\text{NO}_3$  exposure levels in atm sec (bottom axis) and in total exposure time [h] at an atmospheric  $\text{NO}_3$  concentration of 50 ppt (top axis). ..... 106

Figure 9.4: UDT IR spectrum calculated from an UDT sample exposed to  $1.21 \times 10^{-6}$  atm sec of  $\text{NO}_3$  (50 ppt for 6.7 h) and an unoxidized UDT SAM as reference sample (see text). Negative peaks correspond to features only present or more prominent in the unexposed UDT SAM, positive peaks show features only present or more prominent in the exposed UDT SAM. .... 109

Figure 9.5: Negative ion ToF-SIMS spectra of UDT on gold in the  $m/z$  1 – 600 region. Spectrum (a) was obtained on a UDT sample without  $\text{NO}_3$  exposure, spectrum (b) was obtained after an  $\text{NO}_3$  exposure of  $9.1 \times 10^{-6}$  atm sec (equivalent to 50 ppt for 50 h). ..... 110

Figure 9.6: Millipore grade  $\text{H}_2\text{O}$  droplets on UDT monolayers before (image A) and after  $\text{NO}_3$  exposure (equivalent to 50 ppt for 3 weeks, image B). ..... 111

Figure 9.7: Proposed reaction mechanism for an alkene surface with  $\text{NO}_3$  in the presence of  $\text{NO}_2$  and  $\text{O}_2$  based on gas-phase chemistry. .... 112

Figure A.1: Schematic illustration of diffusion, uptake, and reaction of gas-phase species on and in a liquid film, adapted from Finlayson-Pitts and Pitts<sup>1</sup> and Davidovits et al.<sup>160</sup> ..... 136

Figure A.2: Schematic of the resistance model treating individual chemical and physical processes involved in the uptake of a gas-phase species into a liquid as resistances in an electrical circuit. Processes considered are gas-phase diffusion  $\Gamma_{\text{diff}}$ , surface accommodation  $S$ , rates of solvation and desorption ( $k_{\text{sol}}$  and  $k_{\text{des}}$ ), solubility (liquid phase saturation) and diffusion  $\Gamma_{\text{sat}}$ , reaction in the bulk  $\Gamma_{\text{rxn}}$ , and reaction at the surface  $\Gamma_{\text{surf}}$ , adapted from Davidovits et al.<sup>160</sup> ..... 137

## ACKNOWLEDGEMENTS

I would like to begin these acknowledgements by thanking the person who has had the biggest impact on the success of my studies. Allan, you have been the best supervisor I could have hoped for. You always had the big picture in mind when I got entangled in the little challenges and made me focus on what's important. I am very grateful that you were always there when I had a problem or a question.

I want to thank all the past and present members of the Bertram group (Lori, Sarah, Emily, Magda, Jackson, Matt, Michael, Mike, Ben, Daniel, Sebastien, Pedro, Donna, Aidan, Jason, and Richard) for being wonderful colleagues. The great atmosphere we had made every day in the lab so much brighter. I especially want to acknowledge Daniel who taught and helped me so much during my first two years. I am also very happy that I had Lori and Jackson beside me when we struggled with the CIMS and especially with producing  $N_2O_5$ .

I want to thank everybody in the machine shop, electronics shop, and Brian in glassblowing for building, changing, and repairing my equipment so many times.

A big thank you also to everybody who helped me analyze my samples: Dan Bizzotto for help with IR spectroscopy, Ken Wong for all the XPS measurements, Zihua Zhu at PNNL for ToF-SIMS measurements, Mary Fletcher for SEM, and Mario Beaudoin for profilometer measurements. I am very grateful to Larry Fiegland and John Morris for synthesizing undecenethiol for me. Without their generous help a big part of my monolayer studies would not have been possible.

I also want to thank two people who have had nothing to do with this thesis in particular, but who laid the foundation for all this by teaching me chemistry, scientific methods, thinking, and writing: my highschool chemistry teacher Gabriel Hetz and my Diplom thesis supervisor Bruno Glaser.

Mama and Papa, you have supported and encouraged me throughout my life – even when that meant living 8000 km apart. Danke for everything you have done for me! I'm very grateful to have such wonderful parents.

Finally, a very big thank you to Matthias who has been by my side throughout this whole journey – through thick and thin.

# 1 AEROSOL PARTICLES IN THE LOWER TROPOSPHERE

## 1.1 Introduction and Importance

The most general definition of an aerosol is a suspension of liquid or solid material in a gas. In the context of atmospheric sciences, the term aerosols refers to particulate matter of the size range  $0.002 - 100 \mu\text{m}$  suspended in ambient air.<sup>1,2</sup> The lower end of the size range for aerosols is not well defined as the transition between clusters of a few molecules and particles is gradual. The upper end of the range ( $\sim 100 \mu\text{m}$ ) is determined by gravity, as bigger particles settle to the ground rapidly and are not suspended long enough to be considered aerosols. The upper size limit of interest for atmospheric chemistry is usually considered to be  $10 \mu\text{m}$ .<sup>1</sup>

Typical concentrations of liquid and solid aerosol particles in the troposphere range from  $10^2$  up to  $10^8$  aerosol particles in  $1 \text{ cm}^3$  of ambient air. While marine and remote continental regions usually only contain concentrations of  $10^2$  to  $10^4 \text{ cm}^{-3}$ , urban areas typically contain aerosol number concentrations above  $10^5 \text{ cm}^{-3}$ .<sup>1,3-5</sup> Due to this high abundance (especially in highly populated regions) aerosols play a very important role in a variety of atmospheric processes and human health.

Aerosol particles in the atmosphere have a direct influence on the Earth's radiation balance through absorption and reflection of both incoming radiation from the sun, as well as outgoing terrestrial radiation. As aerosols absorb and scatter sunlight, less solar radiation reaches the surface of the Earth. This phenomenon is known as global dimming and is believed to have a cooling effect on the Earth-atmosphere system.<sup>1,6</sup> However, the effect of aerosol particles on the Earth's radiation budget is not only due to this direct influence, but also due to an indirect effect. Ice and water clouds form via nucleation of water vapour onto aerosol particles, so called ice nuclei or cloud condensation nuclei, respectively. The effectiveness of aerosols as nuclei depends on their chemical composition.<sup>1,7</sup> Clouds have a strong impact on both weather and climate. Aerosol concentrations and their chemical composition may influence cloud formation



and may therefore have an additional (indirect) effect on the radiation budget.<sup>1</sup> Overall, the direct and indirect effects of aerosols on climate and global warming are still poorly understood even qualitatively and atmospheric scientists are far from determining their quantitative influence.<sup>8</sup>

The presence of high concentrations of aerosols, especially in the size range of  $\sim 0.1 - 1 \mu\text{m}$ , is also known to have a pronounced impact on visibility, an effect which can be easily noticed in urban and polluted environments. This is due to the absorption and scattering of sunlight by particles in this size range.<sup>1,9</sup>

People have been aware of adverse health effects due to the inhalation of aerosol particles for centuries; a prominent example being the “London Smog” where thousands of excess deaths resulted from sulfur dioxide, acidic aerosols, and soot.<sup>1</sup> When considering the health risks from aerosol particles, researchers usually focus on particulate matter  $< 2.5 \mu\text{m}$  in diameter (called  $\text{PM}_{2.5}$ ), since these particles get transported deep into the lungs when inhaled. Larger particles are typically removed from the inhaled air in the nose and the upper parts of the respiratory tract.<sup>10</sup> Those chemicals that reach the lungs as aerosol particles, or adsorbed onto aerosols, are typically absorbed by the human body much more efficiently than chemicals ingested or in contact with the skin. This makes it extremely important for public health to understand both the chemical composition of aerosols as well as changes in composition due to reactions in the atmosphere that can lead to even more toxic species than the precursor compounds.<sup>1,11,12</sup>

## **1.2 Sources and Composition**

### **1.2.1 Sources of Aerosol Particles**

In general, sources of atmospheric aerosols can be divided into two groups: natural and anthropogenic. Natural aerosols originate from ocean surfaces (sea salt and spray), volcanoes, soil and desert surfaces (mineral dust), forest fires, plants (leaf abrasion, seeds, pollen), and microorganisms (bacteria, fungi, algae), among others.<sup>2,13,14</sup> Major anthropogenic sources of aerosols are fossil fuel combustion, biomass burning, and industrial processes,<sup>2</sup> but locally other contributions such as cigarette smoking or meat cooking may also be significant.<sup>15,16</sup> Apart from being emitted directly into the atmosphere, aerosol particles can also form from gas-phase precursor substances via

nucleation, condensation, and reactions decreasing the volatility of organic gas-phase molecules.<sup>1,17</sup> Due to the large variety of aerosol particle sources, it is not surprising that field measurements have confirmed a broad variety of different aerosol compounds, both organic and inorganic, of anthropogenic and natural origin.

### 1.2.2 Composition of Aerosol Particles

Abundant components of inorganic aerosols are  $\text{SO}_4^{2-}$ ,  $\text{Cl}^-$ ,  $\text{NO}_3^-$ ,  $\text{NH}_4^+$ , and  $\text{Na}^+$ .<sup>1,2</sup> While these few substances dominate the inorganic fraction of aerosols worldwide, the composition of the organic fraction is much more complex. The organic fraction is usually in the range of 10 – 90% of all aerosols.<sup>16</sup> Figure 1.1 shows typical relative compositions of aerosols in two different environments (A urban, B remote continental). As these numbers are only from one specific field study, individual air masses may have significantly different compositions.

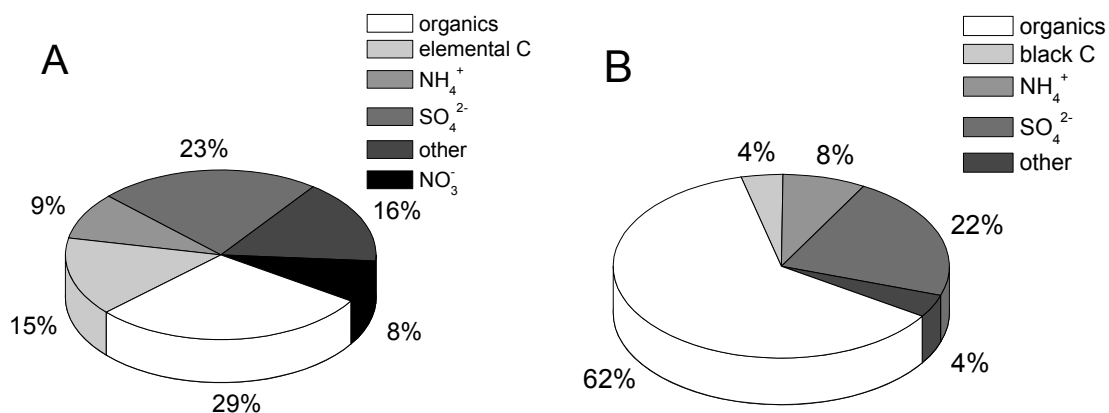


**Figure 1.1: Composition of aerosol particles in A) an urban air mass (Los Angeles) and B) a rural setting in Hungary. A) adapted from Rogge et al.<sup>18</sup> B) adapted from Krivacsy et al.<sup>19</sup>**

The organic material in aerosols can be in the form of purely organic particles, or alternatively the organics can be mixed with inorganic material. These mixtures may exist as homogenous mixtures (e.g. water-soluble organics in aqueous particles) or an organic coating on an inorganic particle.

Due to the complex origins and complex chemical compositions of aerosols, it is not surprising that field studies have observed aerosol particles that seem to consist of more than one phase or contain an immiscible surface film.<sup>20-22</sup>

Due to the abundance of water vapour in most air masses, aqueous droplets are almost ubiquitous in the troposphere. And as methyl, methylene, and vinyl groups are major organic components of atmospheric particulate matter and form hydrophobic parts of molecules, it is reasonable to assume that they partition to the air-particle interface of aqueous aerosols. As outlined below, long chain aliphatic acids are also a dominant class of organics in the troposphere. These acids are surface active due to their hydrophilic headgroup (COOH) and their hydrophobic tail (hydrocarbon chain). Therefore, in mixed inorganic/organic aerosols the organic material can form coatings on the surface of aqueous particles,<sup>20,23</sup> or organic coatings adsorbed on the surface of solid particles.<sup>24</sup> A schematic drawing of an aqueous aerosol coated with a film of a surface active organic is shown in Figure 1.2.

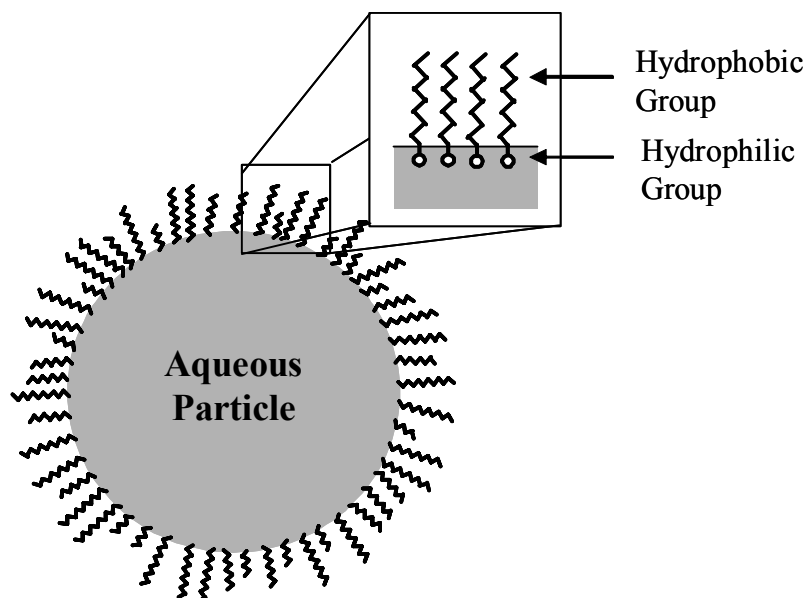


**Figure 1.2: Model of a surface active organic film coating an aqueous aerosol core.**

Examples of these coated particles are aqueous ocean spray droplets covered by water insoluble biomolecules (e.g. fatty acids) from marine organisms<sup>20,23</sup> or mineral dust particles with adsorbed organics, as described by Usher et al.<sup>24,25</sup> and references therein.

This thesis focuses on reactions of liquid and solid organics (simulating purely organic aerosols) and reactions of organic monolayers on an inorganic substrate (simulating reactions of organic coatings on inorganic aerosols) with atmospheric oxidants.

The different organics selected for this work were chosen as representatives of different functional groups identified in field measurements. Different alkanes, alkenes, aromatics, fatty acids, alcohols, and organic bases, among others, are typically found in samples of atmospheric particulate matter.<sup>1,26</sup> However, these identified compounds and their concentrations vary greatly between locations, seasons, and analytical techniques (e.g. solvents used for extraction).<sup>1,27,28</sup> Rogge et al.<sup>18</sup> analysed organics in aerosols from Los Angeles and a town downwind of Los Angeles and the major identified classes of organics were aliphatic dicarboxylic acids and n-alkanoic acids; smaller contributions came from aromatic polycarboxylic acids, n-alkanes, diterpenoid acids, n-alkenoic acids, and polycyclic aromatic hydrocarbons (PAHs). Figure 1.3 shows the data obtained in Los Angeles.

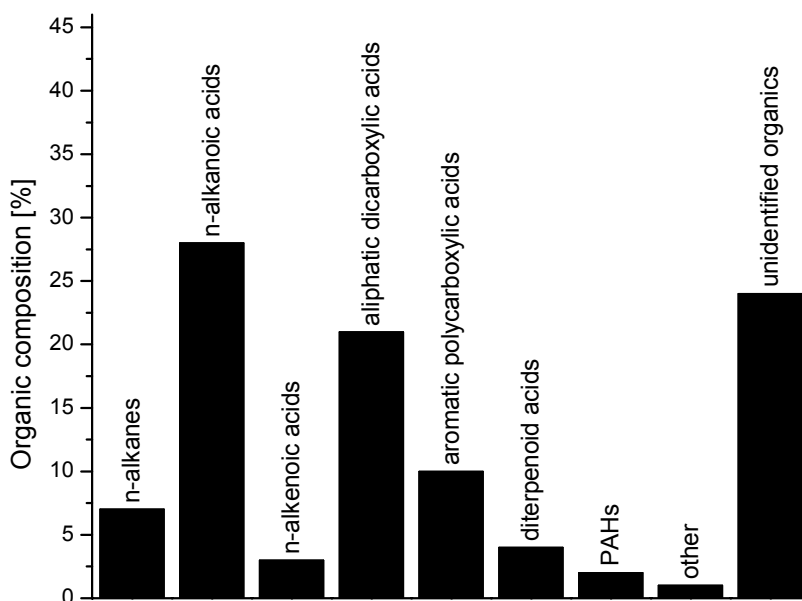


**Figure 1.3: Composition of the resolvable elutable organics in aerosol particles in Los Angeles, adapted from Rogge et al.<sup>18</sup>**

As each of these classes of compounds contains a variety of organics and hundreds of different substances are present, it is not feasible to study atmospheric reactions of all these compounds and include them all into modelling studies. It is therefore necessary to focus on the different organic functional groups present and choose model compounds as typical representatives of certain classes of organic aerosol components. Model compounds used in the present thesis represent some of these major aerosol components (n-alkane, n-alkene, n-alkenoic acid, alkanoate, polyalcohol, and PAH).<sup>26,29</sup> Sources and concentrations of these compound classes are described in the following paragraphs.

Alkanes, alkenes, and carboxylic acids are ubiquitous components in the organic aerosol fraction and are often present in significant concentrations. Ketseridis et al.<sup>26</sup> measured  $14.0 \text{ ng m}^{-3}$  of aliphatic alkanes and  $39.5 \text{ ng m}^{-3}$  of organic acids in a marine environment<sup>1,26</sup> and the data by Rogge et al.<sup>18</sup> showed approximately  $70 \text{ ng m}^{-3}$  of n-alkanes and  $600 \text{ ng m}^{-3}$  of different organic acids for the urban environment of Los Angeles. Sources of alkanes are both biological and anthropogenic and range from plant waxes and cigarettes<sup>16</sup> to automobiles, diesel trucks, and natural gas appliances.<sup>1</sup> Sources of organic acids are living and dead organisms (material from microbes, plant wax, and cell membranes), meat cooking processes<sup>15</sup> – releasing saturated and unsaturated aliphatic acids, and fossil fuel combustion – releasing both aliphatic and aromatic acids. Additionally, these acids are secondary products from the oxidation of atmospheric precursor substances, i.e. alkanes and aldehydes released from plants.<sup>1</sup> Carbon chain lengths of aliphatic organics typically extend up to  $\sim \text{C}_{35}$ .<sup>1,27</sup>

Alcohols are also usually of biogenic origin, primarily released from plants.<sup>1</sup> For example, several unsaturated alcohols have been confirmed in emissions from wounded plants after harvesting and lawn mowing.<sup>30</sup>

Another class of compound that is observed in environmental samples worldwide is polycyclic aromatic hydrocarbons (PAHs). Although their concentrations are typically lower than alkanes or organic acids, their occurrence in the atmosphere is of particular concern. This is caused by the fact that they constitute a health risk to the population due to their allergenic, mutagenic, and carcinogenic properties.<sup>1</sup> Sources of PAHs are incomplete combustion processes in diesel and gasoline engines, and biomass or coal

burning.<sup>1,31</sup> PAHs have a wide range of vapour pressures (e.g. the vapour pressure of the 2-ring PAH naphthalene is  $7.8 \times 10^{-2}$  torr and that of coronene (7 aromatic rings) is  $1.5 \times 10^{-12}$  torr).<sup>1</sup> As a result, PAHs are found in the gas phase (2- and 3-ring PAHs) as well as on and in atmospheric particulate matter (PAHs with 5 or more aromatic rings). PAHs with 3 or 4 rings are semi-volatile and are observed both in the gas-phase and adsorbed to particles. Concentrations of individual particle-phase PAHs in atmospheric samples are usually in the range of a few  $\text{ng m}^{-3}$  for urban areas around the world, but can reach as high as  $900 \text{ ng m}^{-3}$  during heavy traffic conditions or during biomass burning episodes.<sup>1,32-38</sup>

## 2 ATMOSPHERIC CHEMISTRY

As mentioned in the previous chapter, there is a huge variety of different compounds present on and in atmospheric aerosol particles. In addition to organic and inorganic substances in a condensed state, there is also a large number of different gas-phase species in the troposphere – ranging from major components like  $O_2$  to trace gases like  $CO_2$ ,  $NO_2$ , or volatile organic compounds. Concentrations of different substances vary widely and due to the complex composition of the atmosphere, an endless list of possible reactions may occur. In general, atmospheric chemistry is divided into two main categories: homogeneous reactions occurring in the gas phase and heterogeneous reactions between gas-phase species and solid or liquid aerosol particles. Below I give a brief discussion of both to set the stage for the rest of this thesis.

### 2.1 Homogeneous Reactions in the Atmosphere

As many potentially reactive species in the troposphere are present in the gas phase, these reactions are of considerable importance in atmospheric science and have been studied in some detail for many years. Due to the scientific interest in tropospheric homogeneous reactions, there is a reasonably large data base available describing these reactions and many rate constants for reactions of different atmospheric oxidants like OH,  $O_3$ , or  $NO_3$  with gas-phase organics have been determined.<sup>1,39-42</sup> For example, these studies have shown the atmospheric relevance of ozone.<sup>40</sup> They also found that additionally OH radicals dominate gas-phase reactions during the day and that nitrate radicals ( $NO_3$ ) are one of the most important nighttime gas-phase oxidants.<sup>1</sup> Homogeneous reaction rates are typically lower for  $NO_3$  reactions compared to OH. But the fact that  $NO_3$  concentrations can be up to four orders of magnitude higher at night compared to OH during the day<sup>1</sup> makes  $NO_3$  overall an important radical in homogeneous tropospheric reactions.

## 2.2 Heterogeneous Atmospheric Chemistry

Heterogeneous reactions occur between reactants in different phases. In the context of atmospheric chemistry, these are reactions between a gas-phase species and a solid or liquid aerosol particle. This is sometimes also referred to as multiphase chemistry. While research on gas-phase reactions is well established (with a range of different techniques available, good agreements among different laboratories, and good understanding of these homogeneous reactions on a molecular level), studies of heterogeneous reactions is a relatively new field of research and provides more challenges. Knowledge about the surface structures of liquid or solid substrates on a molecular level is very limited. In addition, the surface structure may change due to the adsorption of a gas-phase species, and reaction rates and mechanism may change as the surface changes during reaction.<sup>1</sup> Difficulties also arise as non-reactive physical uptake of the gas-phase species as well as uptake due to chemical reaction is possible. Current scientific understanding of aerosol chemistry is very limited, especially with respect to NO<sub>3</sub> radical reactions on organic surfaces, which are the major focus of this thesis.

A quote from Finlayson-Pitts and Pitts<sup>1</sup> shows just how rudimentary our knowledge of heterogeneous reactions is. They say that “we are still in the “dark ages” in terms of understanding kinetics and mechanisms of these processes on a molecular level”.

Despite the fact that heterogeneous reactions are still insufficiently studied, they are of high importance in the atmosphere. Field measurements suggest that these reactions may change the chemical composition of particles and their surfaces.<sup>43</sup> Therefore important properties like aerosol hydrophilicity, toxicity, and optical properties may be altered by these reactions.<sup>1,44</sup> Aerosols may also constitute a sink for the gas-phase reactants.

A prominent example of the importance of heterogeneous reactions in the atmosphere is the depletion of stratospheric ozone over the Arctic and Antarctic regions, the so called ozone “hole”. Parts of this reaction mechanism depend on the presence of ice crystals and particles as substrates for reaction.<sup>45</sup> The heterogeneous reactions involved are much faster than the corresponding homogeneous gas-phase reactions.



In fact, in many cases heterogeneous reactions of atmospheric oxidants with organics have been shown to be faster than the corresponding homogeneous gas-phase reactions<sup>46,47</sup> and in some cases kinetics and reaction mechanisms of the chemical processes occurring at the interface of two phases may be different from the corresponding homogeneous reactions.<sup>48</sup>

In a number of cases, condensed phase products of heterogeneous atmospheric reactions are more toxic than the precursor compounds (e.g. PAHs that are transformed into nitro-PAHs).<sup>11</sup> This makes research on heterogeneous chemistry an important topic for human health. Heterogeneous reactions of NO<sub>3</sub> radicals, NO<sub>2</sub>, and N<sub>2</sub>O<sub>5</sub> may be of special concern as these reactions may be able to form nitrogenated organics. Since 49 different nitrogenated organic compounds are designated as “Hazardous Air Pollutants”,<sup>12</sup> nitration of aerosol particles via reaction with NO<sub>3</sub> (and possibly NO<sub>2</sub> and N<sub>2</sub>O<sub>5</sub>) may produce toxic compounds that constitute a health risk upon inhalation.

As many reactions of aerosols with atmospheric trace gases are oxidations (e.g. OH, O<sub>3</sub>, or NO<sub>3</sub> reactions), they can change formerly hydrophobic alkanes or alkenes into more hydrophilic compounds (due to e.g. nitro-, nitrate-, hydroxyl-, or carbonyl functional groups) that may serve as better cloud condensation nuclei.<sup>49</sup> This may change the formation conditions and properties of clouds.

Heterogeneous reactions may also have implications for source apportionment. Specific organic species are often used as “molecular markers” for sources of organic particles. If heterogeneous reactions change the concentrations of these “molecular markers” they can lead to errors when calculating source strengths.<sup>43</sup>

Aerosol surface coatings or films form the interface between these particles and the atmosphere. Therefore they are of special interest in understanding and characterizing atmospheric chemical processes. Depending on the density or degree of compression of these films or coatings, they may limit the transfer of molecules across the air-aqueous interface, and hence reduce reaction rates between gas-phase species and the aqueous core of the aerosol.<sup>50-54</sup> Heterogeneous reactions may alter the organic surface coatings on droplets and therefore change the properties of this “barrier” between gas phase and aqueous phase. These reactions may enable the uptake of a gas-phase species into the

aqueous phase or evaporation from the droplet which was previously blocked by surfaces active coatings.

The optical properties of aerosols depend on the presence of functional groups and on the phase of the particles.<sup>1,55</sup> Heterogeneous reactions may induce phase changes as alcohols and organonitrates typically have higher melting points than the corresponding alkanes or alkenes. However, heterogeneous reactions can also lead to scission of long chain organic molecules creating fragments with lower melting and boiling points. If a heterogeneous reaction leads to the scission of a hydrocarbon chain, it could destroy the organic aerosol surface, because the smaller, more volatile organic molecules may be released into the gas phase. This has been demonstrated by Molina et al.<sup>56</sup> who showed that the OH-initiated oxidation of an alkane self-assembled monolayer leads to rapid volatilization of the organic substrate. These authors concluded that decomposition of carbon chains and subsequent volatilization of short chain organics due to OH radical reactions may be an important loss process for tropospheric aerosols and may even be comparable to wet deposition. A modeling study has come to the conclusion that these heterogeneous reactions may constitute a significant source of tropospheric volatile organic compounds (VOCs).<sup>57</sup> These conclusions may not only be valid for hydroxyl radicals, but also for other atmospheric oxidants like NO<sub>3</sub>, as pointed out by Kwan et al.<sup>57</sup> As NO<sub>3</sub> is present in the atmosphere in concentrations several orders of magnitude higher than OH, decomposition due to nitrate radicals may be a significant source of atmospheric VOCs. However, this has not been investigated.

In general, there are several different processes involved in heterogeneous reactions. These steps are illustrated in Figure 2.1.

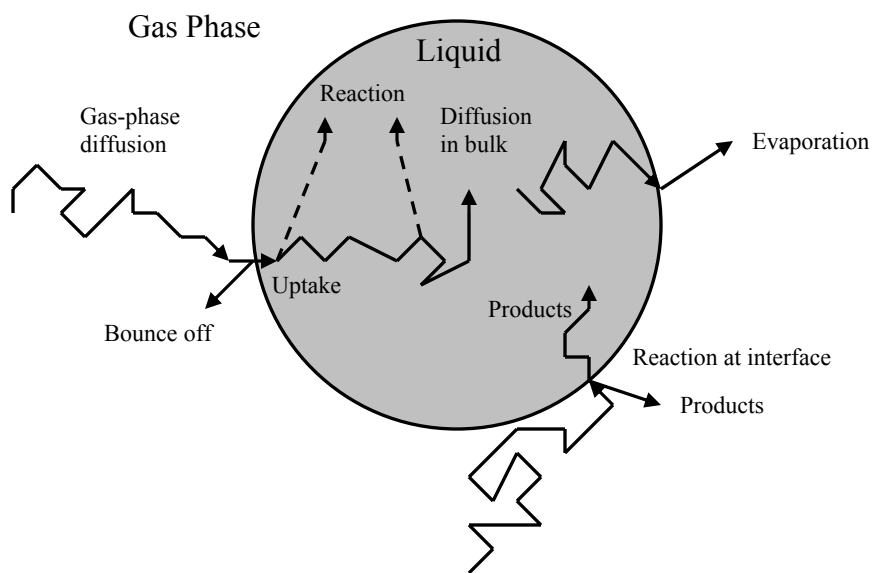


**Figure 2.1: Schematic illustration of diffusion, uptake, and reaction of gas-phase species on and in liquid aerosol particles, adapted from Finlayson-Pitts and Pitts.<sup>1</sup>**

After diffusion through the gas phase, a gaseous molecule either adsorbs onto an aerosol surface or bounces off. If it adsorbs, it is either taken up into the bulk of the particle, reacts directly on the surface, or desorbs again back into the gas phase. In the case of a surface reaction, products may either stay at the interface, diffuse into the bulk of the aerosol, or evaporate into the gas phase. A gas-phase molecule taken up into the bulk diffuses through the particle and either reacts in the bulk or evaporates again into the gas phase.

In many studies on the kinetics of heterogeneous reactions – including the presented thesis – the net loss of a gas-phase species into the condensed phase is measured and an uptake coefficient ( $\gamma$ ) is determined. This reactive uptake coefficient is defined as the fraction of collisions with a surface that leads to reactive loss and describes the overall uptake without deconvoluting the individual steps involved.

The overall uptake process is often described by the resistance model, which is explained in the Appendix.

### 3 THESIS OVERVIEW

Over the past decade scientific interest in the heterogeneous reactions of compounds of atmospheric significance has increased drastically and heterogeneous reactions of aerosol particles and substrates simulating aerosols have been the focus of many studies.<sup>44,46,56,58-75</sup> The majority of the available literature focuses on O<sub>3</sub> reactions, with much less data obtained on reactions of OH, NO<sub>3</sub>, or other atmospheric oxidants (e.g. Cl or Br). Studies investigating NO<sub>3</sub> heterogeneous reactions are few and involve aqueous solutions, mineral dust, soot, and organics as condensed phase reactants.<sup>44,63,66,76-79</sup> As these references show, our knowledge of heterogeneous reactions between organic compounds and NO<sub>3</sub> radicals is extremely limited and many questions are still unanswered. These open questions include the reactivity of different functional groups with NO<sub>3</sub>, the relative differences in reactive uptake between NO<sub>3</sub> and other atmospheric oxidants, as well as the reaction products and mechanisms.

As described in Chapter 1, natural and anthropogenic aerosols are mostly complex mixtures of many components, and in some cases more than one phase.<sup>52,80</sup> Also, the exact chemical composition is still poorly understood. As a first step toward understanding the chemical reactions that may occur in these complex systems, it is beneficial to study model substances that serve as proxies for atmospheric aerosols in controlled laboratory environments. Simple one component substrates are reproducible systems that allow chemical characterization and analysis which is necessary before more complex and realistic aerosols or substrate mixtures may be investigated.

This thesis investigates the reactive uptake coefficients and products of different heterogeneous reactions of atmospheric importance. Gas-phase reaction partners were oxidants present in the lower troposphere in significant concentrations, namely NO<sub>3</sub>, NO<sub>2</sub>, N<sub>2</sub>O<sub>5</sub>, HNO<sub>3</sub>, and O<sub>3</sub>. These gas-phase species were reacted with different solid or liquid organic films and monolayers with different functional groups (alkane, alkene, alkenoic acid, polyalcohol, alkanoate, and PAH). Reactive uptake coefficients were measured, gas-phase products were determined for solid PAH films, and organic

monolayers were analyzed for condensed-phase products. The results from these projects and the atmospheric implications that arise from these results are presented in Chapters 6 – 9.

Chapters 4 and 5 were included to provide additional information on the research presented. Chapter 4 gives an overview of the tropospheric chemistry of the gas-phase species used in this thesis ( $\text{NO}_3$ ,  $\text{NO}_2$ ,  $\text{N}_2\text{O}_5$ ,  $\text{HNO}_3$ , and  $\text{O}_3$ ) and Chapter 5 explains the major experimental and instrumental techniques employed throughout this work.

Chapter 6 investigates reactions of three different solid films of PAH (pyrene, fluoranthene, and benz[a]anthracene) with  $\text{NO}_3$ ,  $\text{NO}_2$ ,  $\text{N}_2\text{O}_5$ ,  $\text{HNO}_3$ , and  $\text{O}_3$ . Three different types of experiments were performed. The first set of experiments consisted of measuring the reactive uptake coefficient of the gas-phase oxidants on “fresh” (i.e. unreacted) PAH surfaces by monitoring the decay of the gas-phase reactants using a coated wall flow tube reactor connected to a chemical ionization mass spectrometer (CIMS). The presented study is complimentary to many of the previous studies of PAH heterogeneous chemistry, since in experiments in this work the loss of the gas-phase reactant was monitored, whereas most of the previous studies examined the loss of the PAH material. Since in this thesis the loss of a range of different atmospheric oxidants on the same PAH surfaces was measured, a direct comparison between the five different oxidants was possible.

The second type of experiments investigated the  $\text{NO}_3$  uptake on PAH surfaces as a function of time to determine if this reaction was catalytic or if the reaction rate decreased with time due to oxidation of the surface-bound PAH molecules. This information is needed to extrapolate laboratory results to the atmosphere. For this study, PAH films were exposed to  $\text{NO}_3$  for prolonged time periods and changes in the  $\text{NO}_3$  signal were monitored using CIMS.

The last set of experiments consisted of a gas-phase product study for the reaction of  $\text{NO}_3$  with pyrene at room temperature to aid in the understanding of the reaction mechanism. The study described in Chapter 6 has been published in Gross and Bertram<sup>81</sup> and Mak et al.<sup>82</sup>

Chapter 7 presents measurements of the reactive uptake coefficient of  $\text{NO}_3$  and  $\text{N}_2\text{O}_5$  on different organic films (an alkanoate, an alkenoic acid, and a polyalcohol). All

experiments were performed on solid and liquid films of the same compound in order to examine the effect of the phase on  $\gamma$ . The reactivity comparison between different phases gives information on whether reactions occur in both the bulk and at the surface or at the surface only. Differences between the uptake coefficients of different functional groups are discussed. Atmospheric lifetimes of organics in the presence of different gas-phase oxidants were calculated for both liquid and solid aerosol particles and the possible importance of heterogeneous reactions on secondary organic aerosol studies is discussed. The content of Chapter 7 has been submitted to *Physical Chemistry Chemical Physics*.

Self-assembled monolayers (SAMs) of organics were used for the projects presented in Chapters 8 and 9. SAMs of an alkanethiol (Chapter 8) and a terminal alkenethiol (Chapter 9) on gold substrates simulated organic aerosol surfaces or organic amphiphilic aerosol coatings (e.g. carboxylic acids on aqueous aerosols), as described in Chapter 1.2.2.

Chapter 8 presents experimental results providing information on condensed-phase reaction products of  $\text{NO}_3$  radicals on an alkane monolayer. For these experiments, SAMs on gold coated silicon wafers were exposed to  $\text{NO}_3$  radicals for different periods of time and these surfaces were subsequently analyzed using X-ray photoelectron spectroscopy (XPS), infrared (IR) spectroscopy, and time-of-flight secondary ion mass spectrometry (ToF-SIMS).  $\text{H}_2\text{O}$  contact angles were also determined using a CCD camera. The data obtained were used to investigate surface oxidation and to determine the condensed phase reaction products. A reaction mechanism and atmospheric implications were derived from these findings. The study described in Chapter 8 has been published in Knopf et al.<sup>83</sup> and Gross and Bertram.<sup>84</sup>

The experiments described in Chapter 8 were repeated in Chapter 9 for the terminal alkene monolayer using identical procedures and instruments. In addition, two other types of experiments were carried out: in the first set, the flow tube reactor coupled to CIMS (mentioned above) was used to determine the reactive uptake coefficient ( $\gamma$ ) of  $\text{NO}_3$  on the unsaturated hydrocarbon surface. As well, the  $\text{NO}_3$  uptake on the alkene surface was investigated as a function of  $\text{NO}_3$  exposure time in a manner similar to the second type of experiments described for PAHs in Chapter 6. The study described in Chapter 9 has been published in Gross and Bertram.<sup>84</sup>

## 4 BACKGROUND INFORMATION ON GAS-PHASE SPECIES

This thesis investigates the heterogeneous reactions of five different gas-phase species,  $\text{NO}_3$ ,  $\text{N}_2\text{O}_5$ ,  $\text{NO}_2$ ,  $\text{HNO}_3$ , and  $\text{O}_3$ . Lewis structures of all five compounds are shown in Figure 4.1. This Chapter was added to give information on the gas-phase concentrations, sources, sinks, and lifetimes of these species.

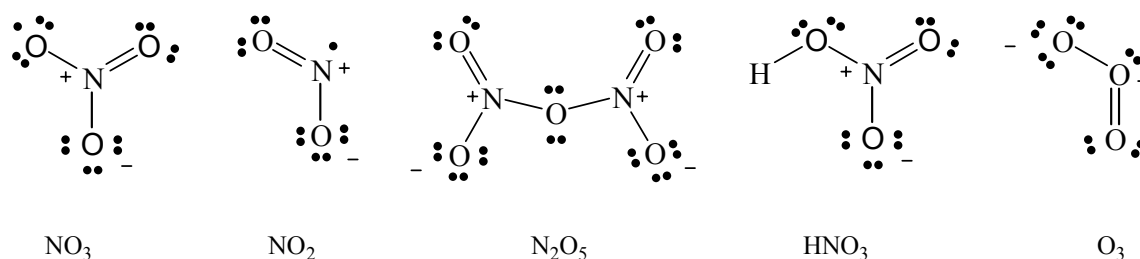


**Figure 4.1: Lewis structures of inorganic gas-phase species used in this thesis.**

All of the processes described below as well as the heterogeneous reactions studied in this thesis are thought to be of relevance in the troposphere. The troposphere is the lower region of the Earth's atmosphere from ground level up to an altitude of approximately 10 – 20 km, depending on latitude and season.<sup>1,2</sup> The temperature within the troposphere normally decreases with increasing altitude. At the top of the troposphere (i.e. the tropopause) the temperature is approximately -55 °C.<sup>1,2</sup>

### 4.1 $\text{NO}_3$ Chemistry in the Troposphere

The significance of the nitrate radical  $\text{NO}_3$  in the atmosphere was first recognized in the 1970s and the first tropospheric field measurement of its concentration by Platt et al.<sup>85</sup> in 1979 confirmed that concentrations at night were high enough in polluted urban environments to significantly affect nighttime chemistry.  $\text{NO}_3$  is a reactive oxidant, formed by the reaction of  $\text{NO}_2$  and  $\text{O}_3$  according to Reaction R4.1,



and is present in polluted nighttime atmospheres in concentrations of up to 430 ppt.<sup>1</sup>

Concentrations of NO<sub>3</sub> in the day are small since NO<sub>3</sub> strongly absorbs visible light and is therefore rapidly photolysed (Reactions R4.2 and R4.3):



The tropospheric lifetime at noon in sunlight is only about 5 s<sup>86</sup> and reaction R4.3 (leading to NO<sub>2</sub> and O) is 8 times faster than reaction R4.2.<sup>87</sup>

NO<sub>3</sub> reacts very quickly with NO according to R4.4 ( $k = (2.4 - 3.0) \times 10^{-11} \text{ cm}^3 \text{ molecule}^{-1} \text{ s}^{-1}$ );<sup>1,88,89</sup> and therefore the two compounds do not coexist in high concentrations:



At night, in absence of photolysis, removal processes of NO<sub>3</sub> from the troposphere include reactions with gas-phase organics and the reaction with NO<sub>2</sub> to form N<sub>2</sub>O<sub>5</sub> (reaction R4.5), which subsequently can be taken up by aqueous aerosols and is removed by precipitation (reaction R4.6).<sup>1</sup>



NO<sub>3</sub> lifetimes at night were reported to range from < 2 min up to 4 h.<sup>86,90,91</sup>

## 4.2 NO<sub>2</sub>, N<sub>2</sub>O<sub>5</sub>, HNO<sub>3</sub>, and O<sub>3</sub> Chemistry in the Troposphere

### 4.2.1 Nitrogen Dioxide (NO<sub>2</sub>)

Nitrogen dioxide, NO<sub>2</sub>, is an orange-brown liquid at temperatures below 21 °C (at 1 atm)<sup>92</sup> and an orange-brown gas at higher temperatures. NO<sub>2</sub> is the only gaseous air pollutant that absorbs visible light significantly. As a result it reduces visibility and contributes to the brownish haze over polluted cities.<sup>1</sup> Tropospheric NO<sub>2</sub> stems from different sources including biomass burning, fossil fuel combustion, soils, lightning, and NH<sub>3</sub> oxidation.<sup>49</sup> The primarily emitted compound is typically NO. In the absence of hydrocarbons, NO<sub>2</sub> is then produced from the reaction of NO + O<sub>3</sub>. In the presence of



hydrocarbons NO is also converted to NO<sub>2</sub> through a radical chain reaction as shown in Figure 4.2.<sup>1</sup>

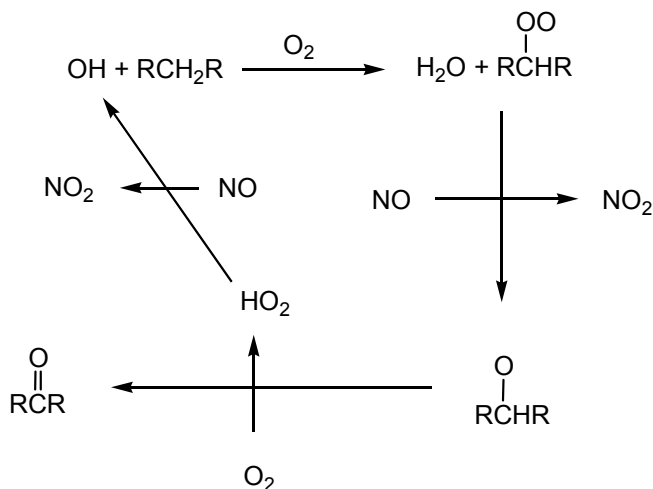


**Figure 4.2: Reaction mechanism for the OH initiated oxidation of alkanes in the troposphere and simultaneous formation of NO<sub>2</sub>. Adapted from Finlayson-Pitts and Pitts.<sup>1</sup>**

Tropospheric concentrations of nitrogen dioxide can reach values of up to 180 ppb<sup>1,93,94</sup> and maximum urban concentrations are typically reached after the morning rush hour when significant amounts of NO and organics have been emitted by cars.<sup>1</sup>

The most important sinks for NO<sub>2</sub> are reactions with OH (to form HNO<sub>3</sub> – during the day) or O<sub>3</sub> (to form NO<sub>3</sub> – at night).<sup>2</sup> After this reaction, NO<sub>2</sub> further reacts with NO<sub>3</sub> to form N<sub>2</sub>O<sub>5</sub> according to reaction R4.5. Additional sinks are the uptake into H<sub>2</sub>O droplets and photolysis during the day:



This reaction R4.7 leads to the production of ozone (from O + O<sub>2</sub>), which subsequently can reform NO<sub>2</sub> from NO according to reaction R4.8<sup>1,2</sup>



The reported lifetime of NO<sub>2</sub> varies enormously from 5 – 21 min in England<sup>95</sup> to 14 h – 2 days in different regions of Asia (reported as lifetime of NO<sub>x</sub>).<sup>96</sup>

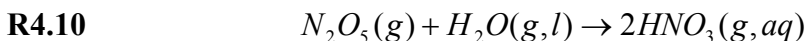
#### 4.2.2 Dinitrogen Pentoxide (N<sub>2</sub>O<sub>5</sub>)

N<sub>2</sub>O<sub>5</sub> is a white solid at room temperature with a vapour pressure of 10 kPa at 3.9 °C.<sup>92</sup> It is an oxidizer and decomposes to HNO<sub>3</sub> in contact with water. Its presence in the atmosphere is limited to the night, as its formation requires the presence of NO<sub>3</sub>.<sup>1</sup>



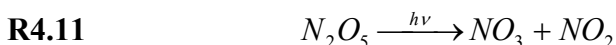
Although N<sub>2</sub>O<sub>5</sub> has never been directly measured in the troposphere,<sup>1</sup> typical atmospheric concentrations at night were calculated to be in the range from < 200 ppt to ~ 15 ppb<sup>97-99</sup> and nocturnal lifetimes of N<sub>2</sub>O<sub>5</sub> vary from < 1 min to ~ 4 h.<sup>86,91,100,101</sup>

The main loss process of N<sub>2</sub>O<sub>5</sub> is reaction with H<sub>2</sub>O to form nitric acid:



This reaction proceeds much faster heterogeneously (on liquid water) than homogeneously with H<sub>2</sub>O(g).<sup>1</sup>

During the day N<sub>2</sub>O<sub>5</sub> photolyses to form NO<sub>3</sub> and NO<sub>2</sub>.<sup>1</sup>



Since NO<sub>3</sub> also rapidly decomposes in sunlight, the reverse reaction does not occur and N<sub>2</sub>O<sub>5</sub> concentrations during the day are minimal.

#### 4.2.3 Nitric Acid (HNO<sub>3</sub>)

Nitric acid is a colourless liquid at room temperature, but due to its relatively high vapour pressure (10 kPa at 28.4 °C)<sup>92</sup> it is also present in the gas phase under ambient conditions. HNO<sub>3</sub> is a strong, corrosive acid. The atmospheric importance of HNO<sub>3</sub> was recognized in the 1970s when the adverse effects of acid rain became evident and HNO<sub>3</sub> was identified as a major contributor to this rain acidity.<sup>102</sup> In the troposphere it is formed in reaction R4.10 above and in the following reaction (R4.12):<sup>2</sup>



In the stratosphere, HNO<sub>3</sub> aids in the formation of polar stratospheric clouds, as reported by Hanson<sup>103</sup> and references therein. Typical tropospheric concentrations are < 100 ppt to 50 ppb.<sup>1</sup> The major removal processes for HNO<sub>3</sub> are dry and wet deposition.

#### 4.2.4 Ozone (O<sub>3</sub>)

Ozone is a bluish gas at atmospheric temperatures and pressures. It absorbs light in the infrared and in the ultraviolet (UV) sections of the radiation spectrum.<sup>1</sup> Its UV absorbance makes O<sub>3</sub> a highly important species in the stratosphere as it shields the Earth from harmful solar UV radiation of wavelength < 290 nm.<sup>1</sup> In the troposphere, however, the presence of ozone contributes to the greenhouse effect and it also has adverse effects on human health as it is highly reactive and toxic.<sup>1</sup> In addition, it is harmful to plants and decreases the yield of many crops.<sup>104</sup>

O<sub>3</sub> in the troposphere is mainly produced by photochemical reactions in the presence of hydrocarbons and NO<sub>x</sub> (= NO + NO<sub>2</sub>)<sup>2</sup>



and its presence is also due in part to ozone formed in the stratosphere and transported down into the troposphere.<sup>105</sup>

Removal of ozone occurs by photolysis which leads to formation of molecular oxygen and an oxygen atom according to reaction R4.18. This process is a source of OH radicals (reaction R4.19).<sup>1,2</sup>



Other sinks for tropospheric ozone are R4.8 and its rapid reaction with unsaturated organics. The lifetime of O<sub>3</sub> toward photochemical loss in the troposphere is typically 2 – 4 weeks,<sup>105</sup> but reactions with unsaturated compounds may shorten this significantly. Ozone concentrations are in the range of about 10 – 100 ppb,<sup>2</sup> but exhibit strong temporal and spatial variations. The highest concentrations are typically found in urban areas in summertime.<sup>105</sup>

## 5 GENERAL OVERVIEW OF EXPERIMENTAL TECHNIQUES USED IN THIS THESIS

### 5.1 Chemical Ionization Mass Spectrometry (CIMS)

Most of the experiments outlined in this thesis required controlled exposure of solid or liquid organic films to gas-phase species. Concentrations of these gases and their depletion due to reaction had to be determined. A quadrupole mass spectrometer was used to separate and quantify the different ionized gas-phase species. Gases were ionized using chemical ionization (CI). A schematic drawing of the CI region and the quadrupole MS is given in Figure 5.1. CI is a very selective ionization technique. Ionization occurs only with a few select compounds and the choice of parent ion depends on the species of interest. The reagent gases used for chemical ionization were  $\text{SF}_6^-$  (for detecting  $\text{N}_2\text{O}_5$ ,  $\text{NO}_3$ ,  $\text{NO}_2$ ,  $\text{HNO}_3$ ,  $\text{O}_3$ , and  $\text{HONO}$ ),  $\text{I}^-$  (for detecting  $\text{NO}_3$ ), and  $\text{O}_2^+$  (for detecting  $\text{NO}$ ). These reagent ions were generated by passing trace amounts of  $\text{SF}_6$  in  $\text{N}_2$ ,  $\text{CH}_3\text{I}$  in  $\text{N}_2$ , or  $\text{O}_2$  in  $\text{He}$  through a  $^{210}\text{Po}$  source to obtain  $\text{SF}_6^-$ ,  $\text{I}^-$ , or  $\text{O}_2^+$ , respectively. As CI is a “soft” ionization technique, a large fraction of the detected masses are from intact molecular ions with little or no fragmentation.<sup>106</sup> Concentrations of the gas-phase species of interest were calculated using their corresponding ionization rate constants with  $\text{SF}_6^-$ ,  $\text{I}^-$ , or  $\text{O}_2^+$ . Uncertainties in these calculated concentrations, based on uncertainties in the rate constants, are 30 – 50%.<sup>107</sup>

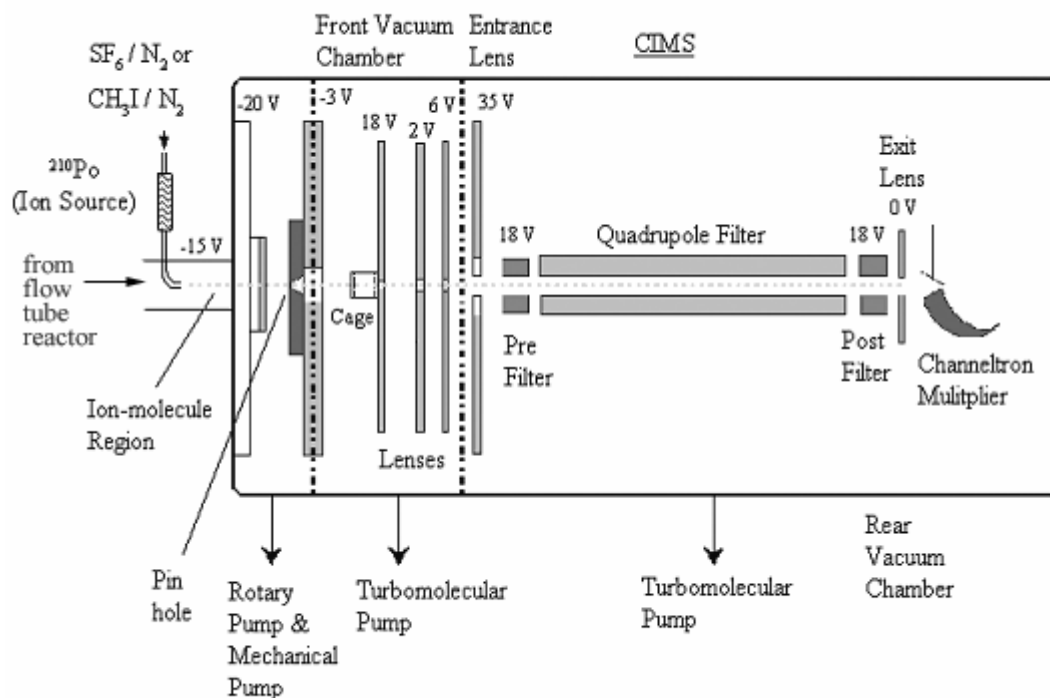


**Figure 5.1: Schematic drawing of the quadrupole mass spectrometer with chemical ionization region at the left-hand side.**

## 5.2 Coated Wall Flow Reactor

All exposures of organics to  $\text{NO}_3$ ,  $\text{N}_2\text{O}_5$ ,  $\text{NO}_2$ ,  $\text{HNO}_3$ , or  $\text{O}_3$  were performed in a coated wall flow reactor upstream of the CIMS. The apparatus used in this work was similar to the one previously used in our laboratory to study heterogeneous loss processes<sup>75</sup> and is depicted in Figure 5.2. The flow tube was constructed of borosilicate glass and included a movable injector through which the gas-phase reactant ( $\text{NO}_3$ ,  $\text{N}_2\text{O}_5$ ,  $\text{NO}_2$ ,  $\text{HNO}_3$ , or  $\text{O}_3$ ) was introduced. The specific setup depicted in Figure 5.2 shows the arrangement for  $\text{N}_2\text{O}_5$  or  $\text{NO}_3$  experiments. The flow tube was equipped with a cooling jacket through which a mixture of ethylene glycol and water could be circulated for temperature control (263 K – 303 K). The main carrier gas (He or He/ $\text{O}_2$  mix) was introduced through a port at the upstream end of the flow reactor. Typical total pressures in the flow reactor were 1.5 – 6 torr. The flow was laminar in all experiments based on the Reynolds number. Reynolds numbers were typically  $< 10$ , while the onset of

turbulent flow occurs at Reynolds numbers of about 2000 or more. Glass and stainless steel parts of the apparatus that were in contact with the gas-phase reactants were coated by an inert lubricant or halocarbon wax.

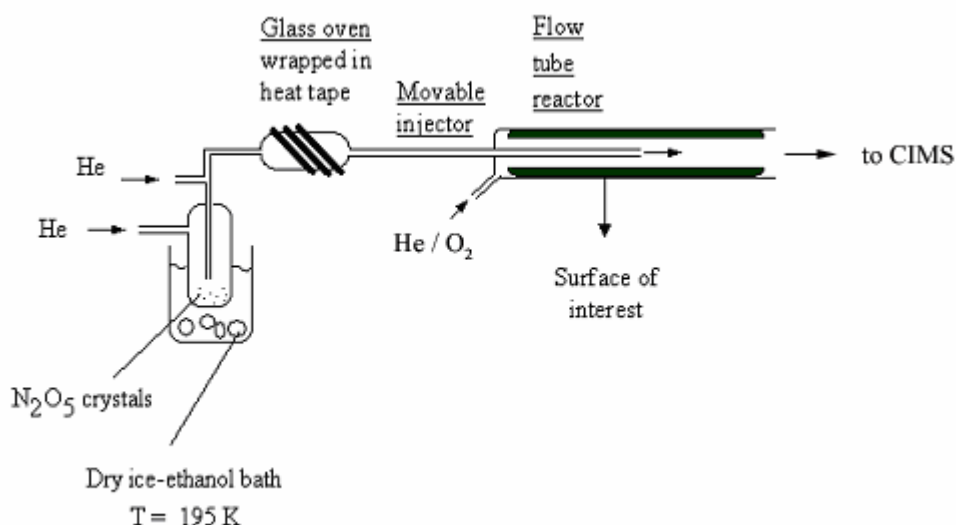


**Figure 5.2: Experimental setup for  $\text{N}_2\text{O}_5$  and  $\text{NO}_3$  experiments. Flow tube reactor with movable injector,  $\text{N}_2\text{O}_5$  glass trap, and oven for thermal conversion of  $\text{N}_2\text{O}_5$  to  $\text{NO}_3$ .**

For most experiments, the organic surfaces of interest were placed inside the flow reactor on the inner wall of a rotating Pyrex cylinder. The rotation assured even coverage of the whole cylinder surface and surface replenishment of the liquid films. The tip of the injector mentioned above could be positioned downstream of the organic surface (position of zero exposure) and was pushed upstream in order to expose the surfaces to either  $\text{NO}_3$ ,  $\text{N}_2\text{O}_5$ ,  $\text{NO}_2$ ,  $\text{HNO}_3$ , or  $\text{O}_3$ . As all the gases were being pumped toward the CIMS, backward diffusion of reactive gases (upstream of the injector tip) did not occur.

As mentioned above, the reactive uptake coefficient ( $\gamma$ ), a parameter often used to describe a heterogeneous process, is defined as the fraction of collisions with a surface that lead to reactive loss of a gas-phase species. In the following chapters,  $\gamma$  is calculated from the irreversible removal of the gas-phase species as a function of reaction time. The reaction time is calculated from the flow velocity in the flow reactor and the position of the movable injector relative to “zero” (i.e. no organics exposed). The slope of a plot of

the natural logarithm of the relative CIMS signal of the gas versus the reaction time was used to obtain the observed first-order loss rate,  $k_{\text{obs}}$ . Examples for this plot using sample data sets are shown in Figures 6.3 and 7.2. This loss rate  $k_{\text{obs}}$  was corrected for concentration gradients due to reactive uptake close to the flow-tube wall<sup>108</sup> which gave the wall-loss rate,  $k_{\text{wall}}$ .  $k_{\text{wall}}$  was then used to calculate  $\gamma$  by a standard procedure, given in equation 5.1.<sup>75</sup>

$$5.1 \quad \gamma = \frac{2rk_{\text{wall}}}{c_{\text{avg}} + rk_{\text{wall}}}$$

In this equation,  $r$  is the flow tube radius and  $c_{\text{avg}}$  is the mean thermal molecular velocity of the gas-phase species. This procedure assumes that the surface area available for reaction is equal to the geometric surface area of the Pyrex tube. The gas-phase diffusion coefficients of  $\text{NO}_3$  reported by Rudich et al.<sup>109</sup> were used when correcting for concentration gradients. When measuring  $\gamma$ , the total exposure time of the surface to the gas-phase reactants was kept short and the concentrations of gas-phase reactants were kept small to minimize oxidation of the surface.

The flow tube technique utilized in this research is typically capable of measuring reactive uptake coefficients greater than  $10^{-6}$ . However, for our flow rates and pressures, reactive uptake coefficients greater than approximately 0.1 were significantly influenced by gas-phase diffusion to the reactive surface. In these cases, the reaction was so fast that diffusion became a limiting factor and a small uncertainty in  $k_{\text{obs}}$  or in the diffusion coefficient resulted in a large uncertainty in the reactive uptake coefficients. For this reason, when the reactive uptake coefficient was greater than approximately 0.1, it was only possible to report a lower limit.

### 5.3 X-Ray Photoelectron Spectroscopy (XPS)

X-ray photoelectron spectroscopy (XPS) is a technique used to determine the chemical composition of a sample surface. Elements present on (and in) the sample are identified due to the different binding energies of their core electrons. These electron binding energies can be used as a fingerprint for the different elements present in the sample. The higher the nuclear charge of an atom the higher the binding energy of a

given core level (e.g. the binding energy for an O(1s) level will be greater than that for a C(1s)).<sup>110</sup> Additionally, slight shifts in the binding energy are characteristic of different functional groups. For example a carbon atom, when bound to a more electronegative atom (O, N, F, Cl) will have a lower valence electronic density and so the repulsion experienced by electrons in inner shells will be lower. This leads to a higher binding energy.<sup>111</sup> For example, each bond with an oxygen atom induces a shift of the binding energy of the C(1s) electrons of approximately + 1.5 eV.<sup>112</sup> Therefore, XPS is capable of determining not only the identity of the elements present at the surface of a sample, but also their chemical state.<sup>113</sup> Detection limits for elements are in the range of 0.1 – 1 atomic%.<sup>114,115</sup>

XPS is based on the photoelectric effect which was explained by Einstein: “photons can induce electron emission from a solid provided the photon energy is greater than the work function”.<sup>116</sup>

The technique uses photons to eject core level electrons. Photons of a known energy are emitted from an X-ray source and hit the surface of interest. Surface atoms then emit core shell electrons and an energy analyzer determines the kinetic energy of these electrons. The binding energy of the electrons can then be calculated using the following equation 5.2.<sup>116</sup>

$$5.2 \quad E_B = h\nu - E_K - \Phi$$

where  $E_B$  is the binding energy of the electron,  $h\nu$  is the energy of the impinging photon,  $E_K$  is the kinetic energy of the ejected electron ( $= \frac{1}{2} m v_e^2$ ,  $m$  = photoelectron mass,  $v_e$  = velocity of electron), and  $\Phi$  is the work function of the emitting material. The binding energy of a core level electron is measured with respect to the highest occupied level of the solid, the Fermi level. The work function  $\Phi$  is defined as the minimum energy required to remove an electron from the highest occupied energy level in the solid to ‘vacuum level’ (this term refers to the energy of an electron at rest in a vacuum far removed from neighbouring particles). For many samples it is in the range of 5 eV.

While the penetration depth of the X-ray beam (which is equal to the mean free path of the photons) is relatively deep ( $\sim 1 \mu\text{m}$ ), the depth of the sample actually analysed is much shallower. Most electrons emitted from atoms at a depth of approximately 10 nm or greater are incapable of reaching the sample surface and are therefore not detected in



the hemispherical energy analyzer.<sup>112</sup> However, some of them are detected as background signal, as they have lost some but not all of their kinetic energy.

XPS measurements are performed under ultra high vacuum to remove adsorbed gases from the sample, eliminate adsorption of contaminants on the sample, prevent arcing and high voltage breakdown, and increase the mean free path for electrons and photons.

XPS measurements reported in this thesis were performed using an achromatic Al K $\alpha$  X-ray source at a photon energy of 1486.6 eV and an electron take-off angle of 90°.

## **5.4 Time-of-Flight Secondary Ion Mass Spectrometry (ToF-SIMS)**

Time-of-flight secondary ion mass spectrometry (ToF-SIMS) is a qualitative and semi-quantitative method used to determine the chemical composition of a surface.<sup>117</sup> While XPS can only supply information on overall elemental composition and oxidation states, ToF-SIMS can provide more structural information on the molecules present. In ToF-SIMS the surface is bombarded with ions (the so called primary ions) in the energy range of 0.5 - 15 keV. Upon ion bombardment, surface molecules are sputtered into vacuum and the primary bombarding particles are implanted into the condensed phase.<sup>117</sup> The mass spectra of sputtered ions (either positively or negatively charged) from the sample (so called secondary ions) are analysed in a time-of-flight mass spectrometer. The characteristic that governs the yield of negative ions is generally the electron affinity of the sample molecules.<sup>118</sup>

For ToF analysis secondary ion beams are generated in short pulses. In ToF-MS, a voltage applied to a grid accelerates the secondary ions to a certain kinetic energy. The ions are expelled into a drift tube and their time of flight in this field free region is determined.<sup>119</sup> The time of flight is used to calculate the velocity of the ions, which leads to the determination of the mass to charge ( $m/z$ ) ratio when the kinetic energy is known. ToF-MS is usually preferred for SIMS as it has the advantage of very high ion transmission that is constant over the whole mass range with a typical overall transmission of some 10%. The sensitivity factor is much higher (up to a factor of  $10^5$ ) than for quadrupole MS.<sup>117</sup>

If measurements are performed in “static SIMS” mode, there is virtually no disturbance of the composition and structure of the uppermost layer of the sample. Due to the very low primary ion current density (i.e. the flux onto the sample surface,  $10^{-9} \text{ A cm}^{-2}$ ), the lifetime of a monolayer is usually on the order of hours. Therefore, in static SIMS, second-order effects are avoided. This means that the intensity of the primary ion beam is so low that virtually no surface molecule is hit twice. This ensures that the secondary ions come from previously unaffected areas.<sup>117</sup>

The ToF-SIMS measurements reported in this thesis were performed using a Physical Electronics, PHI TRIFT II ToF-SIMS instrument with a 15 keV  $\text{Ga}^+$  primary ion beam. The pulse duration was 5 ns with a current of 500 pA. Sample areas of  $100 \times 100 \mu\text{m}^2$  were irradiated, total MS acquisition time was 10 min and negative ion spectra were obtained. The total ion dose was well below static limit, i.e. all experiments were performed in static SIMS mode.  $\text{Ga}^+$  primary ions were obtained from a liquid metal ion source which was exposed to a high electrostatic field.

## 6 REACTIVE UPTAKE OF $\text{NO}_3$ , $\text{N}_2\text{O}_5$ , $\text{NO}_2$ , $\text{HNO}_3$ , AND $\text{O}_3$ ON THREE TYPES OF POLYCYCLIC AROMATIC HYDROCARBON SURFACES

### 6.1 Introduction

Polycyclic aromatic hydrocarbons (PAHs) are observed in environmental samples worldwide. Their occurrence in the atmosphere constitutes a health risk to the population due to their allergenic, mutagenic, and carcinogenic properties. Sources of PAHs are incomplete combustion processes as mentioned in Chapter 1.<sup>1</sup> Understanding the lifetime and fate of PAHs in the atmosphere is important for health risk assessments.

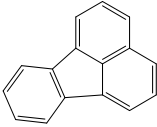
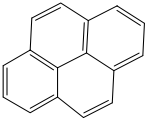
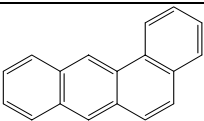
As PAHs have a wide range of vapour pressures,<sup>1</sup> they are found both in the gas phase as well as on and in atmospheric particulate matter. PAHs with 3 or 4 rings are semi-volatile and observed both in the gas phase and adsorbed to particles. Additionally, aromatic compounds can also contribute to surface coatings on urban surfaces where aromatics account for ~ 20% of the organic carbon mass of “urban grime” on buildings, windows etc.<sup>120,121</sup> The fact that significant portions or the entirety of a PAH of higher molecular weight is found in the condensed phase shows that it is necessary to investigate not only gas-phase reactions of PAH molecules, but also to study reactions between atmospheric oxidants and PAHs adsorbed on or in aerosol particles and urban surfaces. Reactions between gas-phase oxidants and surface-bound PAHs may be an important loss process of PAHs in the atmosphere and a source of even more toxic and mutagenic PAH derivatives, i.e. nitro-PAHs.<sup>1,11</sup> Nitro-PAHs are PAH derivatives that are either directly emitted from fossil fuel combustion or formed by atmospheric reactions in the gas phase or heterogeneously. Their concentrations are low, but they are up to 100,000 times more mutagenic and 10 times more carcinogenic than unsubstituted PAHs.<sup>11</sup>

Until now most scientific work on PAHs has focused on gas-phase homogeneous chemistry, with only a limited amount of work reported on heterogeneous reactions.

However, the available data on heterogeneous chemistry suggests that, in general, heterogeneous reactions can differ dramatically from homogeneous reactions in the observed rates, mechanisms, and products.<sup>1,46,47,122,123</sup> Heterogeneous reactions between condensed-phase PAHs and the following gas-phase oxidants have been explored: OH,<sup>67,72,124</sup> NO,<sup>72</sup> NO<sub>2</sub>,<sup>35,72,124-128</sup> O<sub>3</sub>,<sup>123,129-134</sup> HNO<sub>3</sub>,<sup>135</sup> N<sub>2</sub>O<sub>5</sub>,<sup>87,98</sup> and NO<sub>3</sub>.<sup>98</sup> In a number of these studies reactive uptake coefficients ( $\gamma$ ), a parameter often used to describe a heterogeneous process, were not determined. Studies that focus on determining  $\gamma$  for the atmospheric oxidants mentioned above on a range of PAH surfaces would therefore be beneficial. Heterogeneous reactions between NO<sub>3</sub> and PAHs and N<sub>2</sub>O<sub>5</sub> and PAHs are two reactions that are especially in need of further study. The reactive uptake coefficients of N<sub>2</sub>O<sub>5</sub> and NO<sub>3</sub> on PAH surfaces have not been previously determined.

To add to the relatively short list of studies on heterogeneous reactions between gas-phase oxidants and surface-bound PAHs, we have investigated the reactive uptake coefficients of NO<sub>3</sub>, N<sub>2</sub>O<sub>5</sub>, NO<sub>2</sub>, HNO<sub>3</sub>, and O<sub>3</sub> on three types of solid PAH surfaces using a coated wall flow tube reactor. The PAH surfaces that we studied were composed of pyrene (PYR), benz[a]anthracene (BEN), or fluoranthene (FLU), all of which are 4-ring systems with vapour pressures between  $9.2 \times 10^{-6}$  and  $2.1 \times 10^{-7}$  torr at 298 K (see Table 6.1). These PAHs are typically distributed between gas and particle phase more or less equally in the atmosphere (depending on ambient conditions).<sup>1</sup> Understanding heterogeneous reactions on solid PAH surfaces is a first step toward understanding heterogeneous reactions of PAHs adsorbed on or in aerosol particles.

**Table 6.1: Polycyclic aromatic hydrocarbons studied, their molecular structures, molecular weights, melting points, vapour pressures, and typical tropospheric concentrations.**

PAH	molecular structure	molecular weight [g mol <sup>-1</sup> ]	melting point [°C]	vapour pressure at 298 K [torr]	atmospheric concentration [ng m <sup>-3</sup> ]
Fluoranthene		202.3	111	$9.2 \times 10^{-6}$	2.8 – 12.4
Pyrene		202.3	156	$4.5 \times 10^{-6}$	0.54 – 38
Benz[a]anthracene		228.3	160	$2.1 \times 10^{-7}$	0.25 – 5.59

Experiments consisted of measuring the reactive uptake coefficient of the gas-phase oxidants on “fresh” (i.e. unreacted) PAH surfaces by monitoring the decay of the gas-phase reactants. Most of the previous studies monitored the loss of the PAH material. Therefore, our studies are complimentary to many of the previous studies of PAH heterogeneous chemistry. Since we studied the loss of a range of different atmospheric oxidants on the same PAH surfaces, a direct comparison between the oxidants was possible.

For the NO<sub>3</sub> heterogeneous reaction, we also investigated NO<sub>3</sub> uptake as a function of time to determine if this reaction was catalytic (i.e. a reaction takes place at the surface but the surface is not an active participant) or if the reaction rate decreased with time due to oxidation of the surface-bound PAH molecules. This information is needed for extrapolating laboratory results to the atmosphere. The time dependence of the NO<sub>3</sub> uptake on PAH surfaces has not been investigated in previous studies.

Additionally, we carried out preliminary gas-phase product studies for the reaction of NO<sub>3</sub> with pyrene at room temperature to aid in the understanding of the reaction mechanism.

## 6.2 Experimental

### 6.2.1 Experimental Setup and Procedure

The apparatus used in this work consisted of a coated wall flow tube reactor coupled to a chemical ionization mass spectrometer (CIMS) as described in Chapter 5. The inside wall of a Pyrex tube (1.75 cm inside diameter and 11 - 15 cm in length) was coated with the PAH film and then inserted into the flow tube reactor. These coatings provided the surfaces for the heterogeneous studies. Total pressure in the flow reactor was 1.5 – 4.1 torr. Reagent gases for chemical ionization were  $\text{SF}_6^-$  (for detecting  $\text{N}_2\text{O}_5$ ,  $\text{NO}_3$ ,  $\text{NO}_2$ ,  $\text{HNO}_3$ ,  $\text{O}_3$ , and  $\text{HONO}$ ),  $\text{I}^-$  (for detecting  $\text{NO}_3$ ), and  $\text{O}_2^+$  (for detecting  $\text{NO}$ ). Concentrations of the gas-phase oxidants used in our studies were  $(0.8 - 5.7) \times 10^{12}$  molecule  $\text{cm}^{-3}$  for  $\text{N}_2\text{O}_5$ ,  $(0.3 - 3.7) \times 10^{11}$  molecule  $\text{cm}^{-3}$  for  $\text{NO}_3$ ,  $(2.0 - 9.6) \times 10^{13}$  molecule  $\text{cm}^{-3}$  for  $\text{O}_3$ ,  $(0.17 - 4.9) \times 10^{12}$  molecule  $\text{cm}^{-3}$  for  $\text{HNO}_3$ , and  $(4.4 - 6.4) \times 10^{13}$  molecule  $\text{cm}^{-3}$  for  $\text{NO}_2$ . These concentrations were calculated using the corresponding rate constants of these species with  $\text{SF}_6^-$  or  $\text{I}^-$ . Uncertainties in these calculated concentrations, based on uncertainties in the rate constants, are 30 – 50%.<sup>107</sup>

Three different types of experiments were carried out. The first set of experiments involved measuring the reactive uptake coefficients of  $\text{NO}_3$ ,  $\text{NO}_2$ ,  $\text{N}_2\text{O}_5$ ,  $\text{O}_3$ , and  $\text{HNO}_3$  on “fresh” PAH surfaces at 273 K and at room temperature. We refer to the reactive uptake coefficient on “fresh” (or unreacted) surfaces as the initial reactive uptake coefficient ( $\gamma_0$ ), and we refer to these experiments as *measurements of the initial reactive uptake coefficients*. The gas-phase reactant entered the flow cell through the injector and moving the injector upstream exposed more and more of the PAH films to the gas-phase reactant, while pushing it downstream terminated the reaction. The initial reactive uptake coefficients  $\gamma_0$  were determined from the irreversible removal of the gas-phase species as a function of injector position (and therefore reaction time). The slope of a plot of the natural logarithm of the gas CIMS signal versus the injector position was used to obtain the observed first-order loss rate,  $k_{\text{obs}}$ . This loss rate was corrected for concentration gradients close to the flow-tube wall<sup>108</sup> and was then used to calculate  $\gamma_0$  using a standard procedure.<sup>75</sup> This procedure assumes that the surface area available for reaction is equal

to the geometric surface area of the Pyrex tube. Below we show that this is a reasonable approximation.

The second set of experiments involved investigating the time dependence of the NO<sub>3</sub> reactive uptake to determine if this reaction was catalytic or if the reaction rate decreased with exposure time due to oxidation of the surface. We refer to these experiments as *processing studies*. For these measurements the tip of the injector was initially positioned at the front of the flow cell so the surface was not exposed to NO<sub>3</sub> radicals, and then a flow of NO<sub>3</sub> was established. Next the injector was quickly withdrawn 5 cm so that the PAH surface was exposed to NO<sub>3</sub>. The signal of NO<sub>3</sub> was then monitored for an extended period of time (60 min) to determine if the surface was deactivated or processed from prolonged exposure to NO<sub>3</sub>. In contrast to experiments determining  $\gamma_0$ , these experiments were conducted in the presence of O<sub>2</sub> ((0.95 – 2.1) × 10<sup>16</sup> molecule cm<sup>-3</sup>) to better mimic atmospheric conditions.

The third set of experiments involved the measurements of gas-phase products for the reaction between NO<sub>3</sub> and pyrene at 297 ± 1 K. We refer to these experiments as *gas-phase product studies*. For these studies, the release of NO<sub>2</sub>, HNO<sub>3</sub>, HONO, and NO to the gas phase during a 60 min NO<sub>3</sub> uptake experiment on pyrene was monitored with CIMS. The general procedure was identical to the second set of experiments, but instead of monitoring the NO<sub>3</sub> signal, the CIMS signal of a possible gas-phase reaction product (NO<sub>2</sub>, HNO<sub>3</sub>, HONO, or NO) was monitored at its respective m/z during 60 minutes of NO<sub>3</sub> exposure.

### 6.2.2 Chemicals

Pyrene (purity 95%), benz[a]anthracene (99%), and fluoranthene (99%) were purchased from Sigma-Aldrich and used without further purification. NO<sub>2</sub> (99.5%) was purchased from Matheson, N<sub>2</sub> (99.999%), O<sub>2</sub> (99.993%), and He (99.999%) were purchased from Praxair. Gas-phase nitric acid was produced by flowing He over an aqueous solution containing nitric acid and sulphuric acid at ~ 197 K. This solution was prepared by combining an aqueous solution of nitric acid (69% wt %, Fisher Scientific) and sulphuric acid (96% wt %, Fisher Scientific) in a 3:1 ratio by volume.<sup>136</sup> Ozone was generated by passing O<sub>2</sub> through an ultraviolet light source. N<sub>2</sub>O<sub>5</sub> was generated by

reacting  $\text{NO}_2$  with an excess amount of  $\text{O}_3$  in a flow system as described by Schott and Davidson<sup>137</sup> and Cosman et al.<sup>51</sup> The solid  $\text{N}_2\text{O}_5$  crystals were stored at 197 K.  $\text{NO}_3$  radicals were obtained by thermal conversion of gaseous  $\text{N}_2\text{O}_5$  to  $\text{NO}_3$  and  $\text{NO}_2$  at 430 K in a Teflon coated glass oven.

### **6.2.3 Preparation and Characterization of the PAH Films**

Solid PAH films were prepared by first distributing solid PAH powder on the inner wall of glass cylinders with an inner diameter of 1.75 cm (for experiments in the flow reactor) or on planar glass slides (for film characterization using scanning electron microscopy (SEM) and profilometry). The glass cylinders or slides were then heated on a hotplate under a small flow of ultra high purity  $\text{N}_2$  to a temperature just above the melting point of the corresponding PAH material (see Table 6.1). Rotation of the cylinder ensured even distribution of the molten PAH. The PAHs rapidly crystallized upon cooling, resulting in a relatively smooth film, as discussed below. This resulted in films of approximately 0.5 mm thickness. To test whether the reactive uptake coefficient depended on the method of film preparation, we also prepared some pyrene films by dissolving pyrene in xylene, then this solution was applied to the inside walls of the glass cylinder, and the solvent was allowed to evaporate, leaving behind a coating of pyrene.

To characterize the PAH surfaces, we recorded images of PAH films using SEM, and we measured the roughness using profilometry. The SEM and profilometry measurements were performed using glass slides rather than Pyrex tubes. However, the slides were prepared using the same techniques that were used to prepare the glass cylinders. SEM pictures of PAH films (coated with gold) were obtained using a Hitachi S-3000N scanning electron microscope and profilometer scans were taken with a Tencor alpha-step 200 profilometer.

## **6.3 Results and Discussion**

### **6.3.1 Surface Properties of PAH Films**

As mentioned above, to assess the surface properties of the PAH films, SEM and profilometer measurements were conducted. The electron microscope images (see Figure



6.1) confirmed that the PAH films were relatively smooth (i.e. close to the geometric surface area of the glass), nonporous, and completely covered the glass substrate.

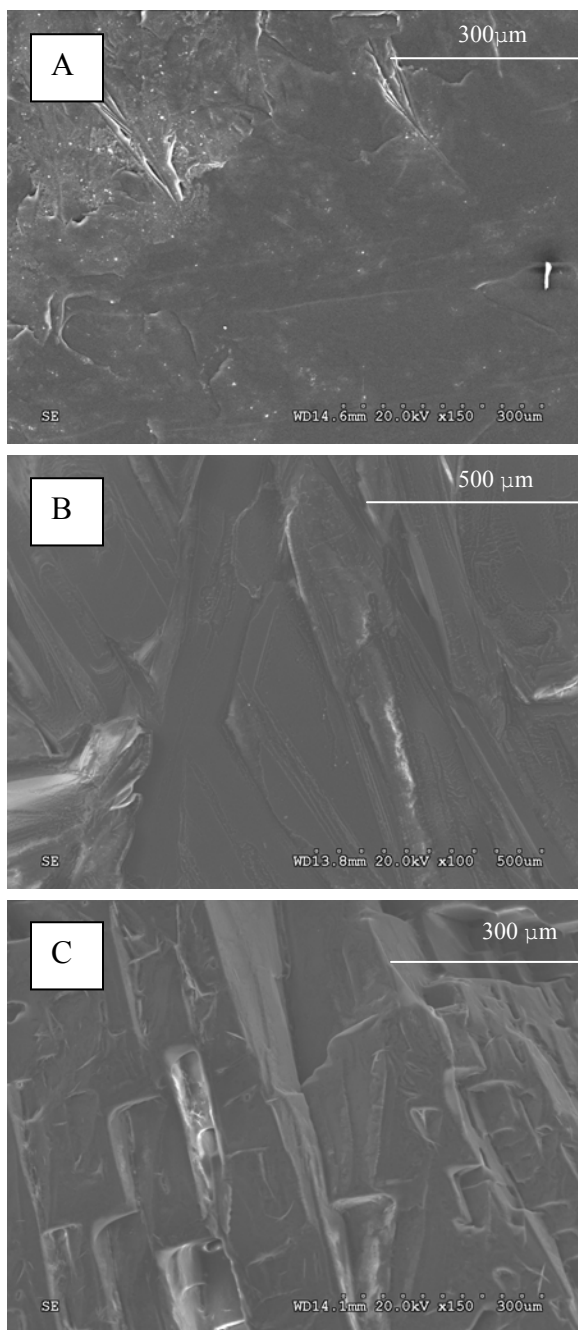


**Figure 6.1: Scanning electron microscope images of solid PAH surfaces (A: benz[a]anthracene, B: fluoranthene, C: pyrene).**

The profilometer measurements indicated that the surface area of these films deviated from the surface area of the glass substrate by a maximum of 2%, indicating the

films were smooth. Therefore, when calculating  $\gamma_0$  we assumed the surface area available for heterogeneous reactions was equal to the geometric surface area of the Pyrex tubes as discussed above. However, we cannot rule out the presence of small steps and cracks on the surfaces which may have been preferred sites for reaction and may have increased the total surface area.

### **6.3.2 Measurements of the Initial Reactive Uptake Coefficients for $\text{NO}_3$**

As mentioned above, the reactive uptake coefficients on “fresh” surfaces were determined from the irreversible removal of the gas-phase species as a function of injector position. Shown in Figure 6.2 is an example of the raw data from a typical measurement with  $\text{NO}_3$ . This plot shows that  $\text{NO}_3$  interacted strongly with the PAH surface and also that the loss of the  $\text{NO}_3$  signal was irreversible. If the uptake had been reversible, we would have expected the signal to increase to more than its original intensity when the injector was pushed back to “0” at the end of the experiment. As no  $\text{NO}_3$  was released from the surface after the reaction was stopped, the uptake was irreversible. An example of (partially) reversible uptake is given in Figure 6.4.

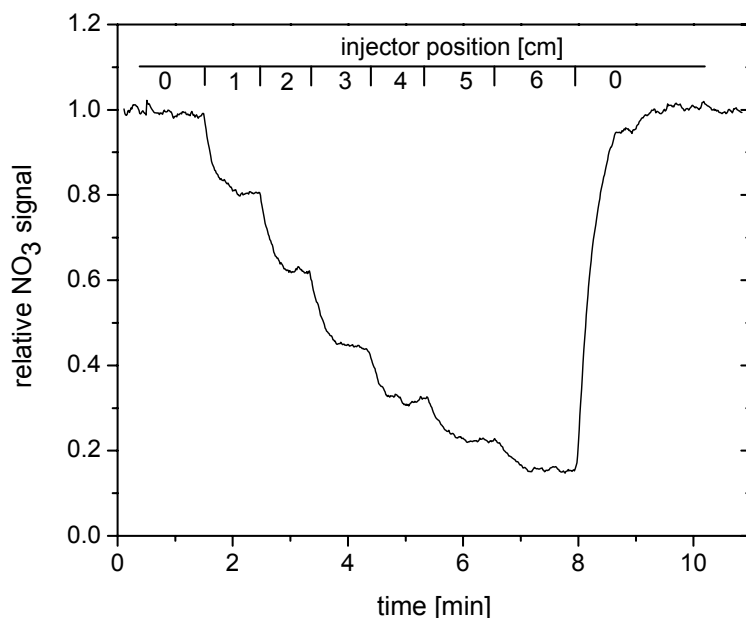


**Figure 6.2:**  $\text{NO}_3$  signal as a function of time for a typical uptake experiment of  $\text{NO}_3$  on fluoranthene at 273 K. Each step down corresponds to an increase of the reactive surface (i.e. the injector is pulled back in 1 cm increments). At the end, the signal recovers as the injector is pushed back to its original position (“0” position, no exposure). Scale within the graph corresponds to the positions of the  $\text{NO}_3$  injector during the different steps of the experiment.

A typical plot for the natural logarithm of the normalized  $\text{NO}_3$  signal versus injector position for PYR is shown in Figure 6.3. The slope of this plot was then used to calculate  $\gamma_0$ . Listed in Tables 6.2 and 6.3 are the  $\gamma_0$  values for  $\text{NO}_3$  on PYR, FLU and BEN obtained at 273 K and room temperature. The reported uncertainties include a 7.2% uncertainty in the diffusion coefficient of  $\text{NO}_3$  in helium.<sup>109</sup> The data in Tables 6.2 and 6.3 show that the reactive uptake coefficient of  $\text{NO}_3$  on all three PAHs is large, and that the temperature dependence of the uptake coefficient over the range of 273 - 298 K is small.

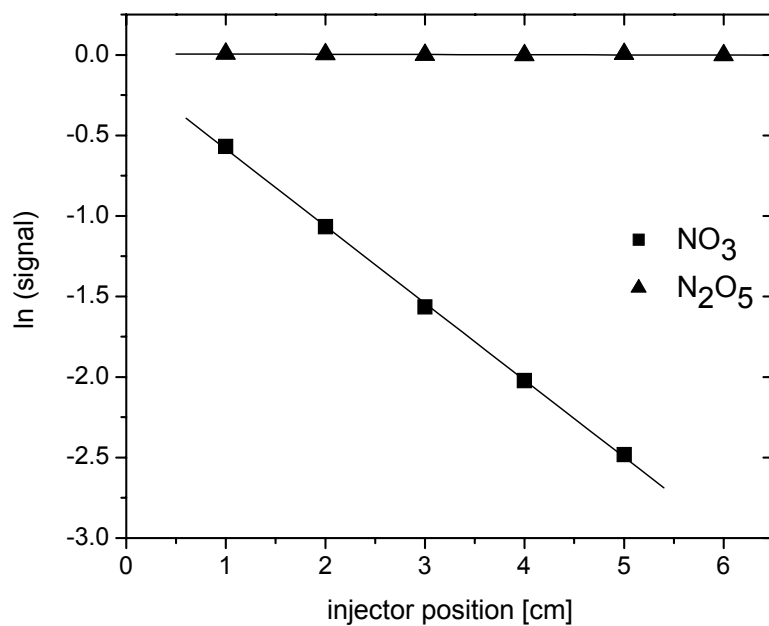


**Figure 6.3:** Plot of the natural logarithm of the CIMS signals vs. the injector position for  $\text{NO}_3$  and  $\text{N}_2\text{O}_5$  during typical experiments on pyrene solid surfaces at 273 K.

**Table 6.2: Results of the uptake experiments at 273 K. Uptake coefficients of N<sub>2</sub>O<sub>5</sub>, NO<sub>2</sub>, HNO<sub>3</sub>, and O<sub>3</sub> are reported as upper limits. Uptake coefficients of NO<sub>3</sub> on PAHs reported with upper limit of 1 indicate that these experiments were diffusion limited.**

	[oxidant] <sub>atm</sub> <sup>a</sup>	reactive uptake coefficient $\gamma_0$			$\gamma_0 \times [\text{oxidant}]_{\text{atm}}/\text{molecule cm}^{-3}$	$\tau_{\text{atm}}$ <sup>b</sup>
		BEN	FLU	PYR	PYR	PYR
NO <sub>3</sub>	50 ppt	0.059 <sup>+ 0.11</sup> - 0.049	0.52 <sup>+ 0.48</sup> - 0.45	0.38 <sup>+ 0.62</sup> - 0.30	$\geq 4.8 \times 10^8$	$\leq 28$ sec
N <sub>2</sub> O <sub>5</sub>	10,000 ppt	$\leq 2.1 \times 10^{-6}$	$\leq 8.7 \times 10^{-6}$	$\leq 4.9 \times 10^{-6}$	$\leq 1.2 \times 10^6$	$\geq 4$ h
NO <sub>2</sub>	100,000 ppt	$\leq 1.0 \times 10^{-6}$	$\leq 4.5 \times 10^{-7}$	$\leq 5.7 \times 10^{-7}$	$\leq 1.4 \times 10^6$	$\geq 2.2$ h
HNO <sub>3</sub>	10,000 ppt	$\leq 2.4 \times 10^{-5}$	$(8.6 \pm 2.3) \times 10^{-6}$	$\leq 2.7 \times 10^{-5}$	$\leq 6.8 \times 10^6$	$\geq 32$ min
O <sub>3</sub>	100,000 ppt	$\leq 1.6 \times 10^{-6}$	$\leq 5.7 \times 10^{-7}$	$\leq 9.7 \times 10^{-7}$	$\leq 2.4 \times 10^6$	$\geq 1.3$ h

<sup>a</sup> typical atmospheric concentration; converted into total molecules cm<sup>-3</sup> for calculations in last two columns<sup>1</sup>

<sup>b</sup> atmospheric lifetime of pyrene at an oxidant concentration equal to the concentration given in column [oxidant]

**Table 6.3: Results of the uptake experiments at 293 – 297 K. See Table 2 for explanations. n.d.= not determined.**

	[oxidant] <sub>atm</sub> <sup>a</sup>	reactive uptake coefficient $\gamma_0$			$\gamma_0 \times [\text{oxidant}]_{\text{atm}}/\text{molecule cm}^{-3}$	$\tau_{\text{atm}}$ <sup>b</sup>
		BEN	FLU	PYR	PYR	PYR
NO <sub>3</sub>	50 ppt	0.13 <sup>+ 0.53</sup> - 0.096	0.087 <sup>+ 0.28</sup> - 0.063	0.79 <sup>+ 0.21</sup> - 0.67	$\geq 9.9 \times 10^8$	$\leq 13$ sec
N <sub>2</sub> O <sub>5</sub>	10,000 ppt	$\leq 5.7 \times 10^{-6}$	$\leq 8.5 \times 10^{-6}$	$\leq 4.1 \times 10^{-6}$	$\leq 1.0 \times 10^6$	$\geq 4.6$ h
NO <sub>2</sub>	100,000 ppt	n.d.	n.d.	$\leq 1.0 \times 10^{-6}$	$\leq 2.5 \times 10^6$	$\geq 1.2$ h
HNO <sub>3</sub>	10,000 ppt	n.d.	n.d.	$\leq 6.6 \times 10^{-5}$	$\leq 1.7 \times 10^7$	$\geq 13$ min
O <sub>3</sub>	100,000 ppt	n.d.	n.d.	$\leq 7.6 \times 10^{-7}$	$\leq 1.9 \times 10^6$	$\geq 1.6$ h

Note that the PAHs investigated in our study have very low vapour pressures and that the homogeneous reaction of PAHs with NO<sub>3</sub> in the gas phase is slow. Hence, the gas-phase reaction between NO<sub>3</sub> and PAHs did not influence our heterogeneous studies. Specifically, the gas-phase reaction will contribute less than 1% to the total loss of NO<sub>3</sub> in our experiments, based on saturated vapour pressures of the PAH material and the rate coefficients for the gas-phase NO<sub>3</sub>-PAH homogeneous reactions.<sup>1</sup>

We have also carried out some tests to determine if the method of preparing the films or the presence of O<sub>2</sub> in the flow reactor influenced the reactive uptake coefficients. Within the uncertainty of our measurements, the reactive uptake coefficient of NO<sub>3</sub> on pyrene did not depend on the presence of O<sub>2</sub> in the flow reactor at room temperature. Also, within the uncertainty of our measurements, the reactive uptake coefficient measured at 273 K for NO<sub>3</sub> was the same on pyrene surfaces prepared by melting pyrene crystals and on pyrene surfaces prepared by dissolving pyrene crystals in xylene and then coating the Pyrex tubes with the resulting solution. In short, the reactive uptake coefficients appeared to be independent of both the method of preparing the films and the presence of O<sub>2</sub> in the flow reactor.

To compare the rate of the reaction between NO<sub>3</sub> and pyrene on a surface with the same reaction in the gas phase, we calculated an enhancement factor for the surface reaction, similar to Moise and Rudich.<sup>46</sup> The enhancement factor is defined as the following:

$$6.1 \quad R = \frac{\text{surface reaction probability}}{\text{gas phase reaction probability}} = \frac{\gamma}{k_{\text{gas-phase}} / 10^{-10}}$$

The gas-phase reaction rate for NO<sub>3</sub>,  $k_{\text{gas-phase}}$  depends on NO<sub>2</sub> concentrations.<sup>1,41</sup> Using a NO<sub>2</sub> concentration of 10 ppb,  $k_{\text{gas-phase}}$  for NO<sub>3</sub> with PYR and FLU is  $4 \times 10^{-16}$  and  $1 \times 10^{-16}$  cm<sup>3</sup> molecule<sup>-1</sup> s<sup>-1</sup> at room temperature, respectively.<sup>1,41</sup> Using these values and our measured reactive uptake coefficients from Table 6.3 in eq 6.1, we obtain R-values for room temperature of  $2 \times 10^5$  and  $9 \times 10^4$  for PYR and FLU, respectively. This suggests that the surface reaction is enhanced by approximately 5 orders of magnitude. Enhancement of reactions on surfaces compared to their analogous gas-phase reactions has also been observed previously. For O<sub>3</sub> with aliphatic unsaturated surfaces enhancement factors ranging from 10 – 10<sup>3</sup> have been observed.<sup>46,47</sup> Also, for O(<sup>3</sup>P) with

aliphatic saturated surfaces, Br with aliphatic saturated surfaces, and NO<sub>3</sub> on aliphatic surfaces enhancement factors of 10<sup>3</sup>, 10<sup>4</sup>, and 100 have been observed, respectively.<sup>46</sup> Possible explanations of these results are longer residence times of the gas-phase species at a surface compared to a homogeneous encounter in the gas phase, a lowering of the activation energy barrier of the reaction, or a new reaction channel on the surface that is inaccessible in the gas phase.<sup>46,47,138,139</sup> More research is needed to better understand these drastic enhancement factors.

As mentioned in Chapter 6.1, in many previous heterogeneous studies with PAHs, the reactive uptake coefficient was not determined. Rather, the time to react away a fraction of the surface-bound PAH molecules was determined. To compare our results with these previous measurements, we converted both our measurements and the previous measurements (when  $\gamma$  was not determined) into an atmospheric lifetime with respect to heterogeneous chemistry,  $\tau_{atm}$ . This lifetime is defined as the time in which 63% of the molecules react, and can be thought of as the processing time of a surface-bound PAH molecule. To convert our measurements into an atmospheric lifetime we used the following equation:<sup>46</sup>

$$6.2 \quad \tau_{atm} = \frac{4N_{tot}}{\gamma_0 c_{avg} [\text{oxidant}]_{atm}}$$

where  $N_{tot}$  is the surface concentration of PAH molecules (molecule cm<sup>-2</sup>),  $c_{avg}$  is the mean thermal velocity (cm s<sup>-1</sup>) and  $[\text{oxidant}]_{atm}$  is the typical concentration of the gas-phase oxidants in the atmosphere (molecule cm<sup>-3</sup>). To translate our measured  $\gamma_0$  into  $\tau_{atm}$  we used a surface density of  $1 \times 10^{14}$  reactive sites cm<sup>-2</sup> which is consistent with numbers in the literature.<sup>130</sup> The values for  $[\text{oxidant}]_{atm}$  used in these calculations are listed in Tables 6.2 and 6.3. To convert the previous laboratory studies, where the decay of surface-bound PAH molecules were monitored into  $\tau_{atm}$  we used the following equation:

$$6.3 \quad \tau_{atm} = \tau_{lab} \frac{[\text{oxidant}]_{lab}}{[\text{oxidant}]_{atm}}$$

where  $\tau_{lab}$  is the average lifetime of surface-bound PAH species determined in the laboratory. In cases where  $\tau_{lab}$  was not mentioned we estimated this value based on the reported experimental data.  $[\text{oxidant}]_{lab}$  is the concentration of the gas-phase oxidant used in the laboratory experiments. This equation assumes the lifetime of surface-bound PAH

species is linear with the concentration of the gas-phase oxidant over the extrapolation range.

More than 20 years ago in a pioneering study, Pitts et al.<sup>98</sup> investigated the reaction of NO<sub>3</sub> with pyrene and perylene adsorbed on glass fibre filters in an environmental chamber. In these experiments, the amount of PAH material used resulted in less than a monolayer coverage on the filters. The authors monitored the decay of the PAH material rather than the loss of NO<sub>3</sub>, and an NO<sub>3</sub> concentration of approximately  $2.5 \times 10^{11}$  molecule cm<sup>-3</sup> was used. Under these conditions, the authors concluded that neither adsorbed pyrene nor perylene reacted to any observable extent with the NO<sub>3</sub> radical over a time period of 50 minutes. Based on these values and eq 6.3, we calculate an atmospheric lifetime  $\tau_{\text{atm}}$  of  $> 167$  h at 50 ppt NO<sub>3</sub>. In contrast, from our experimental results and eq 6.2 we estimate an atmospheric lifetime of 13 seconds. A possible reason for the apparent discrepancy between our results and the results presented by Pitts et al. may be the difference in experimental conditions. The experiments by Pitts et al. were carried out in the presence of large concentrations of N<sub>2</sub>O<sub>5</sub> ( $3.8 \times 10^{13}$  molecule cm<sup>-3</sup>). These large concentrations may have interfered with the surface reaction between NO<sub>3</sub> and pyrene by blocking reaction sites. Additionally, it is known that different underlying substrates for PAHs result in different reaction rates for O<sub>3</sub><sup>122,129,130,132,133</sup> and NO<sub>2</sub>.<sup>127</sup> This might also be true for NO<sub>3</sub>. Pitts et al.<sup>98</sup> used PAHs on filter substrates while solid PAH surfaces were used in this study.

The recent aerosol studies by Schauer et al.<sup>140</sup> may also be related to our NO<sub>3</sub> studies. These authors studied the decay of benzo[a]pyrene (BaP) on spark discharge soot particles exposed to ozone. Upon the addition of NO<sub>2</sub> they saw an enhanced loss of BaP, whereas the NO<sub>2</sub> alone did not result in loss of BaP. As indicated by the authors, the enhanced loss was attributed to the formation of reactive intermediates such as NO<sub>3</sub>. In other words, the measurements by Schauer et al. are consistent with a significant reaction between NO<sub>3</sub> and surface-bound BaP, although reaction rates were not quantified.

### 6.3.3 Measurements of the Initial Reactive Uptake Coefficients for N<sub>2</sub>O<sub>5</sub>

The reactive uptake coefficients for N<sub>2</sub>O<sub>5</sub> on fresh PAH surfaces were determined in the same way as NO<sub>3</sub> uptake coefficients. Shown in Figure 6.3 is an example of data



obtained for  $\text{N}_2\text{O}_5$  loss on pyrene. For this case the change in the  $\text{N}_2\text{O}_5$  signal was less than the scatter in the data. In fact, for all PAH surfaces investigated and for both temperatures (273 K and room temperature), the change in the  $\text{N}_2\text{O}_5$  signal was less than the uncertainty in the measurements. From the data we estimated an upper limit of  $\gamma_0$  and these values are listed in Tables 6.2 and 6.3. These upper limits are based on the 95% confidence interval of our experimental results. As shown, the reactive uptake coefficients are small and drastically lower than the reactive uptake coefficients of  $\text{NO}_3$  on the same surfaces.

Two previous studies investigated the reactions of  $\text{N}_2\text{O}_5$  on PAH surfaces; however, reactive uptake coefficients were not measured.<sup>87,98</sup> Our study is the first to report the reactive uptake coefficients of  $\text{N}_2\text{O}_5$  on PAH surfaces. We can nevertheless compare our results with theirs by using atmospheric lifetimes as discussed above. Our results and eq 6.2 lead to an atmospheric lifetime of  $\geq 4.6$  h at room temperature, and the results from Pitts et al. and Kamens et al. and eq 6.3 lead to atmospheric lifetimes of 100 h (Pitts et al.),<sup>98</sup> and 222 h (Kamens et al.).<sup>87</sup> These calculations show that our results do not contradict the previous measurements.

#### **6.3.4 Measurements of the Initial Reactive Uptake Coefficients for $\text{O}_3$**

Uptake coefficients  $\gamma_0$  were obtained for  $\text{O}_3$  in the same way as for  $\text{NO}_3$  and  $\text{N}_2\text{O}_5$ . Similar to  $\text{N}_2\text{O}_5$ , the decrease in the CIMS signal was less than the scatter in the  $\text{O}_3$  data. From the measurements we calculated an upper limit of  $\gamma_0$  based on the 95% confidence interval of our experimental results (see Tables 6.2, 6.3, and 6.4).

In Table 6.4 we compare our results with results obtained in previous studies. In cases where reactive uptake coefficients were not measured, we determined  $\tau_{\text{atm}}$  from the experimental data and eq 6.3, and have included these values for comparison. Note that our results were obtained by monitoring the loss of the gas-phase reactant, while the previous measurements were obtained by monitoring the decay of PAH molecules. Differences may be due to different substrates (see above) and different PAHs used. However, as can be seen in columns for  $\gamma$  and the atmospheric lifetime calculated with 100 ppb  $\text{O}_3$ , our data are broadly consistent with the previous measurements.

**Table 6.4: Summary of measurements of O<sub>3</sub> uptake on PAH surfaces. For calculations of lifetimes ( $\tau_{\text{atm}}$ ), O<sub>3</sub> concentrations of 100 ppb were used for all studies for comparison purposes.**

reference	surface	temperature	$\gamma_0$	$\tau_{\text{atm}}$
This study	solid PYR	273 K	$\leq 9.7 \times 10^{-7}$	$\geq 1.3$ h
	solid FLU		$\leq 5.7 \times 10^{-7}$	
	solid BEN		$\leq 1.6 \times 10^{-6}$	
This study	solid PYR	293-297 K	$\leq 7.6 \times 10^{-7}$	$\geq 1.6$ h
Pöschl et al <sup>129</sup>	BaP on soot <sup>a</sup>	298 K	$\sim 2 \times 10^{-5}$ to $2 \times 10^{-6}$	-
Kwamena et al <sup>130</sup>	BaP on solid organic aerosol <sup>a</sup>	298 K	$\sim 2 \times 10^{-6}$ to $5 \times 10^{-7}$	-
Mmereki et al <sup>123,131</sup>	Anthracene at air-water interface <sup>b</sup>	298 K	$\sim 3 \times 10^{-7}$ to $2 \times 10^{-8}$	-
Van Vaeck and Van Cauwenberghe <sup>134</sup>	BEN	room temperature	-	11 h
Pitts et al <sup>133</sup>	PYR	room temperature	-	$\sim 4 - 5$ h
	FLU			$\sim 6 - 9$ h
	BEN			$\sim 4 - > 9$ h
	BaP on filters			$\sim 4 - 9$ h
Alebic-Juretic et al <sup>132</sup>	PYR	room temperature	-	$\sim 1.4$ h
	FLU			$\sim 17$ h
	BEN on silica gel			$\sim 0.7$ h

<sup>a</sup> The reactive uptake coefficient depended on relative humidity and O<sub>3</sub> concentrations.

<sup>b</sup> The reactive uptake coefficient depended on O<sub>3</sub> concentration and whether or not the air-water interface was coated with an organic monolayer.

### 6.3.5 Measurements of the Initial Reactive Uptake Coefficients for NO<sub>2</sub>

Our measured reactive uptake coefficients,  $\gamma_0$ , for NO<sub>2</sub> were  $\leq 1.0 \times 10^{-6}$  for all three PAHs at 273 K and at room temperature (see Tables 6.2 and 6.3) (based on the 95% confidence interval of our experimental results). The only other study that has investigated the reactive uptake coefficient of NO<sub>2</sub> on PAH surfaces was the work by Arens et al.<sup>125</sup> These authors studied the uptake on a solid layer of anthracene adsorbed onto a glass substrate. They obtained  $\gamma$  values of  $7 \times 10^{-7} - 2 \times 10^{-6}$  at different NO<sub>2</sub> concentrations and relative humidities, which is generally consistent with our numbers.

Esteve et al.<sup>72,124</sup> also studied NO<sub>2</sub> heterogeneous reactions on 13 different PAHs adsorbed on graphite or diesel particles. Their experimental results and eq 6.3 lead to calculated atmospheric lifetimes  $\tau_{\text{atm}}$  of PAHs ranging from 1.1 h to 5.6 h, which is in the same range as the lifetimes calculated for PYR in this study ( $\geq 1.2$  h).

### 6.3.6 Measurements of the Initial Reactive Uptake Coefficients for HNO<sub>3</sub>

The upper limit reported for HNO<sub>3</sub> is slightly higher than those of N<sub>2</sub>O<sub>5</sub>, NO<sub>2</sub>, and O<sub>3</sub> (see Tables 6.2 and 6.3). This is due to the fact that in some uptake experiments we observed a small uptake of HNO<sub>3</sub>, which was at least partially reversible. Shown in Figure 6.4 is an example of the CIMS raw data obtained in a typical HNO<sub>3</sub> experiment. Shown is the HNO<sub>3</sub> signal as the injector is pulled back in equal 1 cm increments and then pushed forward to its original position. When the injector was returned to the starting position, the HNO<sub>3</sub> signal was larger than at the beginning of the experiment, indicating desorption of HNO<sub>3</sub> from the PAH surface. This indicates that at least part of the loss of HNO<sub>3</sub> was due to physical adsorption on the PAH surface. Since at least part of the loss of the HNO<sub>3</sub> signal was due to physical adsorption rather than reaction, the reactive uptake coefficients for HNO<sub>3</sub> determined in our experiments (based on the 95% confidence interval of our experimental results) should be considered as upper limits. Physisorption probably occurred to some extent for all the oxidants used in this study, but only HNO<sub>3</sub> showed physisorption at a detectable amount in our experiments, most likely due to the polarity of the molecule. Strong physisorption of HNO<sub>3</sub> has also been observed on soot.<sup>136,141</sup>

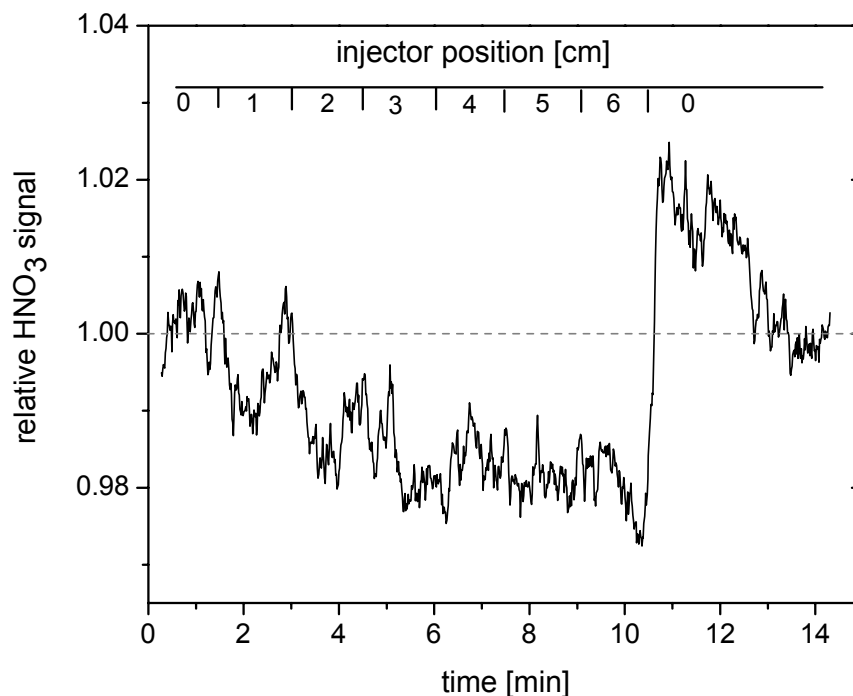


**Figure 6.4:  $\text{HNO}_3$  signal as a function of time for a typical uptake experiment of  $\text{HNO}_3$  on fluoranthene at 273 K. Within the first 10 minutes the injector is pulled back in 1 cm increments, 6 cm total. At the end (at approx. 10 min), the signal increases compared to its original intensity as the injector is pushed back to its original position (“0”, no exposure) and finally decreases to the original intensity. Scale within the graph corresponds to the positions of the injector during the different steps of the experiment.**

To the best of our knowledge, no other group has measured the reactive uptake coefficient of  $\text{HNO}_3$  on PAH surfaces. However, experiments studying the reactivity of  $\text{HNO}_3$  with PAHs have been performed by various researchers. Nielsen<sup>142</sup> studied the reactions of 25 PAHs with  $\text{HNO}_3$  in mixed aqueous and organic solutions and observed PAH half-lives ranging from minutes to years. Vione et al.<sup>143</sup> studied heterogeneous reactions between  $\text{HNO}_3$  and naphthalene in aqueous solution. They concluded that nitration with  $\text{HNO}_3$  in the liquid phase is unlikely to occur in most environments. Similarly, in experiments by Pitts et al.<sup>98</sup>  $\text{HNO}_3$  did not react significantly with PYR or perylene. These results are in agreement with our current measurements. The half-life reported in Kamens et al.<sup>87</sup> for BaP on wood soot with  $\text{HNO}_3$  converts to an atmospheric lifetime of 161 days at typical tropospheric  $\text{HNO}_3$  concentrations of 10 ppb. Our lower

limits for the atmospheric lifetime do not contradict the previous measurements (see Tables 6.2 and 6.3).

### 6.3.7 Processing Studies of NO<sub>3</sub> (i.e. Uptake of NO<sub>3</sub> as a Function of Exposure)

For these measurements, the tip of the injector is initially pushed to the front of the flow cell so the surface is not exposed to NO<sub>3</sub>. Next the injector is quickly withdrawn 5 cm, exposing 27.5 cm<sup>2</sup> of PAH film to NO<sub>3</sub>. The NO<sub>3</sub> signal was then monitored for 60 minutes to determine if the surface is deactivated or processed from exposure to the gas-phase reactant. NO<sub>3</sub> concentrations used in these experiments were  $(1.3 - 3.4) \times 10^{11}$  molecule cm<sup>-3</sup>. All exposure studies were carried out in the presence of  $(0.95 - 2.1) \times 10^{16}$  molecule cm<sup>-3</sup> of O<sub>2</sub>. Experiments were carried out at both  $297 \pm 3$  K and  $263 \pm 2$  K. The lower temperature was chosen to minimize volatilization of PAHs and the products of the NO<sub>3</sub> and PAH reaction. 263 K was used rather than 273 K in order to reduce the volatilization as much as possible. This prohibited replenishment of “fresh” PAH surfaces and enabled studying the “aging” of the PAH films.

Results from the processing studies are shown in Figure 6.5. In this figure the NO<sub>3</sub> signal was normalized to the initial signal intensity before exposure to PAH and the product of the NO<sub>3</sub> concentration and exposure time (i.e. [NO<sub>3</sub>] × t) was plotted on the x-axis rather than just exposure time, since processing is expected to be proportional to both concentration and exposure time.

Shown in Figure 6.5 are results carried out at  $263 \pm 2$  K (Panels A, C, and E) and  $297 \pm 3$  K (panels B, D, and F). At 263 K, the NO<sub>3</sub> signal decreased drastically when the injector was pulled back, indicating a fast initial uptake. However, the signal slowly approached the initial value (relative signal = 1) over the period of 60 minutes, indicating that the reaction slowed down and the surface was being processed or deactivated. This suggests that the surface-bound PAH molecules were active participants in the reaction (i.e. reactants). Observations of the change in colour of the PAH surface with long exposures to NO<sub>3</sub> are also consistent with the conclusion that surface-bound PAH molecules were being oxidized. The surfaces changed from yellow/beige to red/brown during NO<sub>3</sub> exposure.

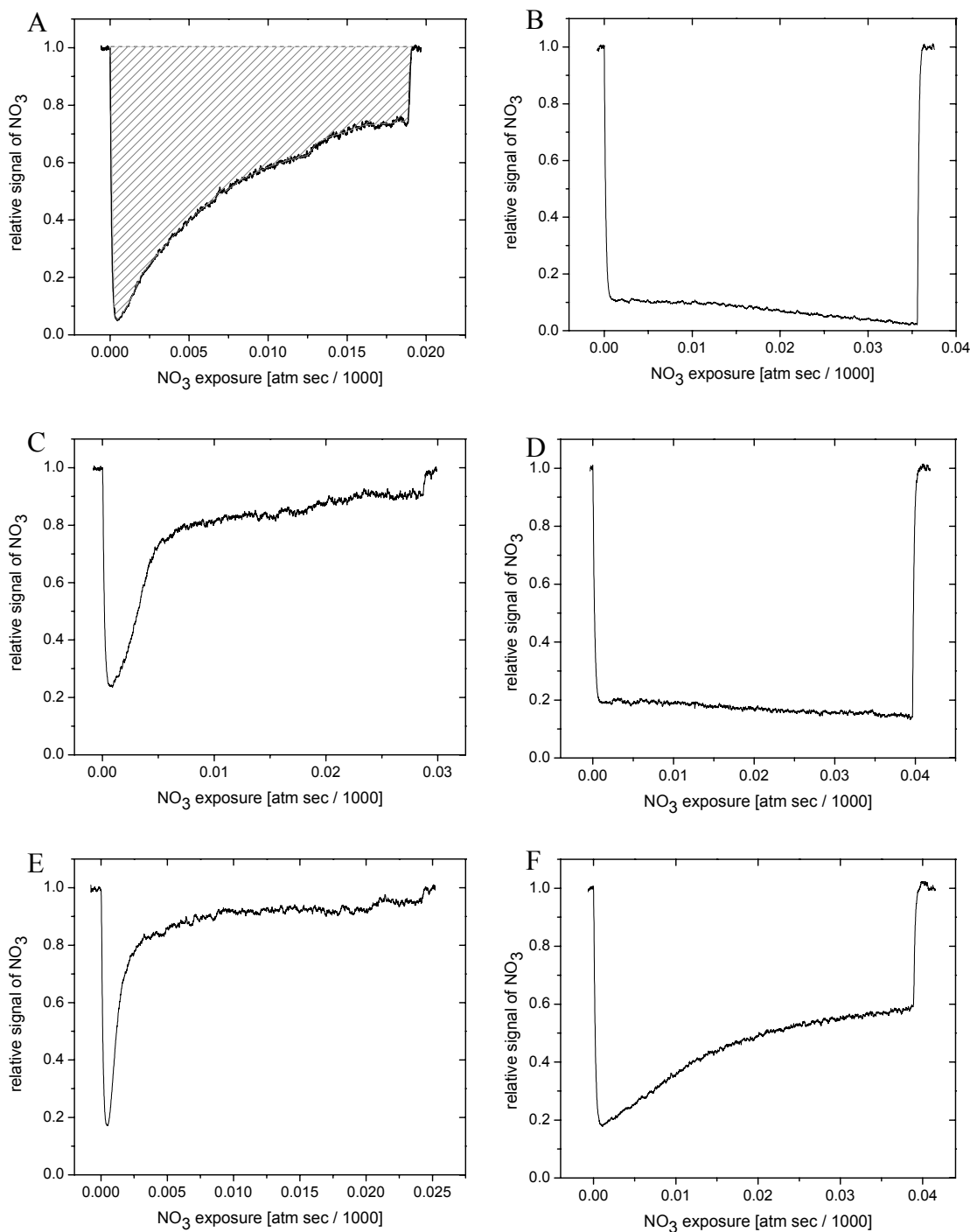


**Figure 6.5: Relative changes of the  $\text{NO}_3$  signal during exposure of PAH surfaces ( $27.5 \text{ cm}^2$ ) to  $\text{NO}_3$  for 60 min.  $\text{NO}_3$  exposure corresponds to the product of  $\text{NO}_3$  concentration and exposure time. Panels A and B: pyrene. Panels C and D: fluoranthene. Panels E and F: benz[a]anthracene. Left-hand side (A, C, E):  $263 \pm 2 \text{ K}$ . Right-hand side (B, D, F):  $297 \pm 3 \text{ K}$ . The shaded region in Panel A corresponds to the area integrated to determine the number of  $\text{NO}_3$  radicals lost during the whole exposure experiment.**

From the plots shown in Figure 6.5 we can determine the total number of NO<sub>3</sub> radicals lost to the surface at 263 K during the 60 min exposure by integrating the loss of the NO<sub>3</sub> signal over the entire exposure time using plots A, C, and E. The plot area of the depleted signal relative to the initial signal intensity (an example is shown for plot A as a gray shaded area), as well as experimental gas flows, concentrations in the flow cell, and the geometric surface area of the PAH films allowed us to calculate the total NO<sub>3</sub> uptake per unit area of PAH. The total number of NO<sub>3</sub> radicals lost to the PAH surfaces during the 60 min exposures were  $4 \times 10^{16}$ ,  $2 \times 10^{16}$ , and  $9 \times 10^{15}$  NO<sub>3</sub> radicals cm<sup>-2</sup> on PYR, FLU, and BEN, respectively. The fact that the number of NO<sub>3</sub> radicals lost per cm<sup>2</sup> is greater than the total number of surface PAH molecules per cm<sup>2</sup> could be because some of the condensed-phase products of the heterogeneous reactions evaporated during the 60 min experiments, exposing a new (i.e. unreacted) PAH surface. Alternatively, some of the NO<sub>3</sub> radicals may diffuse into the bulk and react with sub-surface PAH molecules. In other words the bulk reaction may also contribute to our overall net loss of gas-phase radicals at extended exposure times. It is also possible that more than one NO<sub>3</sub> radical reacted with one surface PAH molecule.

Also from the plots in Figure 6.5, we can estimate the reactive uptake coefficient at the end of the exposure studies. First the  $k_{\text{obs}}$  at the end of the exposure studies was calculated using the relative NO<sub>3</sub> signal just before the end of the 60 min exposure and a reaction length of 5 cm (i.e. the signal change during the movement of the injector from 5 cm exposure back to its “0” position). Then the reactive uptake coefficient was calculated from  $k_{\text{obs}}$ , as described in the experimental section, Chapter 6.2. At the end of the 60 min exposure periods at 263 K,  $\gamma_{\text{NO}_3}$  on PYR, FLU, and BEN had decreased to  $5 \times 10^{-3}$ ,  $1 \times 10^{-3}$ , and  $6 \times 10^{-4}$ , respectively.

In the processing studies, the trend observed at 297 K was drastically different than the trend observed at 263 K. The NO<sub>3</sub> signal did not recover for the experiments with PYR and FLU even up to NO<sub>3</sub> exposures of 0.04 atm sec/1000 (or  $4 \times 10^{-5}$  atm sec). 1 atm sec corresponds to an exposure of 1 atmosphere ( $= 2.5 \times 10^{19}$  molecule cm<sup>-3</sup>) for 1 second. 0.04 atm sec/1000 is equivalent to approx. 65 ppt NO<sub>3</sub> for 1 week. For the full 60 min experiment the NO<sub>3</sub> signal remained constant within experimental uncertainty.

For the BEN surface at room temperature, there was partial recovery of the NO<sub>3</sub> signal, but much less than at 263 K.

At 297 K during the 60 min exposure, the amount of NO<sub>3</sub> radicals lost per cm<sup>2</sup> to the surface was  $5 \times 10^{16}$ ,  $5 \times 10^{16}$ , and  $3 \times 10^{16}$  for PYR, FLU, and BEN, respectively. Again this is greater than a monolayer of PAHs on the surface, indicating that multilayers of the PAHs were reacted. One possible explanation for the continuous loss of NO<sub>3</sub>, even after a monolayer of the PAHs (the surface layer) is reacted, is that the condensed phase products of the heterogeneous reactions evaporated during the exposure studies. The difference between 263 and 297 K is likely due to the higher volatility of condensed-phase products at room temperature compared to 263 K.

Experiments were also performed at 273 K using PYR and an intermediate behaviour between the data at 263 K and 297 K was observed (data not shown).

At room temperature, we observed that the NO<sub>3</sub> signal partially recovered for BEN surfaces during the processing studies, but the signal did not recover for PYR and FLU (see Figure 6.5 B, D, F). This trend can also be explained using an argument similar to the one presented above. BEN has the lowest vapour pressure of the three PAHs investigated, and as a result one would expect the condensed-phase products of this reaction to have a lower vapour pressure than the condensed-phase products for the other two PAHs. If the products of the BEN reaction have a lower vapour pressure and remain on the surface, one would expect the NO<sub>3</sub> signal to recover faster in these experiments, which is the trend observed.

### **6.3.8 Gas-Phase Product Studies for the Reaction of NO<sub>3</sub> with Pyrene**

As mentioned above, we also carried out preliminary gas-phase product studies for the NO<sub>3</sub>-pyrene reaction at  $297 \pm 1$  K. In these studies we focused on HNO<sub>3</sub>, NO<sub>2</sub>, HONO, and NO, since our CIMS and chemical ionization schemes were sensitive to these species. In short, potential gas-phase products (HNO<sub>3</sub>, NO<sub>2</sub>, HONO, and NO) were monitored using CIMS while a pyrene surface was exposed to NO<sub>3</sub>. In Figure 6.6 we present some of the results from these experiments.



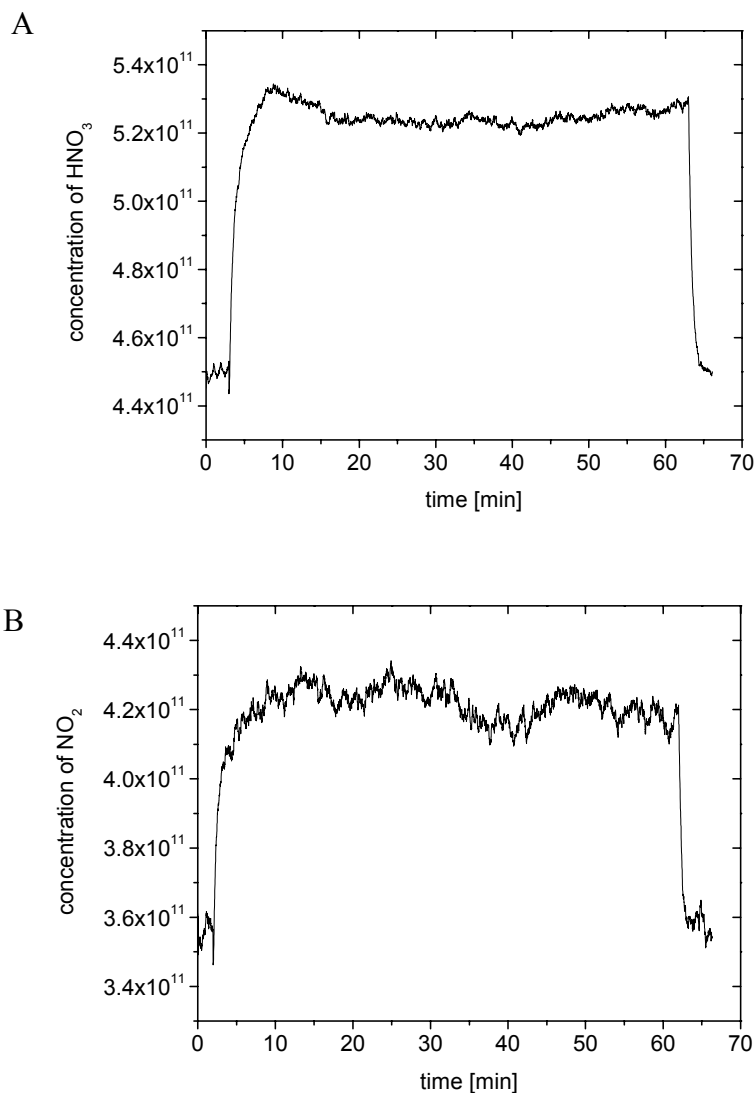


**Figure 6.6: Changes in concentrations of  $\text{HNO}_3$  (panel A), and  $\text{NO}_2$  (panel B) during exposure of pyrene surfaces ( $27.5 \text{ cm}^2$ ) to  $\text{NO}_3$  for 60 min at  $297 \pm 1 \text{ K}$ .  $\text{NO}_3$  concentrations exposed to the surfaces were approximately  $2.5 \times 10^{11} \text{ molecule cm}^{-3}$ .**

For these measurements, the tip of the injector was initially pushed to the front of the flow cell so the surface was not exposed to  $\text{NO}_3$ . Next the injector was quickly withdrawn 5 cm (at  $t \approx 2.5$  minutes), exposing  $27.5 \text{ cm}^2$  of PAH film to  $\text{NO}_3$ . Plotted are the  $\text{HNO}_3$  and  $\text{NO}_2$  signals observed when the pyrene surface was exposed to an  $\text{NO}_3$  concentration of approximately  $2.5 \times 10^{11} \text{ molecule cm}^{-3}$ . Signal intensities of  $\text{NO}_2$  and  $\text{HNO}_3$  increased when  $\text{NO}_3$  radicals were exposed to pyrene while signal intensities of HONO and NO (data not shown) remained constant within experimental uncertainties.

During the 60 min experiments,  $(1.6 \pm 0.5) \times 10^{16}$  NO<sub>2</sub> radicals and also  $(1.6 \pm 0.5) \times 10^{16}$  HNO<sub>3</sub> molecules were produced per cm<sup>2</sup> of pyrene surface in the flow cell in the presence of O<sub>2</sub>, while  $(5 \pm 2) \times 10^{16}$  NO<sub>3</sub> radicals per cm<sup>2</sup> of surface were lost. Considering the mass balance of nitrogen, approx. 1/3 of the total nitrogen exposed to the surface (in the form of NO<sub>3</sub>) reacted and stayed on the surface, most likely forming condensed-phase products like nitro-pyrenes. More on the possible reaction mechanism is included below.

### 6.3.9 Proposed Reaction Mechanism for the Reaction of NO<sub>3</sub> on Pyrene

The mechanisms for NO<sub>3</sub>-PAH surface reactions are unknown. As a starting point, we assume that the NO<sub>3</sub>-PAH reactions that occur in the gas phase can also occur on the surface, although the relative importance of the pathways may be significantly different. Shown in Figure 6.7 is a suggested mechanism based on gas-phase chemistry of PAHs with NO<sub>3</sub>.<sup>144-147</sup> The possible pathways are as follows: first addition of NO<sub>3</sub> radicals to the carbon atoms of the aromatic rings can occur to form an NO<sub>3</sub>-PAH adduct (step a), which can undergo back-decomposition to reactants (step b) in competition with bimolecular reactions with NO<sub>2</sub> (step c) and O<sub>2</sub> (step d). As well, the adduct can undergo unimolecular reactions (step e).

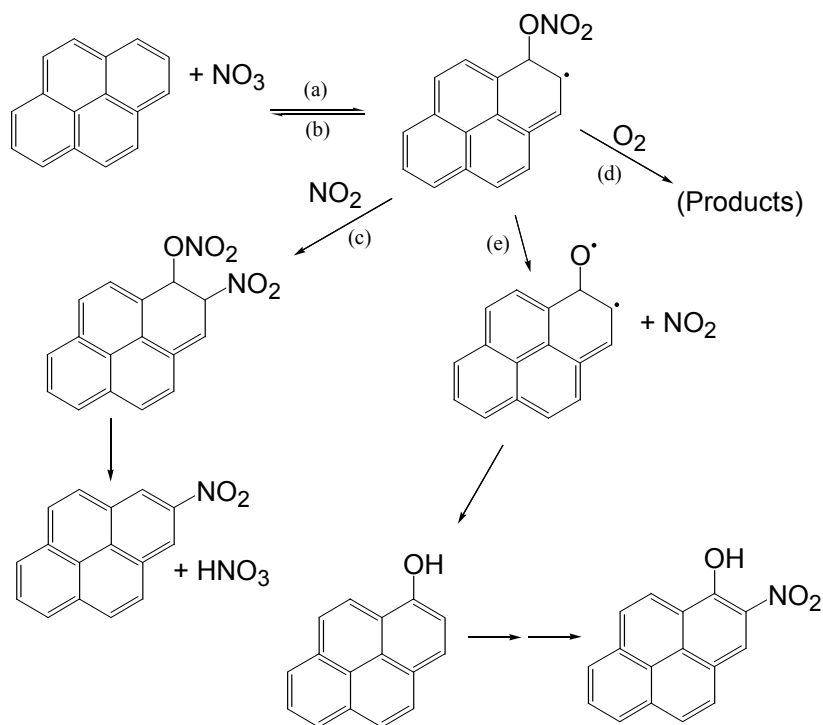


**Figure 6.7: Suggested mechanism for the surface reaction of pyrene with  $\text{NO}_3$  based on gas-phase chemistry of PAHs with  $\text{NO}_3$ . Note that other isomers may be formed as well.**

In our experiments we saw both  $\text{HNO}_3$  and  $\text{NO}_2$  production. This is consistent with channels c and e. If these two channels are in fact dominant we would also expect to see nitro-pyrenes and hydroxyl-pyrenes as surface products. Future experiments focusing on the yields of these products would be beneficial.

## 6.4 Atmospheric Implications

### 6.4.1 Comparison of the Different Oxidants

Here we compare the importance of the different oxidants for heterogeneous oxidation of surface-bound PAHs in the atmosphere.

In Tables 6.2 and 6.3 we have included the product of  $\gamma_0$  and the average atmospheric concentrations of the gas-phase oxidants  $[\text{oxidant}]_{\text{atm}}$ . Compared with just  $\gamma_0$ ,  $\gamma_0 \times [\text{oxidant}]_{\text{atm}}$  is a more relevant parameter for assessing the importance of the various

radicals to atmospheric oxidation, since the number of radicals lost to an organic surface will be proportional to  $\gamma_0 \times [\text{oxidant}]_{\text{atm}}$ . The most important process will generally be the process with the largest  $\gamma_0 \times [\text{oxidant}]_{\text{atm}}$  and therefore the highest oxidative power. As can be seen from these calculations, the oxidative power of  $\text{NO}_3$  is a factor of 60 - 1000 higher than that of all the other oxidants studied.

#### **6.4.2 Lifetime ( $\tau_{\text{atm}}$ ) of Surface-Adsorbed PAHs with Respect to the Different Oxidants**

Above we have used  $\tau_{\text{atm}}$  to compare results from different experiments when  $\gamma_0$  was not measured. Here we use this parameter to assess the atmospheric importance of the various heterogeneous reactions. These lifetimes are reported in the last columns of Tables 6.2 and 6.3. Based on our data the atmospheric lifetime of PYR with respect to  $\text{NO}_3$  heterogeneous loss is only seconds while all other lifetimes calculated from our data are greater than 12 min. In fact, in many cases the lifetimes of the other species based on our data are greater than hours. These results show that under typical atmospheric conditions at nighttime,  $\text{NO}_3$  radicals can be a more important sink for PAHs than  $\text{NO}_2$ ,  $\text{HNO}_3$ ,  $\text{N}_2\text{O}_5$ , or  $\text{O}_3$  and may impact tropospheric lifetimes of surface-bound PAHs.

#### **6.4.3 Direct Acting Mutagenicity of Wood Smoke and $\text{NO}_3$ Heterogeneous Chemistry**

In a series of smoke chamber studies, Kamens et al.<sup>148</sup> have shown that the direct acting mutagenicity of wood smoke increased by 2 to 10 fold in the presence of  $\text{O}_3$  and  $\text{NO}_2$  (and also  $\text{NO}_3$  and  $\text{N}_2\text{O}_5$  since  $\text{O}_3$  and  $\text{NO}_2$  will produce these oxidants). Our results suggest that the increased mutagenicity may have been due in part to the nitration by  $\text{NO}_3$  radicals, since  $\text{NO}_3$  can react more efficiently with PAHs in comparison with  $\text{O}_3$ ,  $\text{NO}_2$ , and  $\text{N}_2\text{O}_5$ .

### **6.5 Summary and Conclusions**

Reactive uptake coefficients were determined for the heterogeneous reactions of  $\text{NO}_3$ ,  $\text{N}_2\text{O}_5$ ,  $\text{NO}_2$ ,  $\text{HNO}_3$ , and  $\text{O}_3$  on three different solid PAH surfaces (pyrene, fluoranthene, and benz[a]anthracene) at 273 K and at 293 – 297 K. These are the first

measurement of the reactive uptake coefficients of  $\text{NO}_3$  and  $\text{N}_2\text{O}_5$  on PAH surfaces. The reaction of  $\text{NO}_3$  radicals with all three PAHs was observed to be very fast, with the reactive uptake coefficient ranging from 0.059 (+ 0.11 / -0.049) for benz[a]anthracene to 0.79 (+ 0.21 / - 0.67) for pyrene. In contrast to the  $\text{NO}_3$  reactions, reactions of the different PAHs with the other gas-phase species ( $\text{N}_2\text{O}_5$ ,  $\text{NO}_2$ ,  $\text{HNO}_3$ , and  $\text{O}_3$ ) were at or below the detection limit ( $\gamma \leq 6.6 \times 10^{-5}$ ) in all cases, illustrating that these reactions are slow or do not occur. The uptake coefficients determined with  $\text{NO}_2$ ,  $\text{HNO}_3$ , and  $\text{O}_3$  showed no discrepancy with values obtained in previous studies. The reaction of  $\text{NO}_3$  on all three PAH surfaces slowed down at 263 K after long  $\text{NO}_3$  exposure times. While benz[a]anthracene showed a similar trend at room temperature,  $\gamma_{\text{NO}_3}$  did not decrease on pyrene and fluoranthene after 60 minutes of  $\text{NO}_3$  exposure at 296 K. This difference is thought to be due to the different volatility of the three different PAHs and their reaction products.

Our results show that under certain atmospheric conditions,  $\text{NO}_3$  radicals may be a more important sink for PAHs than  $\text{NO}_2$ ,  $\text{HNO}_3$ ,  $\text{N}_2\text{O}_5$ , or  $\text{O}_3$  and may affect tropospheric lifetimes of surface-bound PAHs. For example, calculations of oxidative powers ( $\gamma_0 \times [\text{oxidant}]_{\text{atm}}$ ) and atmospheric lifetimes of PAHs with respect to the different gas-phase oxidants showed that under certain atmospheric conditions,  $\text{NO}_3$  reactions should be a more important PAH loss process than the other oxidants studied. Based on our data, atmospheric lifetimes of surface-bound PAH material should be on the order of only seconds to minutes due to heterogeneous reactions with  $\text{NO}_3$  radicals during the night.

Furthermore, heterogeneous reactions between  $\text{NO}_3$  and PAHs could also lead to sampling artefacts when measuring condensed-phase PAHs in the atmosphere with filters. During the collection process, ambient air is drawn through the filters and the gas-phase oxidants can transform the collected particulate matter. It has been shown that the reactions between  $\text{O}_3$  and PAHs adsorbed on filters can lead to sampling artefacts (chemical loss and under-determination of PAHs).<sup>140</sup> The heterogeneous reaction between  $\text{NO}_3$  and PAHs may also lead to sampling artefacts, since this reaction should be competitive with the  $\text{O}_3$  and PAH heterogeneous reaction under certain conditions.

Most likely, there are no pure PAH surfaces in the atmosphere, but the presented results are important first outcomes in the effort to understand heterogeneous PAH reactions under controlled laboratory conditions. More research on the heterogeneous reactions between  $\text{NO}_3$  and PAHs on and in atmospherically realistic particles as well as analysis of condensed-phase products would be beneficial.

## 7 REACTIVE UPTAKE COEFFICIENT MEASUREMENTS OF $\text{NO}_3$ AND $\text{N}_2\text{O}_5$ ON A LIQUID AND FROZEN ALKENOIC ACID, ALKANOATE, AND POLYALCOHOL

### 7.1 Introduction

As mentioned in Chapter 1, the composition of the condensed-phase organic material in the atmosphere is very diverse with hundreds to thousands of different organics identified.<sup>1,16,18,149,150</sup> Some of the classes of compounds in the organic aerosol fraction are alkanes, alkanolic acids, alkenoic acids, dicarboxylic acids, alcohols, and polycyclic aromatic hydrocarbons.<sup>29,49,151</sup>

In the previous chapter we focused on heterogeneous reactions of PAHs. Here we focus on non-PAH organic substrates. In the following we study heterogeneous reactions between  $\text{NO}_3$  and  $\text{N}_2\text{O}_5$  and three types of solid and liquid organic substrates to better understand the atmospheric importance of these reactions. The focus of these studies is to assess the reactive uptake coefficient of these gases on the different organic substrates.

There have only been a few studies that have explored the reactive uptake coefficient of  $\text{NO}_3$  on non-PAH organic substrates. Moise et al.<sup>44</sup> studied the reactive uptake coefficient on the following liquid and solid organics: n-hexadecane, n-octanoic acid, 1-octadecene, 1-hexadecene, heptylmethyl nonane, 1-octanol, 7-tetradecene, conjugated linoleic acid, and nonconjugated linoleic acid. McNeill et al.<sup>73</sup> studied the  $\text{NO}_3$  uptake coefficient on aqueous aerosols coated with a monolayer of sodium oleate. These studies suggest  $\text{NO}_3$  reactions with organics may be important in the atmosphere under certain conditions, but more work in this area is needed to fully understand the significance of these reactions.

In addition, there have been only a few studies of the reactive uptake coefficient of  $\text{N}_2\text{O}_5$  on organics. Thornton et al.<sup>152</sup> studied the uptake coefficient of  $\text{N}_2\text{O}_5$  on solid malonic acid and azelaic acid aerosols. In addition, Lai and Finlayson-Pitts<sup>153</sup> studied the

products formed from the heterogeneous reaction between  $\text{N}_2\text{O}_5$  and 1-palmitoyl-2-oleoyl-*sn*-glycero-3-phosphocholine (an unsaturated lipid), but uptake coefficients were not reported. Due to the dearth of information on this topic, studies of  $\text{N}_2\text{O}_5$  heterogeneous reactions on organics would be beneficial.

In the following, we investigate the reactive uptake of  $\text{NO}_3$  and  $\text{N}_2\text{O}_5$  on liquid and solid organic substrates to better understand heterogeneous reactions on atmospheric aerosols. The reactive uptake coefficients are used to assess the lifetime of these condensed-phase organics in the atmosphere and to speculate on the importance of these reactions in laboratory studies of secondary organic aerosol (SOA) formation. By comparing the results for the liquid and solid compounds, we discuss whether the reaction for the liquid is mainly due to a surface reaction or both surface and bulk reaction.<sup>44</sup>

The specific substances used for this study were diethyl sebacate ( $\text{C}_{14}\text{H}_{26}\text{O}_4$ ), an alkanoate; glycerol ( $\text{C}_3\text{H}_8\text{O}_3$ ), a polyalcohol; and cis-9-octadecenoic acid ( $\text{C}_{18}\text{H}_{34}\text{O}_2$ ), an alkenoic acid. For the remainder of the document we will refer to diethyl sebacate as DES and cis-9-octadecenoic acid as oleic acid. These compounds are depicted in Figure 7.1 and were chosen because of their low vapour pressures and because all have melting points within the temperature range studied (263 K – 303 K). However, liquid glycerol supercooled under our experimental conditions and did not freeze even at the lowest temperature investigated. The fact that oleic acid and DES froze within the temperature range studied, allowed us to investigate differences between solid and liquid surfaces of the same compound. The three organics used in this study represent different functional groups commonly found in atmospheric samples and therefore serve as models for certain organics in the atmosphere. Two of the compounds (oleic acid and glycerol) have been observed in atmospheric field studies and diesters of sebacic acid (decanedioic acid) have recently been used as proxies for saturated organic compounds found in the atmosphere.<sup>69,70,154</sup>



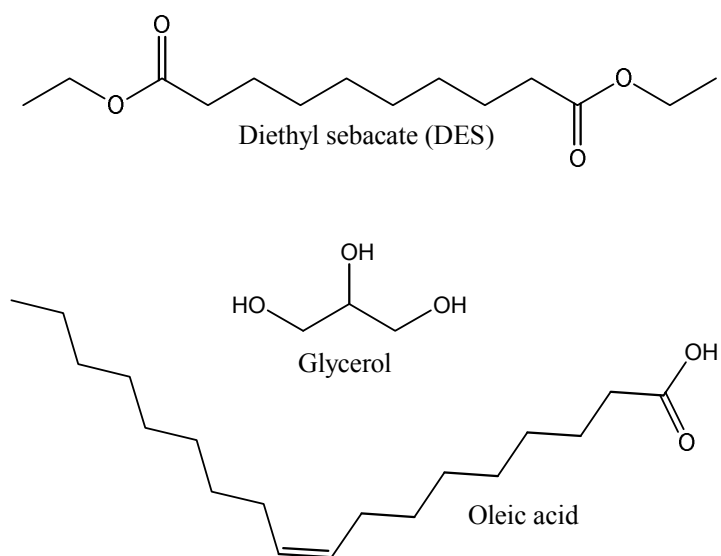


**Figure 7.1: Molecular structures of the three different organic compounds investigated in this study.**

For  $\text{NO}_3$  we find the reactive uptake on the alkenoic acid is much faster than expected based on previous results. This finding may have implications for the atmosphere and studies on the formation of SOA. For  $\text{N}_2\text{O}_5$  we find that the reaction with the polyalcohol is also efficient and may be a reaction that plays an important role in the atmosphere.

## 7.2 Experimental

### 7.2.1 Experimental Setup and Procedure

Experiments were performed in a rotating-wall flow cell coupled to a chemical ionization mass spectrometer (CIMS) described in more detail in Chapter 5. In short, approx. 0.5 – 1 mL of the liquid organic was distributed onto the inner wall of a rotating glass cylinder with an inner diameter of 1.75 cm. A rotation rate of approximately 10 rotations per minute was used in the liquid experiments. Experiments were performed in the temperature range 263 K – 303 K. For experiments on solid surfaces, rotating liquid films were rapidly cooled using the cooling jacket of the flow cell. Total pressures in the flow cell were between 2 and 5 torr and velocities in the flow cell ranged from 20–100  $\text{cm s}^{-1}$  for the  $\text{N}_2\text{O}_5$  experiments, and from 380 – 810  $\text{cm s}^{-1}$  for the  $\text{NO}_3$  experiments.

The flow was laminar in all experiments based on the Reynolds number.  $\text{NO}_3$  and  $\text{N}_2\text{O}_5$  were added through a movable injector which allowed varying the reactive distance and therefore the reaction time. The injector was pulled back in steps, exposing an increasing surface area of the organic to  $\text{NO}_3$  or  $\text{N}_2\text{O}_5$ . Changes in the  $\text{NO}_3$  or  $\text{N}_2\text{O}_5$  signal due to reactive uptake on the organic were monitored using CIMS. Observed first-order loss rate coefficients,  $k_{\text{obs}}$ , were calculated from the depletion of the CIMS signal of the gas-phase oxidant with increasing reaction time. Three typical plots of the natural logarithm of the  $\text{NO}_3$  signal vs. reaction time are shown in Figure 7.2 for glycerol, DES, and oleic acid. The slopes of the linear fits were used to determine  $k_{\text{obs}}$ . Next  $k_{\text{obs}}$  was corrected for concentration gradients that form close to the flow-tube wall using the procedure developed by Brown.<sup>108</sup> Uptake coefficients,  $\gamma$ , were calculated from the corrected  $k_{\text{obs}}$  using a standard procedure.<sup>75</sup>

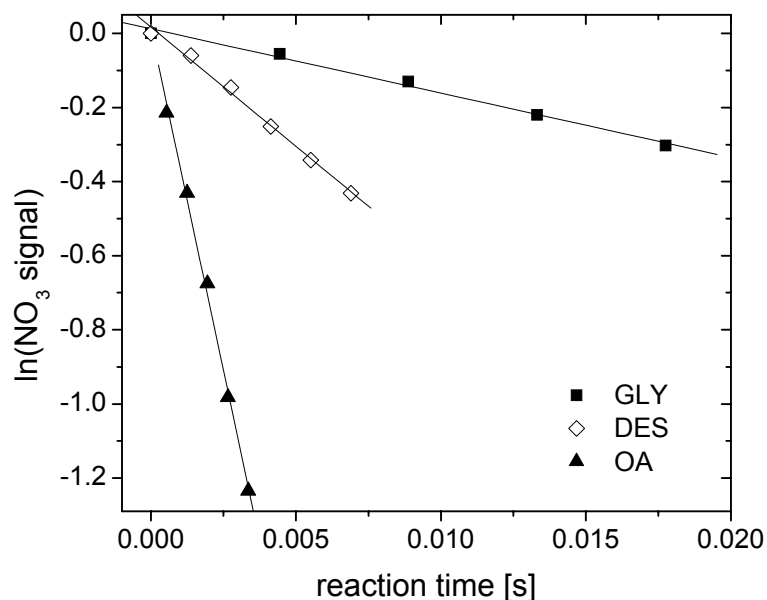


**Figure 7.2:** Plot of the natural logarithm of the CIMS signals of  $\text{NO}_3$  vs. reaction time during typical experiments on liquid surfaces of glycerol (squares), oleic acid (triangles), and DES (open diamonds) at 288 K (for oleic acid and DES) and at 293 K (for glycerol).

$\text{NO}_3$  concentrations ranged from  $7 \times 10^{10}$  to  $2 \times 10^{11}$  molecule  $\text{cm}^{-3}$  and  $\text{N}_2\text{O}_5$  concentrations ranged from  $7 \times 10^{11}$  to  $2 \times 10^{12}$  molecule  $\text{cm}^{-3}$ . All experiments were

performed in the presence of O<sub>2</sub>. O<sub>2</sub> percentages in the flow cell ranged from 10 – 14% (NO<sub>3</sub> experiments) to 38 – 54% (N<sub>2</sub>O<sub>5</sub> experiments) of the total flow. All experiments were repeated at least five times.

As NO<sub>2</sub> is always present in our NO<sub>3</sub> experiments (due to our method of producing NO<sub>3</sub> radicals), we also measured the reactive uptake coefficients of NO<sub>2</sub> for oleic acid, DES, and glycerol at 298 K in the presence of O<sub>2</sub>. Experimental conditions were similar to the conditions discussed above. For all experiments the  $\gamma$  value for NO<sub>2</sub> was at or below our detection limit ( $\gamma \leq 1 \times 10^{-6}$ ).

### 7.2.2 Chemicals

Oleic acid ( $\geq 99.0\%$ ) was purchased from Fluka, DES (98%) from Sigma-Aldrich, and glycerol (99.9%) from Fisher-Scientific. NO<sub>2</sub> (99.5%) was purchased from Matheson, N<sub>2</sub> (99.999%), O<sub>2</sub> (99.993%), and He (99.999%) were purchased from Praxair. N<sub>2</sub>O<sub>5</sub> and NO<sub>3</sub> were generated as described above.

## 7.3 Results and Discussion

Observed uptakes of NO<sub>3</sub> and N<sub>2</sub>O<sub>5</sub> were irreversible for all organics studied. This means that at the end of an uptake experiment, when the injector was pushed forward to its position of zero exposure, no release of NO<sub>3</sub> or N<sub>2</sub>O<sub>5</sub> was observed. All uncertainties reported in this study are 95% confidence limits. Results are shown in Figures 7.3 and 7.4 and are listed in Tables 7.1 and 7.2.

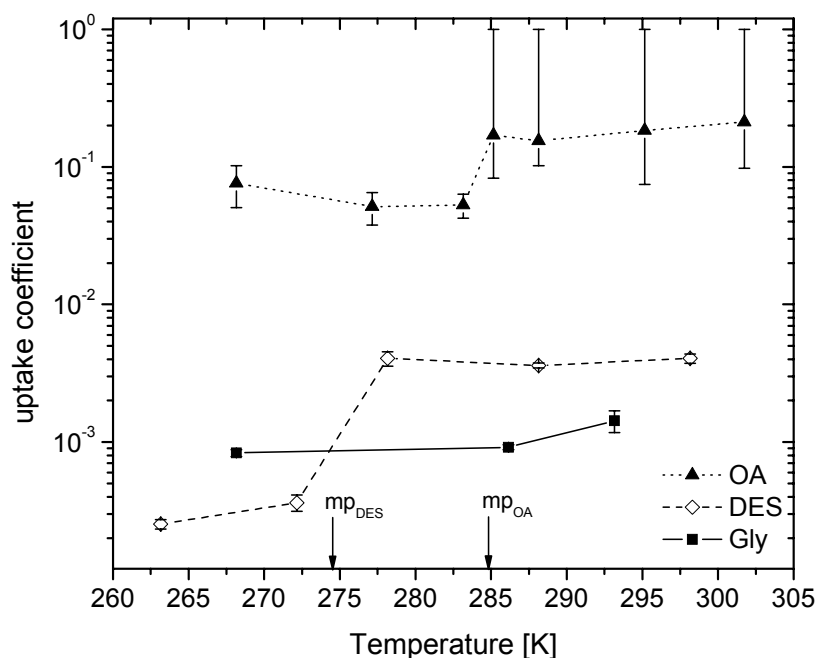


**Figure 7.3: Measured reactive uptake coefficients  $\gamma$  vs. temperature for  $\text{NO}_3$  reactions on different solid and liquid organics. OA = oleic acid, DES = diethyl sebacate, Gly = glycerol. mp denotes melting points of the different compounds.**

### 7.3.1 Reactive Uptake of $\text{NO}_3$ on Oleic Acid (an Alkenoic Acid)

The uptake coefficients for oleic acid (the only unsaturated organic compound investigated) in the liquid state were  $> 0.08$ ,  $> 0.1$ ,  $> 0.07$ , and  $> 0.1$  at 285 K, 288 K, 295 K, and 302 K, respectively.

When the liquid oleic acid froze, the reactive uptake coefficient decreased to a value of  $0.051 - 0.076$ . This suggests that the liquid reaction may be due to both a surface reaction and a bulk reaction since the freezing process is expected to drastically decrease the importance of any bulk reactions in our experiments.<sup>44</sup> An alternative explanation is that the reactive uptake for both the liquid and solid are due to only surface reactions, but the surface in the liquid state is much more favourable for uptake and reactivity.<sup>155</sup> In our experiments we cannot discern between these two different possibilities, but will assume the former (similar to Moise et al.<sup>44</sup>) until further information is available.

The high reactivity observed for the liquid reactions (and also for the solid surface) is due to the addition of the  $\text{NO}_3$  radical to the  $\text{C}=\text{C}$  double bond, based on

recent product studies for NO<sub>3</sub> reactions with liquid oleic acid particles<sup>63,66</sup> and results presented in Chapter 9 of this thesis. Based on the product studies the likely mechanism involves the addition of the NO<sub>3</sub> radical to the double bond to form a C-ONO<sub>2</sub> functional group on one of the two C atoms and an alkyl radical at the other C atom. O<sub>2</sub> can then add to the radical to form a peroxy radical (ROO), which can then undergo a series of radical reactions to form products such as carbonyls, hydroxyls, nitrates or peroxy-nitrates.<sup>63,66</sup>

Since the reactive uptake coefficients in our studies are most likely due to the C=C double bond, we compare our results with previous results for unsaturated organic molecules. The only published data for liquid and frozen unsaturated organics are from Moise et al.<sup>44</sup> The data from this study are shown in Table 7.1. For the liquids our results are 1 to 2 orders of magnitude higher than the results reported by Moise et al.<sup>44</sup> Even for the solids our data are a factor of 5 to 50 higher than the data from Moise et al.

**Table 7.1: Comparison of the reactive uptake coefficient  $\gamma$  for NO<sub>3</sub> reactions with unsaturated organics between this study and results by Moise et al.**

Reference	Surface	T [K]	$\gamma_{\text{liquid}}$	T [K]	$\gamma_{\text{solid}}$
this study	oleic acid	285 - 302	$\geq 0.1$	268 - 283	$(5.1 - 7.6) \times 10^{-2}$
Moise et al. <sup>a</sup>	1-octadecene	293	$1.6 \times 10^{-3}$	283	$1.4 \times 10^{-3}$
Moise et al. <sup>a</sup>	1-hexadecene	277	$2.3 \times 10^{-3}$	254 - 274	$1.8 \times 10^{-3}$
Moise et al. <sup>a</sup>	7-tetradecene	246	$5.8 \times 10^{-3}$	238	$5.2 \times 10^{-3}$
Moise et al. <sup>a</sup>	conjugated linoleic acid	273	$7.9 \times 10^{-3}$	253 - 263	$7.8 \times 10^{-3}$
Moise et al. <sup>a</sup>	nonconjugated linoleic acid	288	$1.5 \times 10^{-2}$	248 - 263	$1.1 \times 10^{-2}$

<sup>a</sup>Moise et al.<sup>44</sup>

The reason for the difference between our results and the results from Moise et al. is not clear. Both our experiments and the experiments by Moise et al. were performed with a rotating-wall flow reactor, and both experimental apparatus were validated by studying known gas-phase reactions. Moise et al.<sup>44</sup> studied the gas-phase reaction of 1-butene with NO<sub>3</sub> and obtained rate constants consistent with literature values. We measured the second order rate constant for the gas-phase reaction of NO<sub>3</sub> with NO at room temperature using our flow cell. We obtained  $2.96 (\pm 0.15) \times 10^{-11} \text{ cm}^3 \text{ molecule}^{-1} \text{ s}^{-1}$  which agrees well with the established literature values ( $2.4 \times 10^{-11}$  to  $3.0 \times 10^{-11} \text{ cm}^3 \text{ molecule}^{-1} \text{ s}^{-1}$ ).<sup>1,88,89</sup>

One difference between our work and the work of Moise et al. was the  $\text{NO}_3$  concentrations used. Moise et al. used  $5 \times 10^{11} - 5 \times 10^{12}$  molecule  $\text{cm}^{-3}$ , which is slightly higher than our concentration. This may explain part of the discrepancy. Other experimental conditions such as pressure and temperatures were similar. Another possible reason for the discrepancy may be the organics studied. We studied oleic acid, while Moise et al. used other unsaturated organics. Further work is needed to understand these differences.

In addition to the studies by Moise et al., Ziemann et al. very recently studied the reactive uptake coefficient of  $\text{NO}_3$  on liquid oleic acid aerosols using an environmental chamber (Ziemann P. J., personal communications). These authors determined a value of  $0.13 (\pm 0.02)$  for the reactive uptake coefficient of  $\text{NO}_3$  on liquid oleic acid particles at room temperature, which is consistent with our findings. Our work together with the very recent work by Ziemann et al. suggests that at least for certain unsaturated organics, the reactive uptake coefficient may be larger than previously thought.

Also related to this discussion, McNeill et al.<sup>73</sup> studied the uptake of  $\text{NO}_3$  on aqueous particles coated with a monolayer of sodium oleate and obtained a  $\gamma$ -value of  $< 10^{-3}$ . This study is similar to studies on solid or frozen films where only the surface or top few layers are accessible. As shown in Figure 7.3, for frozen films we obtained values that were at least a factor of 50 greater than the results obtained by McNeill et al. These differences in reactive uptake coefficients could possibly be explained by differences in the structure at the surface of the monolayer and the surface of the frozen sample.

### **7.3.2 Reactive Uptake of $\text{NO}_3$ on Glycerol (a Polyalcohol)**

For the temperature range studied, the glycerol films did not freeze. This was confirmed visually. The uptake coefficients measured for liquid glycerol were in the range of  $8 \times 10^{-4} - 1.4 \times 10^{-3}$ , which is at least 2 orders of magnitude slower than oleic acid and approximately a factor of 4 slower than DES.

There has only been one previous study of the reactive uptake coefficient of  $\text{NO}_3$  on a liquid saturated alcohol. Moise et al.<sup>44</sup> studied 1-octadecanol and obtained a value of  $7.1 \times 10^{-3}$  for the liquid. The differences in molecular structures between glycerol and 1-octadecanol could perhaps account for the difference in reactivity.

The likely mechanism for the  $\text{NO}_3$  reaction with an alcohol, based on gas-phase reactions, is hydrogen abstraction from the carbon atom next to the alcohol functional group to form  $\text{HNO}_3$  and an alkyl radical.<sup>44,156,157</sup> The hydrogen atom on the carbon atom adjacent to the alcohol is expected to be more reactive compared to a hydrogen atom in an alkane molecule.<sup>157</sup> Note that in glycerol all three C atoms contain an OH-functional group. The alkyl radical is then expected to react with oxygen to form a peroxy radical (ROO), which can undergo subsequent radical reactions. The complete reaction mechanism is discussed in previous publications.<sup>1,40,41</sup>

### 7.3.3 Reactive Uptake of $\text{NO}_3$ on DES (an Alkanoate)

The uptake coefficients measured for liquid DES were in the range of  $(3.5 - 4.5) \times 10^{-3}$ . Freezing of DES resulted in a decrease of  $\gamma$  of about one order of magnitude. This suggests that the reactive uptake of  $\text{NO}_3$  on the liquid is due to both a surface and bulk process.

There have been no previous studies of  $\text{NO}_3$  reactive uptake on liquid or solid alkanoates for comparison. Gas-phase measurements suggest the reaction rates for saturated esters are similar to the reaction rates for saturated hydrocarbons.<sup>158</sup> In other words, the presence of the ester functional group does not significantly affect the reactivity of the alkyl chain. As a result we compare in Table 7.2 our results for the alkanoate with previous measurements of the uptake of  $\text{NO}_3$  with solid and liquid alkanes by Moise et al.<sup>44</sup> In this case, our results for the alkanoate are in good agreement with the measurements by Moise et al. using n-hexadecane.

**Table 7.2:  $\gamma$  comparison of  $\text{NO}_3$  reactions with saturated organics between this study and results by Moise et al.**

Reference	Surface	T [K]	$\gamma_{\text{liquid}}$	T [K]	$\gamma_{\text{solid}}$
this study	DES (ester)	278 - 298	$(3.6 - 4.1) \times 10^{-3}$	263 - 272	$(2.5 - 3.6) \times 10^{-4}$
Moise et al. <sup>a</sup>	n-hexadecane	293	$2.6 \times 10^{-3}$	283 - 289	$3.8 \times 10^{-4}$
Moise et al. <sup>a</sup>	heptamethyl nonane	253	$2.1 \times 10^{-3}$	234	$2.6 \times 10^{-3}$

<sup>a</sup>Moise et al.<sup>44</sup>

Based on gas-phase reactions between  $\text{NO}_3$  and alkanoates, the mechanism is likely due to abstraction of a H atom on the carbon followed by the formation of an alkyl

radical which can form a peroxy radical and undergo additional radical chain reactions as mentioned above in Sections 7.3.1 and 7.3.2.

### 7.3.4 Overall Trend in NO<sub>3</sub> Reactivity

Here we first focus on the results for the solids. In solids, reaction should be confined to the surface, while in liquids the reactive uptake coefficient can also be influenced by diffusion and solubility of NO<sub>3</sub>.<sup>44</sup> For the solids, the results show that the trend in reactivity is alkenoic acid > alkanoate. This trend is consistent with the trend observed for gas-phase reactivity, assuming the alkenoic acid reactivity is due to the C=C double bond. For example, the gas-phase reaction rate coefficients for propene and methyl propionate are  $9.5 \times 10^{-15} \text{ cm}^3 \text{ molecule}^{-1} \text{ s}^{-1}$  and  $1 \times 10^{-17} \text{ cm}^3 \text{ molecule}^{-1} \text{ s}^{-1}$ , respectively.<sup>158,159</sup>

The trend in reactive uptake coefficients for the liquids is alkenoic acid > alkanoate > polyalcohol. This suggests that glycerol reacts more slowly with NO<sub>3</sub> than DES or oleic acid. The trend in the gas-phase is different: the reaction rate constant of propanol is in between those of propene and methyl propionate.<sup>158,159</sup> However, in order to obtain a complete physical explanation for the behaviours of the liquids, different components of the overall uptake have to be considered. We therefore use the “resistance model” of gas-liquid interactions which is described in more detail in the Appendix. Based on this model, the overall reactive uptake coefficient for liquids, neglecting gas-phase diffusion can be described by the following equation:

$$7.1 \quad \frac{1}{\gamma} = \frac{1}{S} + \frac{1}{\frac{1}{\frac{1}{S \frac{k_{sol}}{k_{des}}} + \frac{1}{\Gamma_{rxn}}} + \frac{1}{\Gamma_{surf}}}$$

with

$$7.2 \quad \Gamma_{rxn} = \frac{4HRT\sqrt{Dk_{rxn}}}{c_{avg}}$$

where S is the sticking coefficient (fraction of collisions at the surface that result in accommodation on the surface),  $k_{sol}$  is the rate coefficient for the transfer of molecules from the surface into the bulk of the liquid,  $k_{des}$  is the rate coefficient for the transfer of



molecules from the surface into the gas (desorption),  $\Gamma_{\text{rxn}}$  is the rate of reaction in the liquid solution normalized to the gas-phase collision frequency,  $\Gamma_{\text{surf}}$  represents the surface reaction,  $H$  is the Henry's law solubility constant,  $R$  is the gas constant,  $T$  is the temperature,  $D$  is the diffusion coefficient for  $\text{NO}_3$  in the organic liquid,  $k_{\text{rxn}}$  is the first order rate constant for reaction in the liquid, and  $c_{\text{avg}}$  is the mean molecular velocity of  $\text{NO}_3$ .<sup>1,160</sup>

The diffusion coefficient of a species in a liquid is related to the viscosity through the Stokes-Einstein equation

$$7.3 \quad D = \frac{kT}{6 \cdot \pi \cdot \eta \cdot r}$$

where  $k$  is the Boltzmann constant,  $T$  is the temperature,  $\eta$  is the viscosity of the liquid, and  $r$  is the radius of the diffusing species. The viscosity of liquid glycerol is orders of magnitude higher than that of liquid oleic acid or liquid DES. Viscosities at 293 - 298 K for glycerol, oleic acid, and DES are 1500 mPa s,<sup>161</sup> 43.8 mPa s,<sup>162</sup> and 5.88 mPa s,<sup>163</sup> respectively. Eq 7.3 and the liquid viscosity data suggest that the diffusion coefficient of  $\text{NO}_3$  is orders of magnitude smaller in glycerol than in oleic acid and DES.

In order for a bulk reaction to be slow compared to the surface reaction for a liquid (based on eq 7.1 and 7.2), either the product  $H\sqrt{Dk_{\text{rxn}}}$  must be small or the product  $S(k_{\text{sol}}/k_{\text{des}})$  must be small. The differences in viscosity and therefore diffusion coefficient (together with eq 7.1 and 7.2) lead one to speculate that the reason for the slow  $\text{NO}_3$ -glycerol reaction is not a slow reaction rate constant in the liquid, but the small diffusion coefficient of  $\text{NO}_3$  in liquid glycerol which results in a small  $H\sqrt{Dk_{\text{rxn}}}$  value in eq 7.1 and 7.2.

### 7.3.5 Reactive Uptake of $\text{N}_2\text{O}_5$ on Glycerol

As shown in Figure 7.4 for the three substances investigated, the  $\text{N}_2\text{O}_5$  reactive uptake coefficient was the largest on glycerol. Uptake coefficients ranged from  $4 \times 10^{-4}$  to  $8 \times 10^{-4}$  for the liquid.

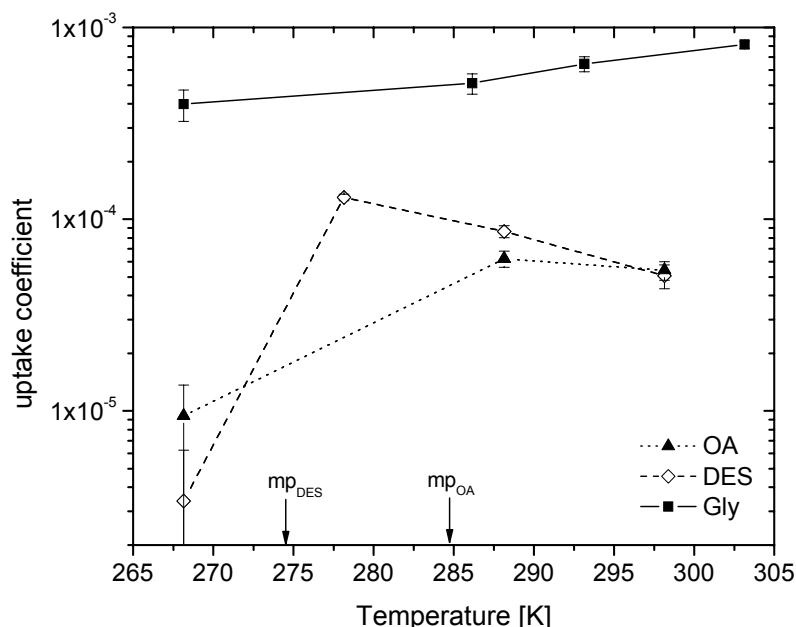


**Figure 7.4: Measured reactive uptake coefficients  $\gamma$  vs. temperature for  $\text{N}_2\text{O}_5$  reactions on different solid and liquid organics. OA = oleic acid, DES = diethyl sebacate, Gly = glycerol. mp denotes melting points of the different compounds.**

Our studies are the first measurements of the reactive uptake coefficients of  $\text{N}_2\text{O}_5$  on a liquid alcohol. However, reactions between  $\text{N}_2\text{O}_5$  and saturated alcohols have been observed in the gas phase.<sup>156,157</sup> It has also been suggested that in previous gas-phase experiments, the reaction between  $\text{N}_2\text{O}_5$  and the alcohols may have occurred heterogeneously on reactor walls.<sup>157</sup> In addition, the condensed-phase reaction between  $\text{N}_2\text{O}_5$  and saturated alcohols is known to produce organonitrates.<sup>164</sup>

The mechanism for the  $\text{N}_2\text{O}_5$  reaction with an alcohol has been suggested to occur via a six membered ring leading to an organic nitrate and  $\text{HNO}_3$ ,<sup>156</sup> see Figure 7.5. To further investigate this mechanism we monitored changes in the  $\text{HNO}_3$  signal during exposure of glycerol to  $\text{N}_2\text{O}_5$ . However,  $\text{HNO}_3$  was not released into the gas phase in these reactions. It is possible that  $\text{HNO}_3$  was too “sticky” to be emitted from the glycerol solid or liquid surface and remained adsorbed or dissolved in the organic.

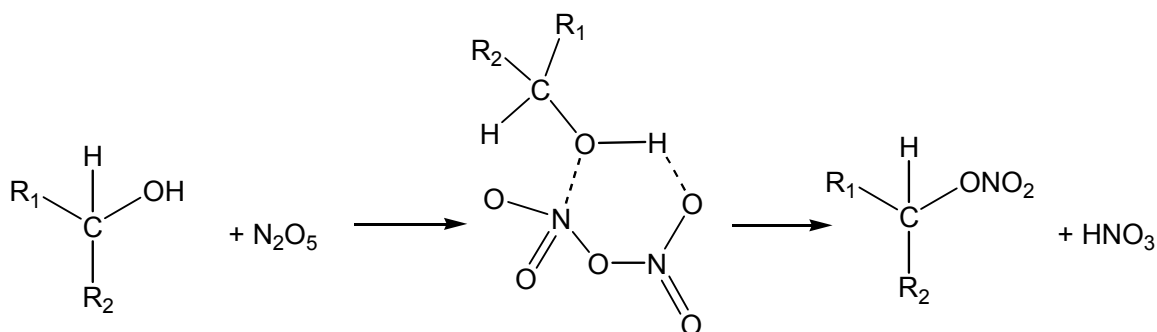


**Figure 7.5: Reaction mechanism of  $\text{N}_2\text{O}_5$  with a saturated alcohol based on the gas-phase mechanism of methanol and  $\text{N}_2\text{O}_5$  suggested by Langer and Ljungström.<sup>156</sup>**

### 7.3.6 Reactive Uptake of $\text{N}_2\text{O}_5$ on Oleic Acid

For the alkenoic acid, the reactive uptake was  $(5 - 6) \times 10^{-5}$  for the liquid and  $< 1 \times 10^{-5}$  for the solid. The decrease in the reactive uptake coefficient below the freezing point suggests that the reaction for the liquid was due to a combination of surface and bulk reactions.

There have been no previous studies of the reactive uptake coefficients of  $\text{N}_2\text{O}_5$  on a liquid or solid alkenoic acid. Lai and Finlayson-Pitts studied the heterogeneous reaction between  $\text{N}_2\text{O}_5$  and 1-palmitoyl-2-oleoyl-*sn*-glycero-3-phosphocholine (unsaturated organic compound) on the inside surface of a glass reaction cell; however, uptake coefficients were not reported. Major products identified in this previous study included nitro and nitrate functional groups. The initial step in the reaction mechanism was thought to be direct reaction of  $\text{N}_2\text{O}_5$  with the double bond leading to a nitronitrate which could undergo subsequent reactions. This was consistent with an early study by Stevens and Emmons.<sup>165</sup> In a related series of experiments, we studied the reactive uptake coefficient of  $\text{N}_2\text{O}_5$  on solid PAH surfaces and reported very small reactive uptake coefficient ( $\gamma \leq 8.7 \times 10^{-6}$ ) of  $\text{N}_2\text{O}_5$  with fluoranthene, pyrene, and benz[a]anthracene as described in Chapter 6.

### 7.3.7 Reactive Uptake of $\text{N}_2\text{O}_5$ on DES

Reactive uptake coefficients determined for liquid DES were in the range of  $4.3 \times 10^{-5}$  to  $1.3 \times 10^{-4}$ , and were  $< 6 \times 10^{-6}$  for the solid. As  $\gamma$  dropped significantly upon

freezing, this again suggests that reaction on the liquid occurs both at the surface and in the bulk.

As shown in Figure 7.4, a significant negative temperature dependence was observed for liquid DES. In order to explain this trend we again use the “resistance model”, which is described in more detail in the Appendix. We assume the reaction for the liquid occurs mainly in the bulk, which is supported by the change in the reactive uptake coefficient upon freezing. In this case, the reactive uptake coefficient can be explained with the following equation:

$$7.4 \quad \frac{1}{\gamma} = \frac{1}{\alpha} + \frac{c_{avg}}{4HRT\sqrt{Dk_{rxn}}}$$

where  $\alpha$  is the probability that a molecule that strikes the surface enters into the bulk with

$$7.5 \quad \frac{1}{\alpha} = \frac{1}{S} + \frac{k_{des}}{Sk_{sol}}$$

$c_{avg}$ ,  $H$ ,  $R$ ,  $T$ ,  $D$ , and  $k_{rxn}$  have been defined above.  $H$ ,  $D$ ,  $k_{rxn}$ , and  $c_{avg}$  may all be temperature dependent. Diffusion coefficients and rate constants typically show a positive temperature dependence. Increasing either  $D$  or  $k_{rxn}$  would lead to higher results for  $\gamma$  and cannot explain the negative temperature dependence for DES with  $N_2O_5$ .  $c_{avg}$ , the mean molecular velocity, also has a positive temperature dependence and therefore leads to a negative temperature dependence for  $\gamma$ . However, increasing the temperature from 278 K to 298 K increases  $c_{avg}$  by only 3.5%, while  $\gamma$  of DES +  $N_2O_5$  decreased by a factor of 2.6 over this temperature range. Therefore the observed temperature dependence cannot be due to changes in the molecular velocity.  $H$ , Henry’s law solubility constant, also has a negative temperature dependence<sup>49,55,166</sup> and we therefore assume that the observed increase in  $\gamma$  at lower temperature is due to the higher solubility of  $N_2O_5$  in the liquid which leads to more  $N_2O_5$  in the bulk of the liquid and therefore a higher probability of reactive uptake.

There have been no previous studies of  $N_2O_5$  on liquid or solid alkanoates for comparison. Also, we are not aware of any gas-phase reactions between  $N_2O_5$  and an alkanoate. The only other heterogeneous studies for pure saturated organics that we are aware of is a study by Thornton et al.<sup>152</sup> These authors measured the uptake of  $N_2O_5$  on solid malonic acid and azelaic acid aerosols and determined uptake coefficients to be

$< 10^{-3}$  and  $(5 \pm 3) \times 10^{-4}$ , respectively. The values they obtained for azelaic acid are slightly higher than our results for DES, but the difference may also be due to the presence of water in the experiments by Thornton et al.<sup>152</sup> The relative humidity used in the azelaic acid experiments by Thornton et al. was 85%, whereas we had a dry carrier gas.

Others have also studied the reactive uptake coefficient of  $\text{N}_2\text{O}_5$  on aqueous organic particles, but we have not included this in the discussion, since the reactivity in these experiments was most likely due to the hydrolysis reaction of  $\text{N}_2\text{O}_5$  not a reaction between  $\text{N}_2\text{O}_5$  and the organic.<sup>50,51,53,54,73,152</sup>

### 7.3.8 Overall Trend in $\text{N}_2\text{O}_5$ Reactivity

A comparison of the uptake coefficients of the solids shows that there is no significant difference in the reactivity of the alkenoic acid and the alkanoate.

For the liquids the trend is polyalcohol  $>$  alkanoate  $\geq$  alkenoic acid. There is very little data on  $\text{N}_2\text{O}_5$ -organic gas-phase reactions for comparison. Pfrang et al.<sup>30,167</sup> measured  $5 \times 10^{-19} - 3 \times 10^{-18} \text{ cm}^3 \text{ molecule}^{-1} \text{ s}^{-1}$  for unsaturated alcohols and Langer and Ljungström<sup>156</sup> measured  $< 5 \times 10^{-19} \text{ cm}^3 \text{ molecule}^{-1} \text{ s}^{-1}$  for saturated alcohols. These two results suggest that (in the gas phase) reaction of  $\text{N}_2\text{O}_5$  is up to an order of magnitude faster in the presence of a  $\text{C}=\text{C}$  double bond. However, Pfrang et al.<sup>167</sup> saw evidence of nitrated unsaturated products, which suggests that in some unsaturated alcohols reaction of the hydroxyl group with  $\text{N}_2\text{O}_5$  was faster than the reaction of the  $\text{C}=\text{C}$  bond.

## 7.4 Atmospheric Implications

### 7.4.1 Oxidation Timescale for Liquid Organic Particles

In order to determine if the reactions we investigated in this study are important in the atmosphere, we calculated the oxidation timescale from our experimental data and compared this timescale with the atmospheric residence time of the aerosol particles. This analysis is similar to the analysis recently used by Robinson et al.<sup>43</sup> to determine the effect of OH and  $\text{O}_3$  reactions on the molecule composition of organic aerosols in the regional context. Following Robinson et al. we calculated the oxidation lifetime using the following equation:

7.6

$$\tau_{liquid} = \frac{N_{tot}}{\Phi} = \frac{4r\rho N_A}{3M\gamma[oxidant]c_{avg}}$$

where  $\tau_{liquid}$  is the oxidation lifetime of a liquid particle,  $N_{tot}$  is the total number of organic molecules in the particle,  $\Phi$  is the flux of oxidant into the particle,  $r$  is the particle radius,  $\rho$  is the particle density (assumed to be the density of the pure liquid),  $N_A$  is Avogadro's number,  $M$  is the molecular weight of the organic molecule,  $\gamma$  is the reactive uptake coefficient,  $[oxidant]$  is the concentration of the oxidant in the gas-phase, and  $c_{avg}$  is the average velocity of the oxidant in the gas-phase.<sup>43</sup> This timescale calculation was derived by setting the total number of oxidation events equal to the initial number of molecules in the particles, i.e. each molecule in the particle reacts once. This simple calculation gives an estimate for the time needed for all the molecules in the particles to be oxidized.

We carried out these calculations for oleic acid, DES, and glycerol. Oxidant concentrations used in the calculations were 50 ppt for  $NO_3$ , 5 ppb for  $N_2O_5$  and 0.04 ppt for OH.  $NO_3$  and  $N_2O_5$  concentrations used in these experiments roughly correspond to heavily polluted conditions, but it should be noted that tropospheric  $NO_3$  and  $N_2O_5$  concentrations are highly variable. For example, recent measurements by Penkett et al.<sup>168</sup> over Western Europe suggest an average  $NO_3$  concentration of 350 ppt, and aircraft measurements by Brown et al. as part of the New England Air Quality Study indicate  $NO_3$  concentrations above the surface, but within the boundary layer, of approximately 20 – 400 ppt.<sup>169,170</sup>

The results of these calculations are shown in Figure 7.6 as a function of particle size. For reference, the size of organic particles in the atmosphere can range from a few nanometres to approximately 10  $\mu m$ , depending on the source and the environment. In an urban environment the mass median diameter for particles in the accumulation mode (particle size range from  $\sim 0.2 \mu m$  to  $2 \mu m$ ) is typically between 0.2 to 0.6  $\mu m$ .<sup>1,49,171</sup> Also for reference, global 3D models of  $^{210}Pb$  and carbonaceous aerosols suggest aerosol residence times of 5 – 15 days.<sup>172,173</sup> Radioactive tracer measurements suggest an atmospheric residence time of the order of 10 days for some regions influenced by pollution.<sup>174</sup> In Figure 7.6 we have indicated with horizontal lines times of 5 and 15 days.

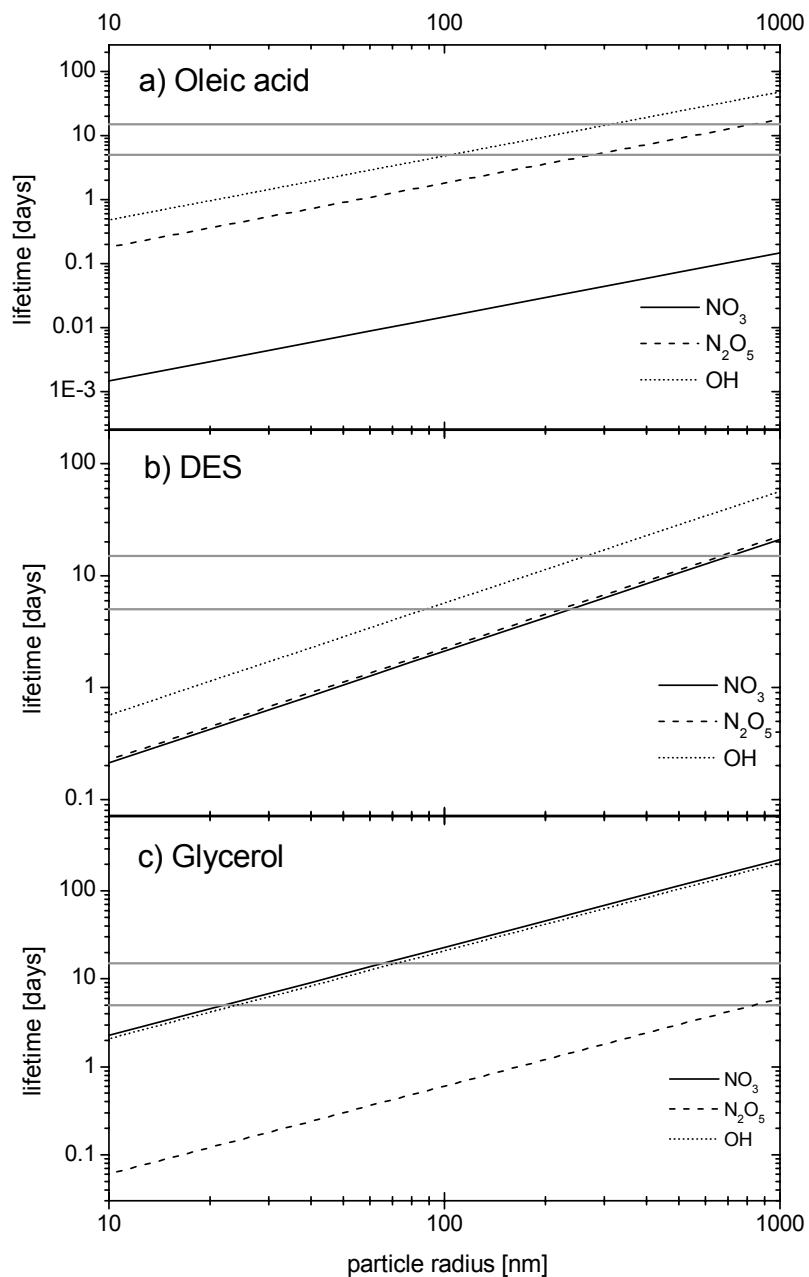


**Figure 7.6: Atmospheric lifetimes  $\tau$  of liquid droplets as a function of particle diameter with respect to oxidation by  $\text{NO}_3$ ,  $\text{N}_2\text{O}_5$  or  $\text{OH}$  at 25 °C. It is assumed that the whole particle consists of oleic acid (panel a), DES (panel b) or glycerol (panel c). Grey horizontal lines indicate lifetimes of 5 and 15 days.**

Figure 7.6, Panel a, shows that the  $\text{NO}_3$  oxidation lifetime for oleic acid-like particles is short compared to aerosol particle residence times. This suggests that  $\text{NO}_3$  heterogeneous reactions may play a role in the oxidation of particles in the atmosphere,

by modifying the chemical composition of these particles. Even for  $\text{N}_2\text{O}_5$ , the oxidation lifetime is comparable to the residence time for oleic acid.

The predicted short lifetimes of oleic acid shown in Figure 7.6 are in contrast to field measurements that suggest lifetimes of oleic acid on the order of days.<sup>15,43</sup> One possible explanation for this discrepancy is a difference in the phase (i.e. liquid vs. solid vs. semi-solid) between the substrates investigated in our work and the oleic-acid containing particles in the atmosphere.<sup>71,75,175-180</sup> One of the main sources of oleic acid in the atmosphere is meat cooking operations. The phase behaviour for these multicomponent particles is not well understood, but based on thermodynamic arguments these particles are likely solid-liquid mixtures.<sup>75</sup> In solid-liquid mixtures the lifetime of the oleic acid can be much longer due to trapping of the oleic acid by the solid structure. This has been shown previously for  $\text{O}_3$  reactions with oleic acid containing particles.<sup>71,75,175-180</sup> Other possible explanations for the difference between the laboratory studies and the field measurements are a difference in diffusion and solubility of  $\text{NO}_3$  in the pure oleic acid compared to oleic acid containing particles in the atmosphere.<sup>175,176,181</sup> Note that although meat cooking aerosols are likely solid-liquid mixtures, a majority of organic particles in the atmosphere are likely liquid, since in most aerosols the concentration of any specific organic is small.<sup>182</sup>

Figure 7.6, Panel b, shows that the oxidation lifetimes associated with  $\text{NO}_3$  and  $\text{N}_2\text{O}_5$  are comparable (or shorter) than the residence time of aerosol particles in the atmosphere. Also, the oxidation lifetimes associated with  $\text{NO}_3$  and  $\text{N}_2\text{O}_5$  are shorter than the oxidation lifetime associated with OH. OH heterogeneous chemistry has received a lot of attention recently, but our results show that  $\text{NO}_3$  and  $\text{N}_2\text{O}_5$  are competitive with OH for DES-like molecules.

Figure 7.6, Panel c, shows that the loss of alcohols with respect to  $\text{N}_2\text{O}_5$  heterogeneous reactions is short compared to the residence time of aerosol particles in the atmosphere. Glycerol has three OH-groups which probably enhance its reactivity compared to alcohols with only one OH-group. Studies of the reactive uptake coefficient of  $\text{N}_2\text{O}_5$  on other alcohols (including molecules with only one OH functional group) would be interesting.



The results in Figure 7.6 were calculated for three specific molecules. More work is obviously needed to determine if these results apply to other unsaturated and saturated organics and to atmospheric aerosol particles. Also, the discrepancies between our work and the work by Moise et al.<sup>44</sup> need to be resolved. However, until more data is available, the results shown in Figures 7.3 and 7.4 may be useful for estimating at least an upper limit to the importance of  $\text{NO}_3$  and  $\text{N}_2\text{O}_5$  on the lifetime of organic species in atmospheric aerosols.

#### **7.4.2 Importance of these Heterogeneous Reactions to Secondary Organic Aerosol (SOA) Studies**

One area where these heterogeneous reactions may be important is in SOA experiments with  $\text{NO}_3$  radicals. In these studies  $\text{NO}_3$  heterogeneous reactions may occur during secondary organic aerosol formation and aging. To illustrate this point we refer to a recent SOA study by Ng et al.<sup>183</sup> These authors studied the SOA formation from reactions of isoprene with nitrate radicals using  $\text{NO}_3$  concentrations of approximately 140 ppt. These authors speculated that heterogeneous reactions may have been important in their studies. Here we use our new reactive uptake results to support this suggestion.

We assume here that in general SOA particles are liquid and that the results from our studies are applicable to particles generated in SOA studies. This of course needs to be verified in future studies, but this analysis is still insightful for estimating an upper limit to the importance of  $\text{NO}_3$  heterogeneous chemistry in SOA laboratory experiments.

To estimate if  $\text{NO}_3$  heterogeneous reactions may be important in the SOA studies conducted by Ng et al.,<sup>183</sup> we calculated the oxidation lifetime of unsaturated and saturated organic molecules in the condensed-phase using eq 7.6 and a particle diameter of 200 nm. For these calculations of the oxidation lifetime we used the reactive uptake coefficient for oleic acid and DES determined in our studies, respectively. Using eq 7.6, we calculated oxidation lifetimes of 7.6 min and 18.2 hours for unsaturated and saturated organics, respectively. The experimental time used by Ng et al. was approximately 1 – 2 hours, so heterogeneous reactions between  $\text{NO}_3$  and saturated organics likely did not play an important role (at least not based on our DES reactive uptake coefficients). However, for the unsaturated organic, the oxidation lifetime is much shorter than the

experimental time, suggesting heterogeneous reactions may have been important. Unsaturated organics were suggested products of the SOA chemistry by Ng et al. Some of these unsaturated organics may have partitioned into the condensed phase and reacted by heterogeneous chemistry as suggested by Ng et al.

### 7.4.3 Oxidation Timescale for Surface Organics

Calculations from section 7.4.1 and 7.4.2 correspond to oxidation of liquid particles. Here we calculate the oxidation timescale for a solid organic surface under atmosphere conditions. To calculate this surface oxidation timescale we use the following equation:<sup>46</sup>

$$7.7 \quad \tau_{solid} = \frac{4N_{tot}}{\gamma c_{avg} [oxidant]}$$

where  $\tau_{solid}$  is the oxidation lifetime of a solid surface, i.e. the time after which 63% of the surface molecules are oxidized, and  $N_{tot}$  is the number of organic molecules at the surface of the aerosol particle. For these calculations we used the reactive uptake coefficient determined for the solids in this study and an  $N_{tot}$  value of  $1 \times 10^{14}$  molecule  $\text{cm}^{-2}$ . For oxidant concentrations, we used the same concentrations as in section 7.4.1 (50 ppt for  $\text{NO}_3$ , 5 ppb for  $\text{N}_2\text{O}_5$ , and 0.04 ppt for OH).

The results for these calculations are shown in Table 7.3. The trends are similar to the trends observed for the liquid, but the oxidation timescales are shorter, since in this case only the surface is oxidized. This suggests that many surface-bound organic species could be rapidly oxidized under certain atmospheric conditions.

**Table 7.3: Atmospheric lifetimes ( $\tau$ ) of solid surfaces with respect to oxidation by  $\text{NO}_3$ ,  $\text{N}_2\text{O}_5$ , or  $\text{OH}$  at 0 °C. It is assumed that the whole surface consists only of the corresponding organic (oleic acid or DES). The number of organic molecules at the surface is assumed to be  $1 \times 10^{14}$  molecule  $\text{cm}^{-2}$ . The uptake coefficients used in the calculations are given in parenthesis under the calculated lifetimes. Uptake coefficients for  $\text{NO}_3$  and  $\text{N}_2\text{O}_5$  are from this study,  $\gamma_{\text{OH}}$  with oleic acid and DES are from Bertram et al.<sup>67</sup> Their values reported for a vinyl-terminated and a methyl-terminated monolayer were used as  $\gamma_{\text{OH}}$  with oleic acid and DES, respectively.**

	[oxidant]	oleic acid	DES
$\text{NO}_3$	50 ppt	2.9 min	8.1 h
		(0.06)	( $3.6 \times 10^{-4}$ )
$\text{N}_2\text{O}_5$	5 ppb	4.1 h	11.3 h
		( $9.4 \times 10^{-6}$ )	( $3.4 \times 10^{-6}$ )
$\text{OH}$	0.04 ppt	3.8 h	3.8 h
		(0.5)	(0.5)

## 7.5 Summary and Conclusions

Reactions of  $\text{NO}_3$  on a liquid alkenoic acid (oleic acid) were determined to be very fast with a reactive uptake coefficient at the diffusion limit ( $\gamma \geq 0.07$ ). This is much higher than previously reported uptake coefficients of unsaturated compounds with  $\text{NO}_3$ . Reactions of the saturated compounds (DES and glycerol) were about two orders of magnitude lower in  $\gamma$ . Reactions of  $\text{N}_2\text{O}_5$  on liquid glycerol were found to be relatively fast ( $\gamma$  ranged from  $4 \times 10^{-4}$  to  $8 \times 10^{-4}$ ).  $\text{N}_2\text{O}_5$  reactive uptake on oleic acid and DES were found to be similar and significantly slower than on the polyalcohol. Both oleic acid and DES showed a slower reaction of the solid surface compared to the liquid film both for  $\text{NO}_3$  and  $\text{N}_2\text{O}_5$ . Because of the high viscosity of glycerol, we suggest that reaction on glycerol occurs mostly at the surface (even on a liquid), while liquid oleic acid and DES have significant bulk reaction contributing to the overall loss of the gas-phase species.

For heavily polluted tropospheric concentrations, we estimated atmospheric lifetimes of purely organic liquid particles and solid aerosol surfaces with respect to  $\text{NO}_3$ ,  $\text{N}_2\text{O}_5$ , and  $\text{OH}$ . The lifetime of oleic acid due to  $\text{NO}_3$  reaction is very short (on the order of minutes). Although lifetimes calculated for the other two compounds and those determined for  $\text{N}_2\text{O}_5$  are considerably longer, these reactions may still be of atmospheric relevance and contribute to the heterogeneous loss of saturated and unsaturated

hydrocarbons and alcohols. In particular, the reactive loss of glycerol with  $\text{N}_2\text{O}_5$  was relatively fast. Studies of the reactions of hydroxyl groups with  $\text{N}_2\text{O}_5$  are scarce and research investigating uptakes or products from reaction of other alcohols with  $\text{N}_2\text{O}_5$  would be important.

## 8 PRODUCTS OF THE REACTIONS OF AN ALKANE MONOLAYER WITH NO<sub>3</sub> RADICALS

### 8.1 Introduction

This Chapter and the following Chapter 9 focus on the heterogeneous reaction of NO<sub>3</sub> on self-assembled monolayers (SAMs) that serve as surrogates for organic aerosol surfaces. Organic material in the atmosphere can be in the form of purely organic aerosol particles, or alternatively the organic substances can be mixed with inorganic material. In the latter case, the organic material can form coatings on the surface of aqueous particles<sup>20,23</sup> or coatings adsorbed on the surface of solid particles, such as mineral dust.<sup>24</sup> As outlined in Chapter 2, these organic surface coatings or films on aerosols form the interface between these particles and the atmosphere and therefore are the primary reactive site in heterogeneous atmospheric reactions. Depending on the density or degree of compression of these films or coatings, they may also limit the transfer of molecules across the air-aqueous interface, and hence reduce reaction rates between gas-phase species and the aqueous phase. While in the atmosphere, organic particles and organic surfaces can be modified by reactions with atmospheric oxidants such as O<sub>3</sub>, NO<sub>3</sub>, and OH.<sup>23,80</sup> These heterogeneous reactions are expected to change the hygroscopicity and toxicity of these particles and surfaces.

Heterogeneous reactions may decompose organic surface molecules and therefore change the properties of this “barrier” between gas phase and aqueous phase. It is expected that the kinetics and reaction mechanisms of chemical processes occurring at the interface of two phases are different from the corresponding homogeneous reactions<sup>48</sup> or reactions between a gas-phase reactant and the bulk of a solid or liquid substrate. This makes surface chemistry of special interest in understanding and characterizing atmospheric chemical processes.

The study described in this Chapter used monolayers of an alkanethiol on gold as proxies for organic aerosol surfaces. Specifically, we investigate the heterogeneous reactions between NO<sub>3</sub> radicals and 1-octadecanethiol (C<sub>18</sub>H<sub>38</sub>S).

Octadecanethiol forms a methyl-terminated, C<sub>18</sub> alkane monolayer in self-assembly via a bond between the sulfur atom and the underlying gold substrate. It is believed that the first step in the self-assembly process is the bond cleavage between S and H in the thiol, followed by chemisorption of the thiol to the gold substrate by formation of a covalent S-Au bond. The interaction of the alkane chains occurs through van der Waals forces.<sup>184</sup> The formation of the S-Au bond takes place rapidly, while the straightening of the carbon chains and the reorientation of the terminal methyl groups are significantly slower processes.<sup>184</sup> The resulting density of alkanethiol monolayers on gold is  $4.6 \times 10^{14}$  molecule cm<sup>-2</sup>.<sup>114,184</sup> These monolayers are tilted by 26 – 30° from the surface normal,<sup>185,186</sup> which results in a total thickness of an ODT monolayer of 22 Å.<sup>187</sup>

We use this SAM as a surrogate for organics adsorbed on solid substrates such as mineral dust particles or urban surfaces in the atmosphere.<sup>24,188</sup> The SAM surface may also serve as a proxy for solid organic particles in the atmosphere and a rough model for some types of organic coatings on aqueous particles in the atmosphere. Studies with this monolayer enabled us to probe the reactive processes that are confined to the gas-surface interface, and to separate surface and bulk processes.<sup>80</sup> The results from these studies may provide insight into the reactivity of organics adsorbed on solid substrates such as mineral dust particles or urban surfaces,<sup>24,121,188,189</sup> and the reactivity of organic coatings on aqueous particles.<sup>23</sup> They may also provide insight into the reactivity of solid surfaces.<sup>48</sup>

We used a flow tube reactor coupled to a chemical ionization mass spectrometer (CIMS) (described in Chapter 5) to expose these monolayers to NO<sub>3</sub>. X-ray photoelectron spectroscopy (XPS, see Chapter 5.3) was used to investigate surface oxidation and to determine if exposure of NO<sub>3</sub> (in the presence of O<sub>2</sub>) leads to volatilization of the organic substrate. These experiments were motivated by a recent study by Molina et al.<sup>56</sup> Using atmospherically relevant exposures of OH, these authors showed that OH-initiated oxidation of alkane self-assembled monolayers (in the presence of O<sub>2</sub>, NO<sub>x</sub>, and H<sub>2</sub>O) leads to rapid volatilization of the organic substrate. Moise and Rudich also studied

heterogeneous reactions on self-assembled alkane monolayers and observed partial loss of the organic surface after exposure to Cl and Br radicals in the presence of O<sub>2</sub>.<sup>46</sup> In the gas phase, the mechanisms of the reactions between NO<sub>3</sub>, OH, Cl, and Br radicals with alkanes are similar (all involve alkyl, alkoxy, and alkylperoxy radicals). However, the NO<sub>3</sub> + alkane reaction in the gas phase is slower compared to gas-phase reactions between OH + alkanes and Cl + alkanes. If the NO<sub>3</sub> + alkane reaction rate on and in the organic monolayer is significantly enhanced compared to equivalent reactions in the gas phase, it seems reasonable to speculate that NO<sub>3</sub> will lead to volatilization of alkane monolayers using atmospherically relevant exposures. Some studies suggest that heterogeneous reactions can lead to rapid volatilization of organic particulate matter.<sup>56,154,190</sup> The reactions may be a significant sink for organic particles<sup>56</sup> and a major source of volatile organic compounds (VOC) in the atmosphere.<sup>23,57</sup> Other studies suggest that under certain conditions these radical heterogeneous reactions may not be a significant source of VOC material.<sup>46,63,69,70</sup> Due to the importance of this process and the insufficient data available, a focus of the SAM studies presented in this thesis was the investigation of potential monolayer loss upon exposure to NO<sub>3</sub>.

In addition to XPS, we used infrared (IR) spectroscopy, time-of-flight secondary ion mass spectrometry (ToF-SIMS), and H<sub>2</sub>O contact angle measurements to further characterize the reacted surfaces and the condensed-phase products. This is an important step toward understanding the mechanism of these reactions and toward determining possible differences in mechanisms for homogenous reactions, reactions of NO<sub>3</sub> in the bulk of a particle, and reactions occurring at the interface itself.

In our experiments, as mentioned above, the NO<sub>3</sub> reactions were performed in the presence of O<sub>2</sub> and NO<sub>2</sub> (NO<sub>2</sub> is a by-product of the method of producing NO<sub>3</sub>). This should complement several previous radical-organic heterogeneous studies which were carried out free of NO<sub>2</sub>. An understanding of the effect of NO<sub>2</sub> concentrations may help explain some of the discrepancies in the literature on radical-organic heterogeneous reactions and they are expected to be of atmospheric relevance, since many atmospheric conditions have high NO<sub>2</sub> concentrations.<sup>1</sup>

## 8.2 Experimental

### 8.2.1 Chemicals

1-Octadecanethiol (98%,  $C_{18}H_{38}S$ , ODT) was purchased from Sigma-Aldrich and used without further purification.  $NO_2$  (99.5%) was purchased from Matheson,  $N_2$  (99.999%),  $O_2$  (99.993%) and He (99.999%) were purchased from Praxair.  $N_2O_5$  and  $NO_3$  were generated as described above (Chapter 6.2). Note that the dissociation of  $N_2O_5$  was almost complete with residual  $N_2O_5$  concentrations in the flow cell of approximately 1 – 3% of  $NO_3$  concentrations.

### 8.2.2 Monolayer Preparation

Monolayers were prepared on gold coated silicon (100) wafers. Gold coatings were 100 nm thick. These wafers were first cleaned in piranha solution ( $H_2SO_4$  (96%) /  $H_2O_2$  (30%) = 3:1) for approximately 15 min, then rinsed with Millipore water (18 M $\Omega$ ) and distilled ethanol. The wafers were then immersed in a 1 mM solution of ODT in distilled ethanol for  $\geq 24$  h.<sup>191</sup> Following this, the samples were cleaned in ethanol using an ultrasonic bath for 1 minute and rinsed with Millipore water for approximately 3 minutes. This cleaning procedure was repeated two more times. SAM coated gold surfaces were then dried under a stream of ultra high purity  $N_2$ .

### 8.2.3 Product Studies as a Function of Exposure

The flow reactor was used to expose SAMs on Au coated Si plates to  $NO_3$  for subsequent XPS, IR,  $H_2O$  contact angle, and ToF-SIMS analysis. The flow cell walls were covered with a Teflon sheet to avoid contact between  $NO_3$  and the glass walls.  $NO_3$  exposure levels ranged from 0 –  $9.3 \times 10^{-5}$  atm sec (an exposure of 0 – 21 days at 50 ppt  $NO_3$ ). Experiments were performed at 298 K, at a pressure of 2.3 – 2.7 torr, using  $NO_3$  concentrations of  $(1 - 5) \times 10^{11}$  molecule  $cm^{-3}$  and  $O_2$  concentrations of  $(1.1 - 1.6) \times 10^{16}$  molecule  $cm^{-3}$ . Helium was used as carrier gas for  $NO_3$ . At the exit of the flow cell,  $N_2O_5$  and  $NO_3$  were detected using chemical ionization with either  $I^-$  or  $SF_6^-$  as the reagent ion. XPS, IR and ToF-SIMS were then used to monitor the oxidation of the monolayer and to identify surface products.  $H_2O$  contact angle measurements were used to determine the hydrophilicity of the monolayer.



Note that in our experiments we were using relatively high NO<sub>3</sub> concentrations ( $(1 - 5) \times 10^{11}$  molecule cm<sup>-3</sup>), whereas in the atmosphere NO<sub>3</sub> concentrations are lower (roughly  $1 \times 10^9$  molecule cm<sup>-3</sup> depending on time and location). Due to experimental constraints it was not possible to use lower NO<sub>3</sub> concentrations in our experiments. In order to extrapolate our results to the atmosphere, we assume that the only important parameter is the total number of collisions between NO<sub>3</sub> radicals and the surface. This, however, requires verification in future experiments.

#### **8.2.4 XPS, IR, ToF-SIMS, and Contact Angle Measurements**

XPS measurements were performed on a Leybold instrument using an achromatic Al K $\alpha$  X-ray source at a photon energy of 1486.6 eV and an electron take-off angle of 90°. Infrared measurements were performed with a Bruker FTIR microscope equipped with a grazing angle objective in the wavenumber range 7000 - 500 cm<sup>-1</sup> (2048 scans per spectrum, 4 cm<sup>-1</sup> resolution). These measurements were done at 1 atm under a purge flow of dry purified air. Time-of-flight secondary ion mass spectrometry (ToF-SIMS) was done using a Physical Electronics, PHI TRIFT II ToF-SIMS instrument with a 15 keV Ga<sup>+</sup> primary ion beam (mass resolution  $\geq 9000$ ). The pulse duration was 5 ns with a current of 500 pA. Sample areas of  $100 \times 100 \mu\text{m}^2$  were irradiated, total MS acquisition time was 10 min, and negative ion spectra were obtained. The total ion dose was well below the static limit. Contact angle estimates were obtained from camera images of a H<sub>2</sub>O droplet (Millipore, 18 M $\Omega$ , static) on unreacted ODT monolayers and SAMs exposed to NO<sub>3</sub>.

### **8.3 Results and Discussion**

#### **8.3.1 X-ray Photoelectron Spectroscopy**

Figure 8.1 shows the C(1s) region of the XPS spectra obtained for different NO<sub>3</sub> exposures. The increasing shoulder at higher binding energies within the C(1s) region that appears with increasing NO<sub>3</sub> exposure indicates the oxidation of the organic surface. For the unexposed sample only one peak at 285 eV was observed. This peak is due to methyl or methylene functional groups. After exposure to NO<sub>3</sub>, the main peak at about

285 eV remains, but a shoulder was observed at higher energies. We fit the total C(1s) region with four overlapping Gaussian-Lorentzian peaks. In Fig. 8.1(b) an enlarged view of the C(1s) region obtained with a NO<sub>3</sub> exposure of  $9.3 \times 10^{-5}$  atm sec is shown as well as the Gaussian-Lorentzian fits to the data. Note that using four peaks gave superior fitting results compared to using three peaks. The chemical shifts discussed here were obtained from the fitting procedure of all XPS spectra and are given as average values with standard deviations. The chemical shift of about  $1.5 \pm 0.5$  eV is consistent with the formation of C-O or C-O-O functional groups on the surface.<sup>112</sup> The chemical shift at about  $3.1 \pm 0.6$  eV is consistent with ketones or aldehydes, and the shift at approximately  $4.7 \pm 0.5$  eV is consistent with carboxylic groups.<sup>112</sup>

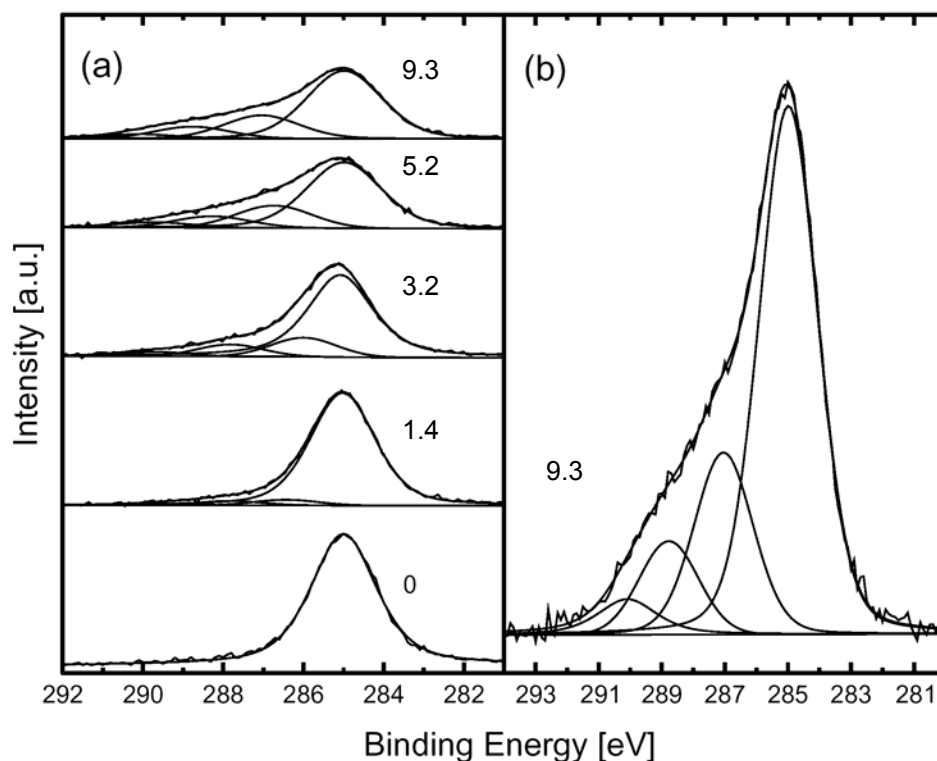


**Figure 8.1:** Panel (a) shows XPS spectra of the C(1s) region for an ODT monolayer exposed to NO<sub>3</sub> concentrations of 0 -  $9.3 \times 10^{-5}$  atm sec. Also included are the Gaussian-Lorentzian peaks from the fitting procedure. The spectra are shifted vertically for better visibility. Panel (b) shows an enlarged view of the best fit of the C(1s) region for an ODT monolayer exposed to NO<sub>3</sub> concentrations of  $9.3 \times 10^{-5}$  atm sec. Numbers in panels represent exposure levels in  $10^{-5}$  atm sec.

To assess the amount of volatilization of the organic surface, we have plotted in Figure 8.2(A) the atomic ratio of the total carbon ( $C_{\text{total}}$ ) to the total gold (Au) derived from the integrated C(1s) and Au(4f) intensities and the necessary atomic sensitivity factors. The error bars (which represent  $\pm 1 \sigma$ ) were derived from 4 independent exposure experiments of ODT using equal  $\text{NO}_3$  concentrations. A linear fit to the data shown in Figure 8.2(A) gives a maximum carbon loss of about 7.5% (with 95% confidence) for  $\text{NO}_3$  exposures of  $3.02 \times 10^{-5}$  atm sec (which represents one week at 50 ppt  $\text{NO}_3$ ). Based on this, we suggest that  $\text{NO}_3$  does not lead to rapid volatilization of organic monolayers under atmospheric conditions.

To determine the fraction of the carbon oxidized as a function of time, we calculated the atomic ratio of the oxidized carbon ( $C_{\text{ox}}$ ) to  $C_{\text{total}}$ , both determined from the fits shown in Figure 8.1(a). These ratios are plotted in Figure 8.2(C). Figure 8.2(C) suggests that approximately 17% of the alkyl chain is oxidized for  $\text{NO}_3$  exposures of  $3.02 \times 10^{-5}$  atm sec. It should be noted that exposure of the organic monolayer solely to  $\text{O}_2$  concentrations of about  $10^{16}$  molecule  $\text{cm}^{-3}$  did not lead to oxidation of the monolayer.

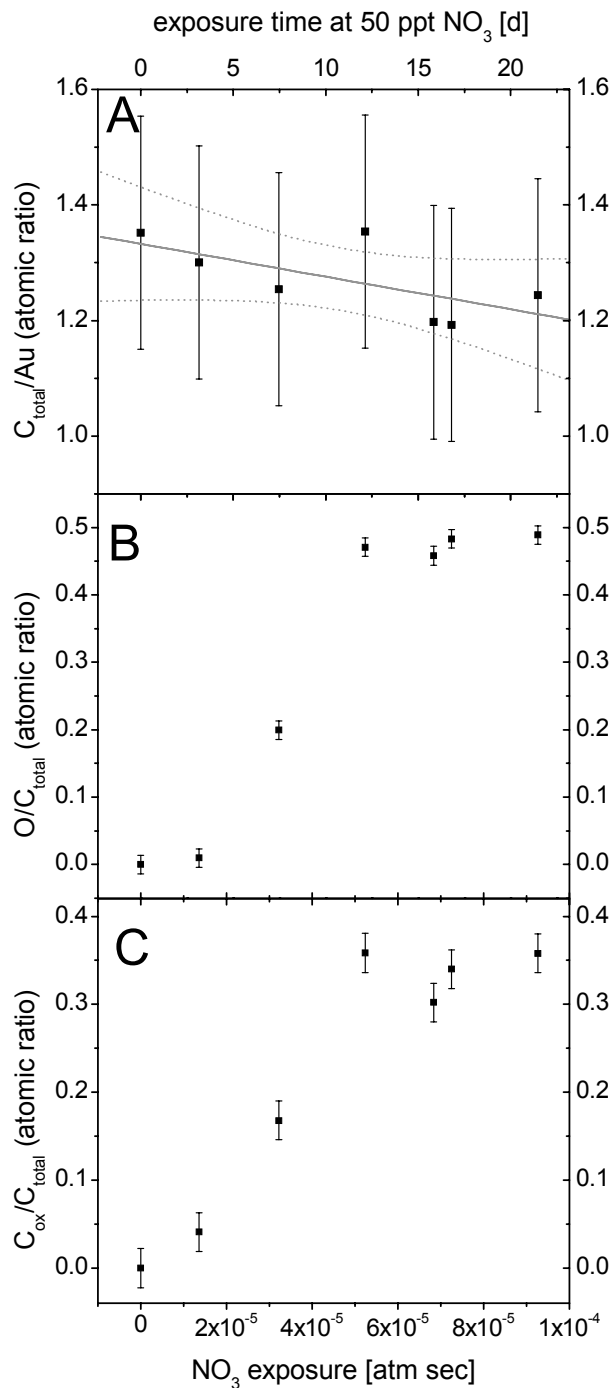


**Figure 8.2: A summary of the XPS results. Panel (A): the atomic ratio of the total carbon,  $\text{C}_{\text{total}}$ , to total gold, Au. The solid line is a linear fit to the data, and the dashed lines correspond to the 95% confidence limit. Panel (B): the atomic ratio of total oxygen, O, to  $\text{C}_{\text{total}}$  as a function of  $\text{NO}_3$  exposure. Panel (C): the atomic ratio of oxidized carbon,  $\text{C}_{\text{ox}}$ , to  $\text{C}_{\text{total}}$  determined by fitting the C(1s) spectrum with Gaussian-Lorentzian peaks (see text for further details).**

From the XPS data, we also calculated the atomic ratio of total oxygen (O) to  $C_{\text{total}}$  as a function of  $\text{NO}_3$  exposure, as determined from the integrated O(1s) and C(1s) intensities and the respective atomic sensitivity factors. The results of these calculations are plotted in Figure 8.2(B) and suggest that the atomic O/ $C_{\text{total}}$  ratio is approximately 0.2 after an exposure of  $3.02 \times 10^{-5}$  atm sec. Both Figures 8.2(B) and 8.2(C) show that  $\text{NO}_3$  led to oxidation of the organic surface using atmospherically relevant exposures.

In addition to monitoring the C(1s) and O(1s) signals, we also monitored the N(1s) signal; however, the XPS measurements only show a very small N(1s) signal. About 1% of the total surface elemental composition has been assigned as nitrogen based on the N(1s) signal at  $\text{NO}_3$  exposures higher than  $3.2 \times 10^{-5}$  atm sec. The binding energy of the N(1s) signal could be attributed to a nitrate group. We have also monitored the S(2p) signal from the monolayer. At exposures less than  $3 \times 10^{-5}$  atm sec, the sulfur is not oxidized. At long exposures of approximately  $8 \times 10^{-5}$  atm sec, the sulfur is oxidized to sulfonate due to reactions with  $\text{NO}_3$ . This, however, can account for only a small amount of the O(1s) signal in the XPS spectrum.

### 8.3.2 IR-Spectroscopy

Grazing angle IR measurements were performed on ODT SAMs that had been exposed to  $\text{NO}_3$  radicals. Listed in Table 8.1 are possible nitrogen species that may form during the  $\text{NO}_3$  chemistry (in the presence of  $\text{O}_2$  and  $\text{NO}_2$ ) and the corresponding IR transition frequencies. For our analysis we only focused on the IR regions from 3000 – 2800  $\text{cm}^{-1}$  and 1700 – 1200  $\text{cm}^{-1}$ . The 3000 – 2800  $\text{cm}^{-1}$  region corresponds to the C-H stretching region. The 1700 – 1200  $\text{cm}^{-1}$  region covers a frequency range where several of the possible nitrogen species have transitions. We did not include in this analysis the regions above 3000  $\text{cm}^{-1}$ , between 2800 – 1700  $\text{cm}^{-1}$ , and below 1200  $\text{cm}^{-1}$  because assigning the baseline in these regions was often difficult and subjective due to large baseline fluctuations, low peak intensities, and interference by water vapour peaks in some areas. Shown in Figure 8.3 are typical results.  $\text{NO}_3$  exposures used in this study were  $3.6 \times 10^{-5}$  atm sec, which is equal to 50 ppt for 8.4 days. 50 ppt (24 hour average) corresponds roughly to polluted conditions. Based on the XPS data shown in Figure 8.2 the amount of carbon oxidation with this exposure was about 20%. The spectrum shown

in Figure 8.3 corresponds to  $(I_{\text{unoxidized}} - I_{\text{oxidized}})/I_{\text{unoxidized}}$ , where  $I_{\text{oxidized}}$  and  $I_{\text{unoxidized}}$  correspond to the intensity of the reflected light from the oxidized and unoxidized film, respectively. The resulting plot is proportional to the difference in the absorbance of the two samples. The results from Figure 8.3 show first that the  $\text{NO}_3$  reaction led to the disappearance of the  $\text{CH}_3$  and  $\text{CH}_2$  groups, which is consistent with the oxidation of the organic chain. Figure 8.3 also shows the appearance of new peaks at  $1643 \text{ cm}^{-1}$  and  $1282 \text{ cm}^{-1}$  after exposure to  $\text{NO}_3$ . The presence of these peaks is consistent with the formation of organonitrates ( $\text{RONO}_2$ ) (see Table 1). Organonitro ( $\text{RNO}_2$ ) groups, peroxy nitrates ( $\text{ROONO}_2$ ), and peroxyacylnitrate surface species were not identified in the IR data. Peroxy nitrates and peroxyacylnitrates are expected to have a short lifetime. Hence, these species may have been lost when transferring the substrates to the analytical instruments for surface analysis.

**Table 8.1: Peak assignment for IR spectroscopy of different nitrogen containing species (R = alkyl chain, PAN = peroxyacetylnitrate). Typical ranges of wavenumbers [ $\text{cm}^{-1}$ ] and references are provided.**

Assignment	Peak Position [ $\text{cm}^{-1}$ ]	Reference
RNO <sub>2</sub>	1580 – 1540	Allen et al., 1994; Hung et al., 2005; Jang and Kamens, 2001; Lai and Finlayson-Pitts, 1991; Tuazon et al., 1999; Williams and Fleming, 1989 <sup>66,153,192-195</sup>
	1390 – 1340	Hung et al., 2005; Jang and Kamens, 2001; Tuazon et al., 1999; Williams and Fleming, 1989 <sup>66,193-195</sup>
RONO <sub>2</sub>	1666 – 1600	Allen et al., 1994; Alvarado et al., 1999; Atkinson et al., 1998; Hallquist et al., 1999; Hung et al., 2005; Jang and Kamens, 2001; Lai and Finlayson-Pitts, 1991; Palen et al., 1992; Tuazon et al., 1999; Williams and Fleming, 1989 <sup>66,153,192-199</sup>
	1286 – 1250	Allen et al., 1994; Alvarado et al., 1999; Atkinson et al., 1998; Cassanelli et al., 2006; Hallquist et al., 1999; Hung et al., 2005; Palen et al., 1992; Tuazon et al., 1999; Williams and Fleming, 1989 <sup>66,192,194-200</sup>
	862 – 843	Allen et al., 1994; Alvarado et al., 1999; Atkinson et al., 1998; Cassanelli et al., 2006; Hallquist et al., 1999; Hung et al., 2005; Palen et al., 1992; Tuazon et al., 1999 <sup>66,192,194,196-200</sup>
ROONO <sub>2</sub>	1724 – 1721	Hallquist et al., 1999; Tuazon et al., 1999 <sup>194,198</sup>
	1298 – 1296	Hallquist et al., 1999; Hung et al., 2005; Tuazon et al., 1999 <sup>66,194,198</sup>
	797 – 789	Hallquist et al., 1999; Tuazon et al., 1999 <sup>194,198</sup>
PAN	1842 – 1830	Allen et al., 2005; Atkinson et al., 1998 <sup>197,201</sup>
	1741 – 1738	Allen et al., 2005; Atkinson et al., 1998 <sup>197,201</sup>
	1302 – 1300	Allen et al., 2005; Atkinson et al., 1998 <sup>197,201</sup>
	794	Allen et al., 2005; Atkinson et al., 1998 <sup>197,201</sup>

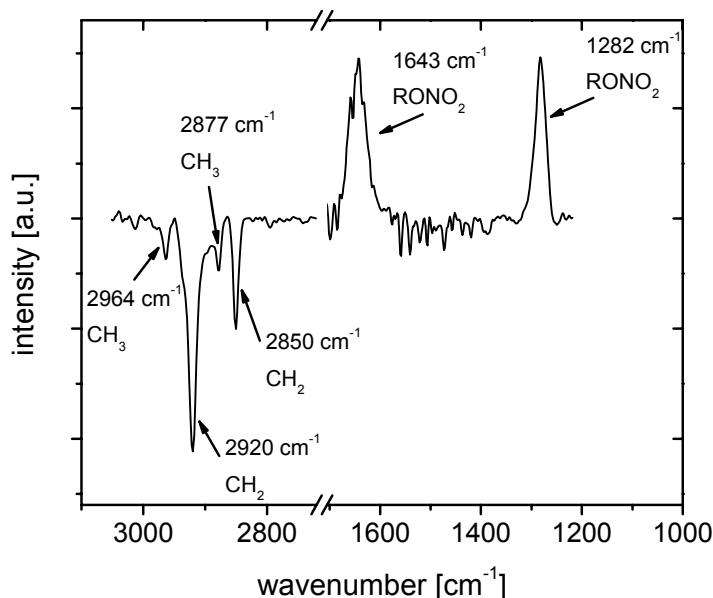


**Figure 8.3: ODT IR spectrum calculated from an ODT sample exposed to  $3.6 \times 10^{-5}$  atm sec of  $\text{NO}_3$  and an unoxidized ODT SAM as reference sample (see text). Negative peaks correspond to features only present or more prominent in the unexposed ODT SAM, positive peaks show features only present or more prominent in the exposed ODT SAM.**

The observation of organonitrate peaks in the IR spectrum is in contrast to the XPS data, which showed very little N(1s) signal. This suggests that the organonitrates decomposed during the XPS measurements. To investigate this further we exposed an ODT monolayer to  $\text{NO}_3$  (exposure level =  $9.06 \times 10^{-5}$  atm sec). We then recorded an IR spectrum of the sample, followed by an XPS spectrum, followed by another IR spectrum. In the first IR spectrum negative peaks in the region from 3000 to 2800  $\text{cm}^{-1}$  were observed due to the disappearance of  $\text{CH}_3$  and  $\text{CH}_2$  surface species, and positive peaks at 1643  $\text{cm}^{-1}$  and 1282  $\text{cm}^{-1}$  were observed due to the formation of alkylnitrates, similar to Figure 8.3. However, in the second IR spectrum (after the XPS measurements) the 1643  $\text{cm}^{-1}$  and 1282  $\text{cm}^{-1}$  peaks were strongly diminished in intensity, while features characteristic of  $\text{CH}_3$  and  $\text{CH}_2$  remained unchanged. This provides further evidence that the N-containing functional groups decomposed during XPS analysis. In general, XPS is considered non-destructive, but some damage to sensitive material has been reported before.<sup>116,202,203</sup> A comparison between the average bond energies shows that O-N bonds



(201 kJ mol<sup>-1</sup>) are much weaker than C-O (358 kJ mol<sup>-1</sup>) or C=O (799 kJ mol<sup>-1</sup>)<sup>204</sup> and therefore organonitrates should be much more prone to decomposition in XPS than the other functional groups expected in our experiments. Alcohols, carbonyl, and carboxyl groups have been analyzed successfully by XPS in the past<sup>205-207</sup> and are not expected to decompose due to the bond strengths.

### 8.3.3 ToF-SIMS Measurements

ToF-SIMS measurements were also carried out to confirm the formation of nitrate functional groups. Figure 8.4 shows negative ion ToF-SIMS spectra of an ODT monolayer prior to exposure to NO<sub>3</sub> (Panel a) and after exposure to NO<sub>3</sub> (Panel b). For these studies an exposure of  $5.4 \times 10^{-5}$  atm sec (equivalent to 50 ppt NO<sub>3</sub> for 12.6 days) was used. Based on the XPS data shown in Figure 8.2, approximately 35% of the carbon is oxidized with this exposure.

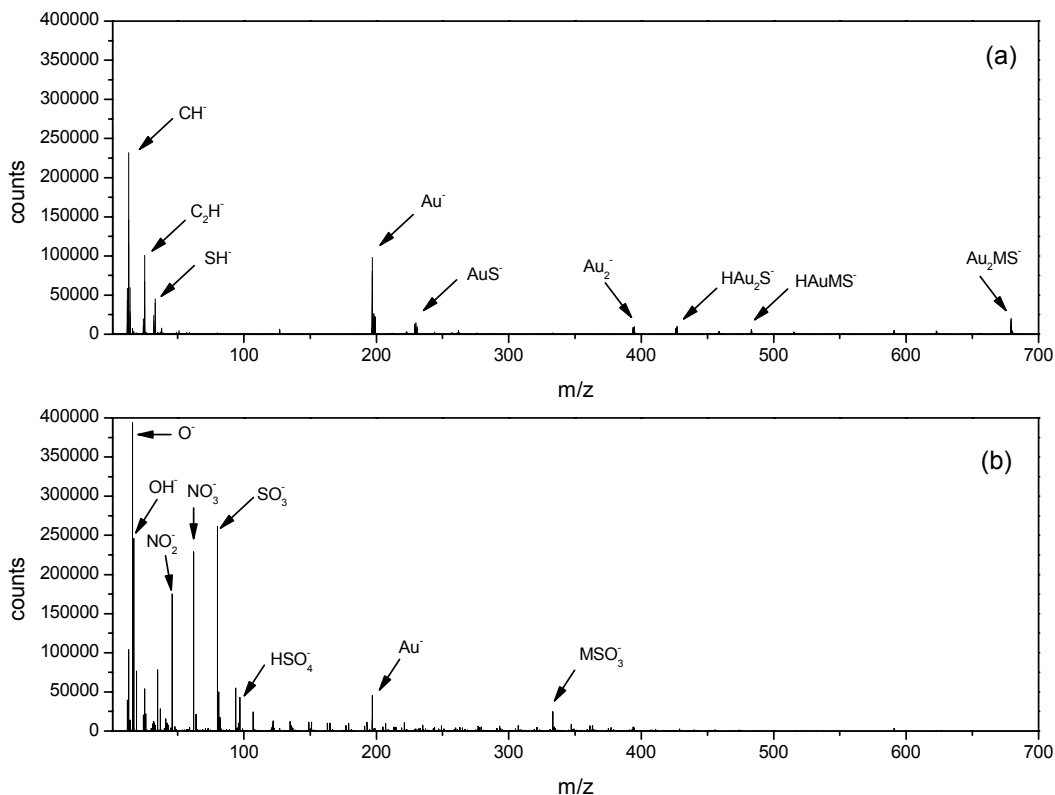


**Figure 8.4: Negative ion ToF-SIMS spectra of ODT on gold in the m/z 1 – 700 region. Spectrum (a) was obtained on an ODT sample without NO<sub>3</sub> exposure, spectrum (b) was obtained after an NO<sub>3</sub> exposure of  $5.4 \times 10^{-5}$  atm sec (equivalent to 50 ppt NO<sub>3</sub> for 12.6 days).**

Spectrum (a) – recorded before NO<sub>3</sub> exposure – shows mostly Au<sub>x</sub>S<sub>y</sub> clusters and low molecular weight fragments of the alkanethiol chains (C<sup>-</sup>, CH<sup>-</sup>, C<sub>2</sub>H<sup>-</sup>, S<sup>-</sup>, SH<sup>-</sup>), but also characteristic peaks for ODT. These peaks included the whole molecule of ODT and are labelled “MS” in the figure with “M” meaning C<sub>18</sub>H<sub>37</sub>. The observed peaks agreed well with those observed in previous ToF-SIMS measurements of alkanethiol SAMs on gold performed by Offord et al.,<sup>208</sup> Sun and Gardella,<sup>209</sup> and Sohn et al.<sup>210</sup>

Comparisons of ODT spectra (a) and (b) showed that after NO<sub>3</sub> exposure, peaks characteristic of the unoxidized hydrocarbon SAM (C<sup>-</sup>, CH<sup>-</sup>, C<sub>2</sub>H<sup>-</sup>, S<sup>-</sup>, SH<sup>-</sup>, HAuMS<sup>-</sup>, and Au<sub>2</sub>MS<sup>-</sup>) decreased or disappeared. New peaks with high intensities formed in the *m/z* region < 100 amu, which can be attributed to O<sup>-</sup>, OH<sup>-</sup>, NO<sub>2</sub><sup>-</sup>, NO<sub>3</sub><sup>-</sup>, SO<sub>3</sub><sup>-</sup>, and HSO<sub>4</sub><sup>-</sup>. Furthermore, a large number of additional peaks emerged in the *m/z* region > 100 amu, but with smaller intensities. These are most likely due to oxidized ODT molecules that fragmented during the sputtering process. Due to the high number of possible fragments in these long chain hydrocarbons, the wide variety of different oxidation levels, and the variety of different oxidation products, it was not possible to identify these products unambiguously.

The identification of NO<sub>2</sub><sup>-</sup> and NO<sub>3</sub><sup>-</sup> peaks by ToF-SIMS confirmed the formation of nitrogen containing species on the surface. These peaks are also consistent with the formation of organonitrates, which fragment to NO<sub>2</sub><sup>-</sup> and NO<sub>3</sub><sup>-</sup> during the sputtering process.

The combined evidence for the presence of organonitrates from IR and ToF-SIMS measurements clearly showed that these compounds were formed during reaction of ODT with NO<sub>3</sub> but were not stable in XPS analysis.

Spectrum (b) in Figure 8.4 also shows peaks due to SO<sub>3</sub><sup>-</sup> and HSO<sub>4</sub><sup>-</sup>. Oxidized sulfur likely results from oxidization of the sulfur group in the monolayer by NO<sub>3</sub> at high exposures. This is consistent with the XPS results that also showed oxidation of the sulfur group at NO<sub>3</sub> exposures greater than 3 × 10<sup>-5</sup> atm sec.

### 8.3.4 Contact Angle Measurements

Contact angles of H<sub>2</sub>O droplets on unexposed and NO<sub>3</sub> exposed ODT monolayers were obtained using camera images. Two exemplary images are shown in Figure 8.5. The

initial contact angle determined for ODT before NO<sub>3</sub> exposure was  $101^\circ \pm 4^\circ$  (error represents one standard deviation). Reported literature values for different long chain alkane monolayers (C<sub>8</sub> – C<sub>18</sub>) range from  $93^\circ$  to  $119^\circ$ .<sup>47,65,67,138,203,208,211-215</sup> These numbers show that our contact angle for ODT is in general agreement with literature values.

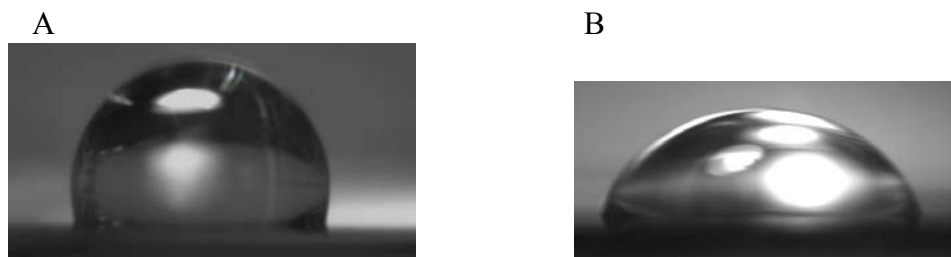


**Figure 8.5: Millipore grade H<sub>2</sub>O droplets on ODT monolayers before (image A) and after NO<sub>3</sub> exposure (equivalent to 50 ppt for 3 weeks, image B).**

ODT samples were exposed to  $9.06 \times 10^{-5}$  atm sec NO<sub>3</sub> (equivalent to 50 ppt for 21 days). This exposure can be seen as an extreme limit of aerosol exposure under polluted conditions. After this exposure, the contact angle on ODT was  $60^\circ \pm 6^\circ$ , a decrease by approximately  $41^\circ$ . This result is consistent with the monolayers becoming more hydrophilic due to oxidation. Previous studies investigating changes in H<sub>2</sub>O contact angles ( $\theta$ ) on hydrocarbon monolayers (C<sub>8</sub> – C<sub>20</sub>) after exposure to gas-phase reactants reported a very broad range of data for alkanes: after F radical exposure  $\theta = 82^\circ$ ,<sup>214</sup> after O<sub>3</sub> exposure  $\theta = 71^\circ$  and  $99^\circ$ ,<sup>65,213</sup> after OH exposure  $\theta = 10^\circ$ ,<sup>67</sup> and after O exposure  $\theta = \sim 35 - 45^\circ$ .<sup>138</sup> Part of the variability is likely due to the different exposure levels used in these experiments and also to different condensed phase products formed (e.g. hydroxyl groups versus carbonyl groups).

To put our values in an atmospheric context, we converted our contact angle results into cloud condensation nucleation activities. Based on data presented in Pruppacher and Klett,<sup>216</sup> an insoluble 200 nm (diameter) particle with  $\theta = 101^\circ$  will have a critical supersaturation ( $S_{\text{crit}} = \text{RH} - 100\%$ ) for water nucleation of  $> 150\%$ . In contrast, an insoluble 200 nm particle with  $\theta = 60^\circ$  will have a critical supersaturation of approximately 100%. This shows that the oxidation by NO<sub>3</sub> radicals can decrease the

critical supersaturation required for water nucleation. However, even after oxidation, the  $S_{\text{crit}}$  is still much larger than  $S_{\text{crit}}$  for water soluble particles. For example,  $S_{\text{crit}}$  for a 200 nm ammonium sulphate particle is less than 0.1%.<sup>49</sup> Also, typical values of supersaturations found in clouds are between about 0.2 and 2%.<sup>1</sup>

### 8.3.5 Proposed Reaction Mechanism

Shown in Figure 8.6 is the proposed mechanism for oxidation of an alkane monolayer by  $\text{NO}_3$  radicals in the presence of  $\text{O}_2$  and  $\text{NO}_2$  based on gas-phase chemistry. We use this as a starting point to discuss our data. We assume that the same reactions can occur on the SAM as in the gas phase, although the relative importance of the pathways can be significantly different on and in the organic monolayer compared to the gas phase. We use our experimental results to speculate on the importance of the different reaction pathways for the saturated hydrocarbon surfaces.

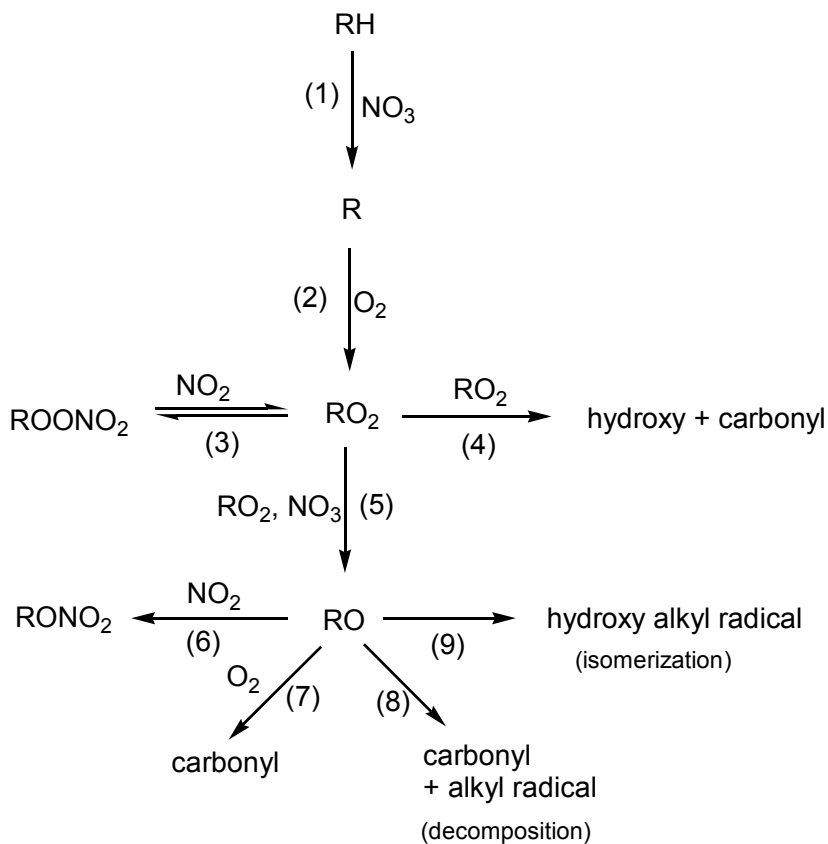


**Figure 8.6: Proposed reaction mechanism for an alkane surface with  $\text{NO}_3$  in the presence of  $\text{NO}_2$  and  $\text{O}_2$  based on gas-phase chemistry.**

As a reminder, XPS showed limited volatilization (i.e. loss of the carbon chain), and the formation of 1) C-O groups, 2) ketones or aldehydes, and 3) carboxylic groups. The IR spectra and ToF-SIMS showed the formation of organonitrates.

The initial reaction (step 1) in the oxidation process is the abstraction of a hydrogen atom from a methyl or methylene group of the alkyl chain to form  $\text{HNO}_3$  and an alkyl radical. Our experiments were not optimized to measure  $\text{HNO}_3$ , and as a result we were not able to determine if this product remained on the surface or evaporated during  $\text{NO}_3$  exposures.

The second reaction step is the transformation of an alkyl radical into a peroxy radical in the presence of  $\text{O}_2$ .<sup>40</sup> In the presence of  $\text{NO}_2$ , peroxy nitrates can form and may subsequently thermally decompose back to the reactants (step 3).<sup>40</sup> Hence peroxy nitrates represent a temporary reservoir of  $\text{NO}_2$ . The peroxy radical can also react with  $\text{NO}_3$  to form an alkoxy radical,  $\text{NO}_2$ , and  $\text{O}_2$  (step 5). Alternatively, the peroxy radical can undergo self reaction, leading to the formation of alkoxy radicals and  $\text{O}_2$  (step 5) or an alcohol and carbonyl (step 4).<sup>40</sup> In the gas phase, the branching ratio for the alcohol + carbonyl channel ranges from about 0.3 to 0.8 for primary and secondary radicals.<sup>40</sup> In the solution phase, however, the self reaction appears to proceed only through the alcohol + carbonyl channel for both primary and secondary radicals.<sup>217</sup> For tertiary radicals the alcohol + carbonyl channel is not accessible.<sup>40,217</sup> If the alkoxy radical forms, it can decompose by scission of a C-C bond (step 8), or can undergo isomerization to form a hydroxyl alkyl radical (step 9). Alternatively the alkoxy radical can react with  $\text{NO}_2$  to form alkyl nitrates (step 6) or react with  $\text{O}_2$  to form ketones or aldehydes (step 7).<sup>40</sup>

The presence of C-O, ketones, and aldehydes can be explained by step 4, step 7, or step 9. As mentioned above, the branching ratio for the alcohol + carbonyl channel ranges from about 0.3 to 0.8 in the gas phase, but in solution the  $\text{RO}_2$  self reaction appears to proceed only through the alcohol + carbonyl channel. Perhaps in our experiments, the self reaction also proceeds mainly through the alcohol + carbonyl channel. The presence of C-O, ketones, and aldehydes, could also be explained by the formation of an alkoxy radical followed by isomerization to form hydroxyalkyl radicals and reaction with  $\text{O}_2$  to form carbonyls. In terms of isomerization, alkoxy radicals could abstract a hydrogen from a neighbouring carbon chain to form C-OH groups.

Carboxylic functional groups observed in the XPS spectra are probably due to C(=O)O formed in secondary reactions, e.g. oxidation of aldehydes to acids (as reported by George et al.<sup>70</sup>).

The results in this manuscript (based on IR and ToF-SIMS data) show that organic nitrates are also a significant product of the heterogeneous oxidation. Organonitrates can be formed by step 6. Alternatively, it has been suggested that organoperoxy nitrates can decompose in the condensed phase to form organonitrates or carbonyls.<sup>63</sup> This pathway (not shown in Figure 8.6) may also be important in our monolayer studies for the production of organonitrates.

The identification of organonitrates in our oxidation studies may be important for a few reasons: first, the formation of organonitrates may explain why we did not see significant decomposition of the carbon chains. Even under extremely polluted conditions, i.e. high NO<sub>3</sub> exposure, the maximum loss of the organic layer we observed was only 10%. This is consistent with our results that show that the formation of organonitrates is a significant pathway. Formation of organonitrates removes RO<sub>2</sub> and/or RO species from the system, and hence will reduce the importance of the decomposition channel. Possibly this is one of the differences between our work with NO<sub>3</sub> and alkane monolayers and the recent studies with OH and alkane SAMs where significant decomposition was observed.

Second, the results suggest that under certain atmospheric conditions, radical-organic reactions may be a source of condensed-phase organonitrates. It is well known that condensation of gas-phase species is an important source of condensed-phase organonitrates. Also another possible source of particle-bound organonitrates is condensed-phase photochemistry.<sup>218</sup> Perhaps under certain conditions of high NO<sub>3</sub> and NO<sub>2</sub> concentrations the formation of condensed-phase organonitrates by radical-organic reactions may also contribute. Field measurements exploring this topic would be interesting.

Third, our results may also have implications for condensed-phase OH-organic reactions. Under many atmospheric conditions, NO<sub>2</sub> concentrations are high. Perhaps for these situations, organonitrates will also form by a mechanism similar to that seen in our experiments (either RO + NO<sub>2</sub> or RO<sub>2</sub> + NO<sub>2</sub> to form RO<sub>2</sub>NO<sub>2</sub> followed by

decomposition to  $\text{RONO}_2$ ) and limit the importance of the decomposition channel (step 8 in Figure 8.6) in the OH-organic reaction. However, Molina et al.<sup>56</sup> studied the oxidation of an alkane monolayer by OH in the presence of  $\text{NO}_x/\text{O}_2/\text{H}_2\text{O}$  in various proportions and they observed significant decomposition of the monolayer. This suggests that the OH-organic reaction mechanism is less susceptible to the presence of  $\text{NO}_2$ .

We observed at most a limited decomposition by scission of organic monolayers (step 8) when employing  $\text{NO}_3$ , while Molina et al.<sup>56</sup> observed complete volatilization when using OH radicals. The reason for this difference is not clear. In our experiments, we assume that  $\text{HNO}_3$  was produced in the initial step of the reaction. It is possible that this species remains on the surface and somehow influences the reaction mechanism. Another issue is possible contamination of the monolayer by hydrocarbons from the ambient laboratory. However, for the unoxidized monolayers, the C/Au ratio was in the range expected for  $\text{C}_{18}$  monolayers, and only one peak was observed in the C (1s) region, due to methyl or methylene groups. This suggests that contamination of the unoxidized monolayers was minor. Also, it has previously been shown that alkanethiol monolayers replace organic contaminants from gold substrates.<sup>187</sup> We have also carried out measurements with a  $\text{C}_{11}$  alcohol terminated monolayer, and the observed C/Au ratios and O/C ratios agreed with theoretical predictions within experimental uncertainty, which suggests that contamination even for a more hydrophilic monolayer was minor. However, contamination cannot be completely ruled out. Moise and Rudich observed partial volatilization (approximately 20%) of the saturated hydrocarbon monolayer when using Cl and Br radicals.<sup>46</sup> Perhaps the presence of  $\text{HNO}_3$  can also explain the difference between  $\text{NO}_3$ , Cl, and Br.

## 8.4 Summary and Conclusions

The results presented above suggest that even under extremely polluted conditions, i.e.  $\text{NO}_3$  concentrations of 100 ppt (24 hour average) persisting for one week,<sup>1</sup> a maximum of 10% of the organic monolayer is volatilized. Our results are relevant to organics adsorbed on solid substrates such as mineral dust particles or urban surfaces. Our results may also be relevant for solid organic particles in the atmosphere and for organic coatings on aqueous particles.

IR spectroscopy and ToF-SIMS confirmed the formation of organonitrates ( $\text{RONO}_2$ ) in the  $\text{C}_{18}$  alkane SAM after exposure to  $\text{NO}_3$ . The observation of organonitrates is in contrast to the XPS data which showed very little  $\text{N}(1s)$  signal. The formation of organonitrates in our experiments may explain why we did not see significant decomposition of the carbon chains in the presence of  $\text{NO}_3$  radicals. Formation of organonitrates removes alkyl peroxy ( $\text{RO}_2$ ) and/or alkoxy ( $\text{RO}$ ) species from the system, and hence will reduce the importance of the decomposition channel. Possibly this is one of the differences between our work with  $\text{NO}_3$  and alkane monolayers and some of the recent studies with OH and alkane SAMs where significant decomposition was observed.



## 9 PRODUCTS AND KINETICS OF THE REACTIONS OF A TERMINAL ALKENE MONOLAYER WITH NO<sub>3</sub> RADICALS

### 9.1 Introduction

The following research expands on the previous study of NO<sub>3</sub> radicals with ODT monolayers described in Chapter 8. Here, we studied the reaction between NO<sub>3</sub> radicals (in the presence of O<sub>2</sub> and NO<sub>2</sub>) and another type of organic self-assembled monolayer (SAM) to further improve our understanding of radical-organic heterogeneous chemistry. The SAM studied in this chapter was a terminal alkene monolayer: undec-10-ene-1-thiol (C<sub>11</sub>H<sub>22</sub>S, hereafter referred to as UDT). In urban air masses, unsaturated organics are dominated by terminal alkenes as shown by Paulson et al.<sup>219</sup> and references therein. This makes a terminal alkene SAM a suitable proxy for atmospheric organic material.

Differences in behaviour between ODT (the alkane monolayer studied in Chapter 8) and UDT can be attributed to the presence of the terminal double bond in UDT and not to the difference in chain length, since properties of hydrocarbon thiols on gold are thought to be independent of chain length for chains of more than 10 C atoms.<sup>211</sup>

To the best of our knowledge there has been no scientific study investigating the interaction of NO<sub>3</sub> with an alkene monolayer, while O<sub>3</sub> reactions on alkene monolayers have been investigated in some detail.<sup>25,47,64,65,220-222</sup> OH,<sup>56,67</sup> Cl, and Br uptake<sup>46</sup> on an alkane and a terminal alkene SAM have also been studied. Uptake coefficients for O<sub>3</sub> reactions on terminal alkene SAMs range from  $9 \times 10^{-6}$  to  $3 \times 10^{-4}$ .<sup>25,47,64</sup> Comparing the reactivity of NO<sub>3</sub> and O<sub>3</sub> on alkenes in the gas phase shows that NO<sub>3</sub> reactions are about 2 – 4 orders of magnitude faster than O<sub>3</sub> reactions,<sup>1</sup> suggesting that the heterogeneous reaction of NO<sub>3</sub> with alkenes in monolayers might also be fast. As mentioned above, gas-phase reactions of alkenes with NO<sub>3</sub> occur much faster than reactions with alkanes. This suggests that the reactive uptake coefficient  $\gamma$  on a terminal alkene SAM might also be 1 – 3 orders of magnitude higher than that of an alkane SAM.

Using the flow tube reactor shown in Figure 5.2, we measured the reactive uptake coefficient  $\gamma$  of  $\text{NO}_3$  on the alkene monolayer as a function of  $\text{NO}_3$  exposure. This data was then used to determine how fast alkene surfaces and monolayers will be oxidized by  $\text{NO}_3$  radicals in the atmosphere. We also carried out detailed surface-product studies. The techniques used are the same as those described for the measurements on ODT SAMs in Chapter 8: X-ray photoelectron spectroscopy (XPS), infrared (IR) spectroscopy, and time-of-flight secondary ion mass spectrometry (ToF-SIMS). These techniques were used to determine the condensed-phase products formed in the UDT +  $\text{NO}_3$  reaction.

The results from these measurements were used to develop a mechanism for the  $\text{NO}_3$ -alkene monolayer reaction.

## 9.2 Experimental

### 9.2.1 Chemicals

Undec-10-ene-1-thiol ( $\text{C}_{11}\text{H}_{22}\text{S}$ , UDT) was synthesized at Virginia Tech, Blacksburg, Virginia, according to the procedure described in Peanasky and McCarley.<sup>223</sup> All other chemicals were identical to those described in Chapter 8.

### 9.2.2 Monolayer Preparation

Monolayers of undecenethiol (UDT) on gold coated silicon wafers for condensed-phase product studies were prepared as described in Chapter 8.2 for ODT. Additionally, UDT SAMs were also prepared on a cylindrical gold coated tube for measurements of reactive uptake coefficients. This cylindrical gold coated tube (inner diameter 1.91 cm, length 15 cm) was cleaned in piranha solution, rinsed with Millipore water (18 M $\Omega$ ) and distilled ethanol as described before. It was then immersed in a 1 mM solution of UDT in distilled ethanol for  $\geq 24$  h.<sup>191</sup> Subsequently, samples were cleaned in ethanol using an ultrasonic bath for 1 minute and rinsed with Millipore water for approximately 5 minutes. This cleaning procedure was repeated two more times. SAM coated gold surfaces were then dried under a stream of ultra high purity  $\text{N}_2$ .

### 9.2.3 Measurements of the Reactive Uptake Coefficient

A temperature controlled, cylindrical flow tube reactor coupled to a chemical ionization mass spectrometer (CIMS) was employed for measurements of the reactive uptake coefficient ( $\gamma$ ) of  $\text{NO}_3$  on alkene monolayers at 298 K. The inner wall of a gold coated tube was coated with a UDT SAM and inserted into the flow reactor.  $\text{NO}_3$  radicals were added through a movable injector as previously described.  $\text{NO}_3$  concentrations of  $(1 - 2) \times 10^{11}$  molecule  $\text{cm}^{-3}$  were used in the presence of  $\text{O}_2$  ( $(1.1 - 1.3) \times 10^{16}$  molecule  $\text{cm}^{-3}$ ). Total pressure in the flow reactor was 2.3 – 2.5 torr.  $\text{NO}_3$  was detected at the exit of the flow cell using chemical ionization with  $\text{I}^-$ . The  $\text{NO}_3$  signal was monitored while the injector was pulled back in equal increments, exposing UDT surfaces to  $\text{NO}_3$  radicals. Calculation procedures for the determination of  $\gamma$  from the depletion of the CIMS signal of the gas-phase reactant (here  $\text{NO}_3$ ) during exposure to an organic surface have been described in previous chapters.

### 9.2.4 Product Studies as a Function of Exposure

The flow reactor was also used to expose UDT SAMs on Au coated Si plates to  $\text{NO}_3$  for subsequent XPS, IR,  $\text{H}_2\text{O}$  contact angle, and ToF-SIMS analysis.  $\text{NO}_3$  exposure levels ranged from 0 –  $9.06 \times 10^{-5}$  atm sec (an exposure of 0 – 21 days at 50 ppt  $\text{NO}_3$ ). Experiments were performed at 298 K, at a pressure of 2.3 – 2.7 torr, using  $\text{NO}_3$  concentrations of  $(1 - 5) \times 10^{11}$  molecule  $\text{cm}^{-3}$  and  $\text{O}_2$  concentrations of  $(1.1 - 1.6) \times 10^{16}$  molecule  $\text{cm}^{-3}$ . Helium was used as carrier gas for  $\text{NO}_3$ .

### 9.2.5 XPS, IR, ToF-SIMS, and Contact Angle Measurements

These techniques are described in detail in Chapter 8.2.4.

## 9.3 Results and Discussion

### 9.3.1 Reactive Uptake Coefficient of $\text{NO}_3$ on an Unoxidized UDT SAM

The  $\gamma$ -value for a UDT SAM was determined to be  $3.4 \times 10^{-2}$  ( $+ 4.4 \times 10^{-2}$  /  $- 1.8 \times 10^{-2}$ ) (the uncertainty reported corresponds to the 95% confidence interval and an uncertainty in the diffusion coefficients of  $\text{NO}_3$  in He and  $\text{O}_2$  of 15%). In comparison, the

value determined for ODT was  $(8.8 \pm 1.0) \times 10^{-4}$ ,<sup>83</sup> a factor of approximately 39 less. This enhancement of UDT reactivity compared to ODT reactivity is in agreement with the enhancement observed for reaction rate constants for different gas-phase reactions of alkanes and alkenes with NO<sub>3</sub>. For example  $k_{\text{propene}} / k_{\text{propane}} = 18$ ,  $k_{\text{1-butene}} / k_{\text{n-butane}} = 305$ ,  $k_{\text{cyclohexene}} / k_{\text{cyclohexane}} = 237$ , where  $k$  represents different gas-phase rate constants for NO<sub>3</sub> reactions.<sup>1,40</sup>

The  $\gamma$ -value of the terminal alkene UDT obtained in this study is consistent with the  $\gamma$ -value of solid oleic acid reported in Chapter 7. Both UDT and oleic acid have one double bond per molecule. However, as was described in Chapter 7,  $\gamma$ -values for unsaturated compounds reported in this thesis are higher than the values obtained by Moise et al.<sup>44</sup> using liquid and solid alkene bulk films. Moise et al.<sup>44</sup> measured  $(1.6 \pm 0.3) \times 10^{-3}$  and  $(1.4 \pm 0.1) \times 10^{-3}$  for liquid and solid 1-octadecene films;  $(2.3 \pm 0.9) \times 10^{-3}$  and  $(1.8 \pm 0.3) \times 10^{-3}$  for liquid and solid 1-hexadecene films;  $(5.8 \pm 2.0) \times 10^{-3}$  and  $(5.2 \pm 2.0) \times 10^{-3}$  for liquid and solid 7-tetradecene films, respectively. Possible reasons for this difference have been described in Chapter 7.

Table 9.1 shows a summary of studies on heterogeneous reactions of different gas-phase oxidants with terminal alkene monolayers. Reactive uptake coefficients  $\gamma$  and average atmospheric concentrations for each oxidant are reported. Direct comparison of  $\gamma$ -values for each oxidant is of minor atmospheric relevance since the concentration of each oxidant is different in the atmosphere. Therefore the last column in Table 9.1 shows the product of  $\gamma$  and the average atmospheric concentrations of the gas-phase oxidants. These numbers are more relevant parameters for assessing the importance of the various gas-phase species to atmospheric oxidation since the number of molecules lost to an organic surface should be proportional to  $\gamma \times [\text{reactant concentration}]$ . The most important process will generally be the process with the largest  $\gamma \times [\text{reactant concentration}]$  and therefore the highest oxidative power. The abundance of NO<sub>3</sub> in the atmosphere is highly variable, since it has a high spatial and seasonal variability. For these calculations we use NO<sub>3</sub> concentrations of 50 ppt and 5 ppt to roughly represent polluted urban and rural conditions.<sup>1,224-226</sup> As can be seen from Table 9.1, the oxidative

power of NO<sub>3</sub> is significantly higher than that of OH, Cl, and Br. Only O<sub>3</sub> is of equal importance to NO<sub>3</sub> due to its much higher tropospheric concentrations.

**Table 9.1: Reactive uptake coefficients ( $\gamma$ ) of different gas-phase oxidants on terminal alkene monolayers, average atmospheric concentrations of the gas-phase species ([oxidant] / molecule cm<sup>-3</sup>) and calculated oxidative powers ( $\gamma \times [\text{oxidant}]$ ). For NO<sub>3</sub> radicals, calculations have been performed for both high NO<sub>3</sub> concentrations (50 ppt) and low concentrations (5 ppt) to represent approximately a range of concentrations encountered in the atmosphere due to spatial and seasonal fluctuations.**

Oxidant	Surface	$\gamma$	[oxidant]	$\gamma \times [\text{oxidant}]$
NO <sub>3</sub>	terminal C <sub>11</sub> alkene <sup>a</sup>	0.034	$1.2 \times 10^9$	$4.1 \times 10^7$
			$1.2 \times 10^8$	$4.1 \times 10^6$
OH	terminal C <sub>3</sub> alkene <sup>b</sup>	0.6	$1 \times 10^6$	$6 \times 10^5$
Cl	terminal C <sub>8</sub> alkene <sup>c</sup>	0.1 - 1	$1 \times 10^4$	$1 \times 10^3 - 1 \times 10^4$
Br	terminal C <sub>8</sub> alkene <sup>c</sup>	0.05	$1 \times 10^6$	$5 \times 10^4$
O <sub>3</sub>	terminal C <sub>3</sub> and C <sub>8</sub> alkenes <sup>d</sup>	$9 \times 10^{-6} - 3 \times 10^{-4}$	$2.5 \times 10^{12}$	$2.3 \times 10^7 - 7.5 \times 10^8$

<sup>a</sup>This study.

<sup>b</sup>Bertram et al.<sup>67</sup>

<sup>c</sup>Moise and Rudich<sup>46</sup>

<sup>d</sup>Dubowski et al., Moise and Rudich, and Usher et al.<sup>25,47,64</sup>

Using the reactive uptake coefficient determined in this study and the equation presented as eq 6.2 in Chapter 6 and in Moise and Rudich,<sup>46</sup> we can calculate the average lifetime of an alkene monolayer at the interface of an aerosol particle in the atmosphere. Assuming an NO<sub>3</sub> concentration of 50 ppt, we obtain a value of 22.6 min. This shows that the lifetime is short in polluted environments and that in regions where NO<sub>3</sub> concentrations are high, surface concentrations of alkenes are expected to be low. A similar conclusion was reached by Moise and Rudich<sup>46</sup> using reactive uptake coefficients determined on bulk liquid and solid alkene films, although their measured uptake coefficients were slightly different.

### 9.3.2 Measurements of the Reactive Uptake of NO<sub>3</sub> as a Function of Exposure Time

Measurements of the reactive uptake coefficient as a function of time were carried out to determine if the surfaces were catalytic (i.e., a reaction takes place at the surface but the surface is not an active participant) or if the reaction rate decreased with time due to oxidation of the monolayer. For these measurements an NO<sub>3</sub> concentration of  $1.0 \times$

$10^{11}$  molecule  $\text{cm}^{-3}$  was used. The change in  $\gamma$  with exposure to  $\text{NO}_3$  is shown in Figure 9.1. The initial fast uptake coefficient is most likely due to a fast reaction with the double bond. Once the double bond was oxidized, the uptake coefficient reached a value consistent with the uptake on an alkane monolayer. The exposure at which the reactive uptake reached a near steady state value is consistent with the time it would take to oxidize all the alkene functional groups on the surface, based on calculations presented by Bertram et al.<sup>67</sup>

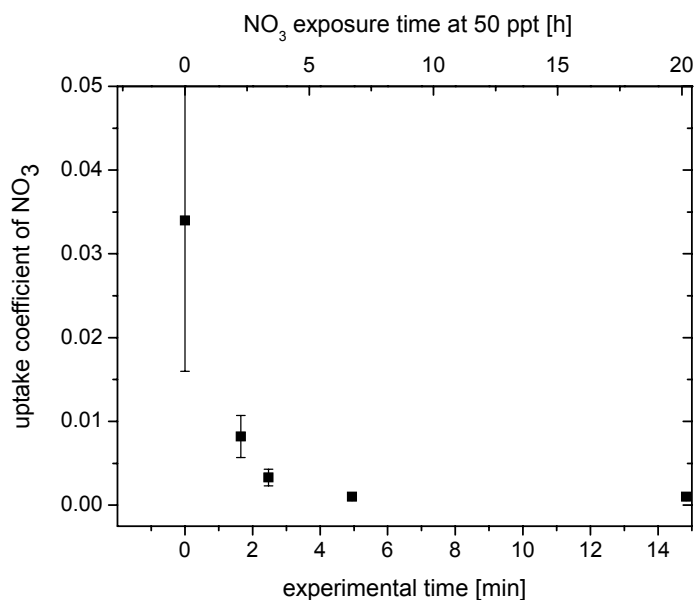


**Figure 9.1: Changes in the reactive uptake coefficient  $\gamma$  with increasing  $\text{NO}_3$  exposure of a UDT SAM. Bottom x-axis corresponds to actual time of the experiment [min] (at an  $\text{NO}_3$  concentration of  $1.0 \times 10^{11}$  molecule  $\text{cm}^{-3}$ ), top x-axis shows the corresponding total  $\text{NO}_3$  exposure time [h] of the SAM at an atmospheric concentration of 50 ppt.**

Next results from XPS, IR, and ToF-SIMS studies of the reaction of  $\text{NO}_3$  with alkene monolayers are presented. The purpose of these measurements was to identify surface products and to determine the mechanism for the oxidation of the double bond. All of these experiments were carried out using exposures of less than  $2 \times 10^{-5}$  atm sec, which is significantly less than the exposures used in our previous alkane SAM studies. As shown in Figures 8.1 and 8.2 in Chapter 8, an alkane monolayer is hardly oxidized at

exposures less than  $2 \times 10^{-5}$  atm sec. Using these low exposure levels, the reaction should be mostly confined to the double bond.

### 9.3.3 X-Ray Photoelectron Spectroscopy

XPS measurements of alkene monolayers were carried out as a function of  $\text{NO}_3$  exposure (ranging from 0 to  $1.8 \times 10^{-5}$  atm sec, equivalent to 0 – 4.2 days at 50 ppt  $\text{NO}_3$ ). Figure 9.2 shows the C(1s) region of the XPS spectra obtained using three different  $\text{NO}_3$  exposures ranging from 0 to  $9.1 \times 10^{-6}$  atm sec (equivalent to 50 ppt for 50 h). For the unexposed sample only one peak at 285 eV was observed. This peak is due to vinyl or methylene functional groups. After exposure to  $\text{NO}_3$ , the main peak at about 285 eV remained, but a shoulder was observed at higher energies within the C(1s) region indicating oxidation of the organic surface. We fit the total C(1s) region with four overlapping Gaussian-Lorentzian peaks, similar to our previous studies of alkane monolayers. The peaks used in the fit were centered at approximately 285 eV, 286.5 eV, 288 eV, and 289.5 eV. The peaks at energies above 285 eV represent oxidized C species (consistent with C-O, aldehyde/ketone, and carboxylic groups, respectively).

To determine the fraction of carbon oxidized as a function of exposure time, we calculated the atomic ratio of oxidized carbon ( $C_{\text{ox}}$ , the three peaks at higher binding energy) to the total carbon peak area ( $C_{\text{total}}$ ). Panel (c) in Figure 9.3 shows these ratios for  $\text{NO}_3$  exposures of 0 –  $1.8 \times 10^{-5}$  atm sec. The error bars (which represent  $\pm 2 \sigma$ ) were derived from 4 different UDT SAMs on gold coated Si wafers exposed to the same amount of  $\text{NO}_3$ . As can be seen, after exposures of only  $2.0 \times 10^{-7}$  atm sec (equivalent to 1.1 h at 50 ppt  $\text{NO}_3$ ), approximately 12% of the C(1s) signal corresponded to oxidized carbon.

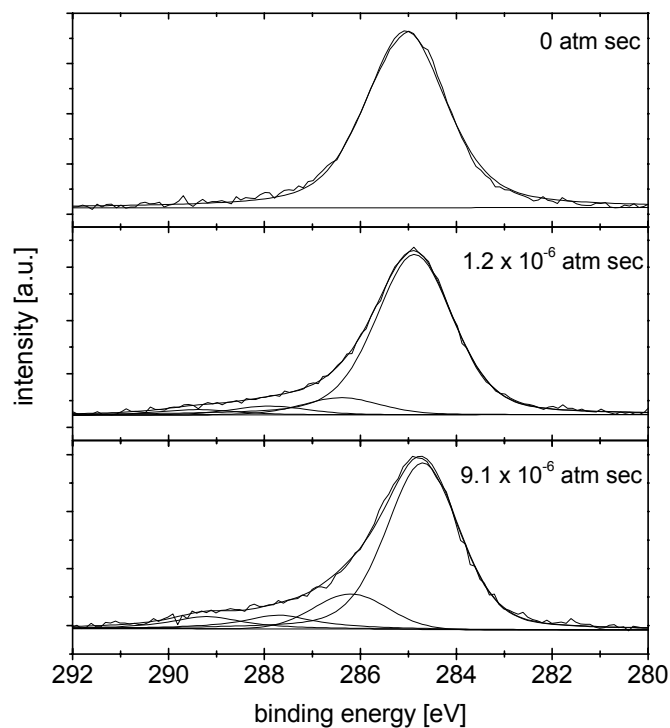


**Figure 9.2: XPS spectra of the C(1s) region for a UDT monolayer before exposure to NO<sub>3</sub> (0 atm sec, top panel) and after exposures of  $1.2 \times 10^{-6}$  atm sec (equivalent to 50 ppt for 6.7 h, centre panel) and  $9.1 \times 10^{-5}$  atm sec (equivalent to 50 ppt for 50 h, bottom panel).**



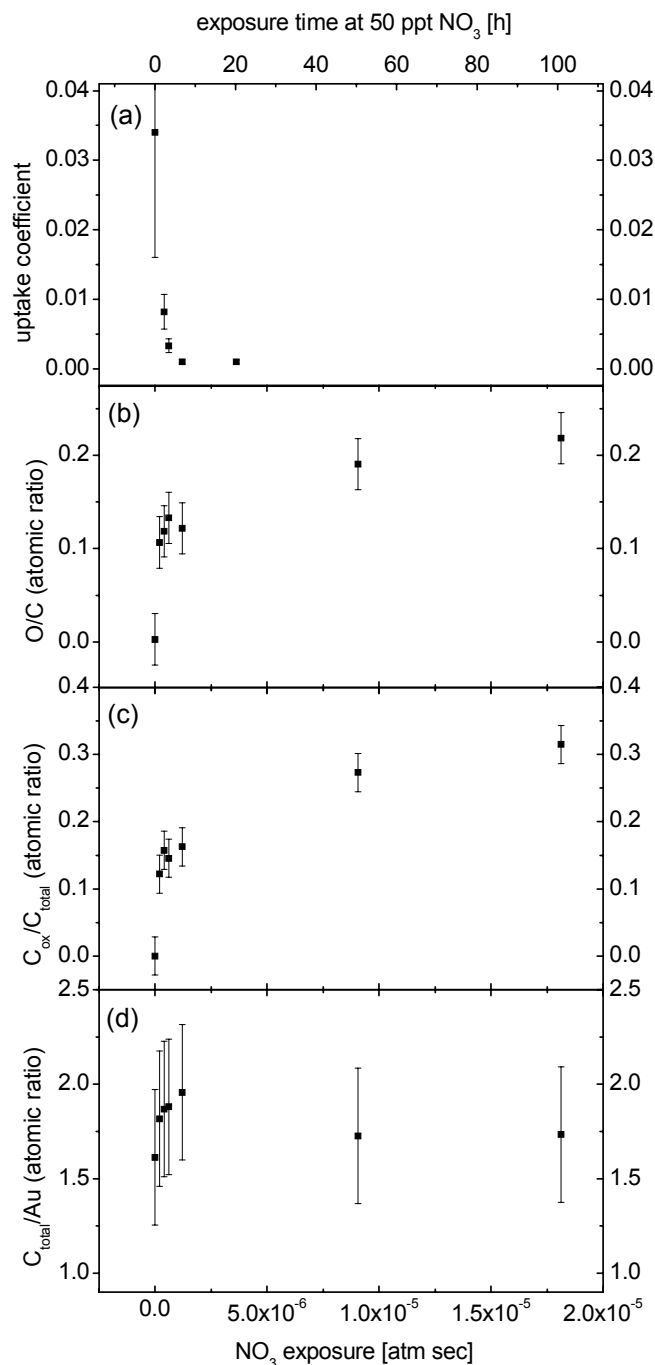


**Figure 9.3: Summary of processing study and XPS results for UDT. Panel (a) shows the changes in  $\gamma$  with increasing  $\text{NO}_3$  exposure. Panels (b)-(d) show changes in atomic ratios obtained in XPS as a function of  $\text{NO}_3$  exposure. (b) Atomic ratio of total oxygen, O, to total carbon, C. (c) Atomic ratio of oxidized carbon,  $\text{C}_{\text{ox}}$ , to total carbon,  $\text{C}_{\text{total}}$ . (d) Atomic ratio of total carbon,  $\text{C}_{\text{total}}$ , to total gold, Au. The two scales on the top and bottom x-axes are valid for all four panels and provide information on  $\text{NO}_3$  exposure levels in atm sec (bottom axis) and in total exposure time [h] at an atmospheric  $\text{NO}_3$  concentration of 50 ppt (top axis).**

Panel (b) of Figure 9.3 shows the increase in O(1s) due to increasing NO<sub>3</sub> exposure. The trend observed is qualitatively the same as for C<sub>ox</sub>/C<sub>total</sub> in panel (c). As with C<sub>ox</sub>/C<sub>total</sub>, after longer exposures ( $1.2 \times 10^{-6}$  -  $1.8 \times 10^{-5}$  atm sec) the reaction slowed down and O/C increased with a smaller slope than in the initial stage of oxidation.

We also exposed the monolayers to O<sub>2</sub> and NO<sub>2</sub> in the absence of NO<sub>3</sub>. After exposure to just these species (using concentrations greater than those used in the NO<sub>3</sub> experiments) the C<sub>ox</sub>/C<sub>total</sub> atomic ratio and O/C atomic ratio were within the error limits for the unexposed sample shown in Figure 9.3.

To assess the amount of decomposition of the UDT SAM, we plotted the atomic ratio of the total integrated C(1s) signal to the total Au(4f) signal intensity (C/Au), Figure 9.3, panel (d). No significant changes in this ratio could be observed within experimental certainty. However, due to the large uncertainties, we can only conclude that less than 21% of the surface was volatilized during the longest exposure experiments. As detachment of the carbon chain is also possible due to oxidation of the sulfur head group, 21% should be considered an upper limit to the amount of carbon loss due to C-C bond scission.

Monitoring the S(2p) signal of UDT SAMs after exposure to NO<sub>3</sub> showed only unoxidized sulfur (peak maximum at  $163.1 \pm 0.2$  eV) for exposures  $\leq 1.2 \times 10^{-6}$  atm sec and both unoxidized sulfur (peak maximum at  $163.1 \pm 0.2$  eV) and oxidized sulfur (peak maximum at  $168.0 \pm 0.2$  eV) for exposures  $\geq 9.1 \times 10^{-6}$  atm sec.

N(1s) signals were below the detection limit in all measurements of exposed and unexposed UDT SAMs. However, the nitrogen-species may have formed during the oxidation reactions but decomposed during XPS measurements, similar to the alkane monolayer experiments. To determine if nitrogen-containing species were formed in these reactions, we carried out IR and ToF-SIMS measurements (see below).

To investigate the behaviour of UDT after long exposures to NO<sub>3</sub> radicals, we also performed a few experiments with large NO<sub>3</sub> exposures. After an exposure of  $4.5 \times 10^{-5}$  atm sec, the monolayers reached oxidized C fractions (C<sub>ox</sub>/C<sub>total</sub>) of 37%, and an O/C ratio of 0.42 (data not shown). These values are similar to the values obtained on ODT monolayers after long NO<sub>3</sub> exposures.

### 9.3.4 IR-Spectroscopy

Spectra were taken of an unexposed UDT sample with per-deuterated ODT as reference to confirm the presence of methylene groups and the absence of CH<sub>3</sub> groups in the original UDT SAMs (data not shown). Following this, IR measurements were performed on samples that had been exposed to NO<sub>3</sub>. For this analysis we focused only on the IR regions from 3000 – 2800 cm<sup>-1</sup> and from 1370 – 1200 cm<sup>-1</sup>. The wavelength range used in these experiments was slightly smaller than the range used in the alkane monolayers experiments. This is because the signal to noise was smaller in the alkene experiments due to the low NO<sub>3</sub> exposures and smaller degree of oxidation of the films. The spectrum shown in Figure 9.4 was obtained the same way as for Figure 8.3 in Chapter 8 for ODT. An exposure level of  $1.21 \times 10^{-6}$  atm sec (50 ppt for 6.7 h) was used in this experiment. As with ODT, NO<sub>3</sub> exposure of UDT resulted in negative peaks in the range 3000 – 2800 cm<sup>-1</sup> due to the decrease of the symmetric and asymmetric stretching modes of CH<sub>2</sub>. At this short exposure to NO<sub>3</sub> we do not expect significant oxidation of the methylene groups in UDT. As peak intensities depend on the orientation of the different vibrational modes,<sup>227</sup> we assume that the negative peaks appearing in the region of 3000 – 2800 cm<sup>-1</sup> were due to increased disorder within the monolayer due to reaction of the double bond. This is consistent with results by Moise and Rudich<sup>46</sup> who observed almost complete disappearance of the CH<sub>2</sub> stretching peaks in IR, while XPS indicated only a 20% reduction in total carbon and a significant fraction of remaining unoxidized C(1s). The IR spectra clearly showed the formation of a peak at 1281 cm<sup>-1</sup>. Based on Table 8.1 in Chapter 8, this could be due to an organonitrate, organoperoxynitrate, or peroxyacylnitrate. It seems unlikely that the identified surface species are organoperoxynitrates or peroxyacylnitrates, since these species typically have a short lifetime and are expected to decompose while the substrates are transferred to the IR spectrometer for analysis, as discussed above. Based on the IR data, we can conclude that nitrogen-species are formed, contrary to the conclusion that could be reached from the XPS data alone.

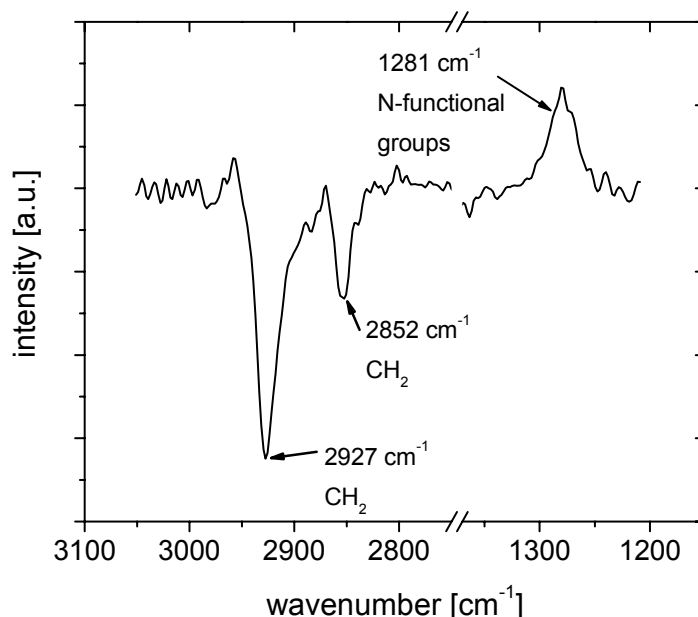


**Figure 9.4: UDT IR spectrum calculated from an UDT sample exposed to  $1.21 \times 10^{-6}$  atm sec of  $\text{NO}_3$  (50 ppt for 6.7 h) and an unoxidized UDT SAM as reference sample (see text). Negative peaks correspond to features only present or more prominent in the unexposed UDT SAM, positive peaks show features only present or more prominent in the exposed UDT SAM.**

### 9.3.5 ToF-SIMS Measurements

Shown in Figure 9.5 are negative ion ToF-SIMS spectra for UDT before (spectrum a) and after exposure to  $\text{NO}_3$  (spectrum b). As with ODT, spectra before  $\text{NO}_3$  exposure showed  $\text{Au}_x\text{S}_y$  clusters, low molecular weight fragments of the monolayer chains ( $\text{C}^-$ ,  $\text{CH}^-$ ,  $\text{C}_2\text{H}^-$ ,  $\text{S}^-$ ,  $\text{SH}^-$ ), and characteristic peaks for the whole UDT molecule. These peaks are labelled M, which indicates  $\text{C}_{11}\text{H}_{21}$ . All peaks characteristic of the unoxidized hydrocarbon SAMs decreased or disappeared upon  $\text{NO}_3$  exposure ( $\text{C}^-$ ,  $\text{CH}^-$ ,  $\text{C}_2\text{H}^-$ ,  $\text{S}^-$ ,  $\text{SH}^-$ ,  $\text{MS}^-$ , and  $\text{Au}(\text{MS})_2^-$ ). New peaks of high intensity formed especially in the  $m/z < 100$  region, which could be attributed to  $\text{O}^-$ ,  $\text{OH}^-$ ,  $\text{NO}_2^-$ ,  $\text{NO}_3^-$ ,  $\text{SO}_3^-$ , and  $\text{HSO}_4^-$ . As with ODT, peaks for  $\text{NO}_2^-$  and  $\text{NO}_3^-$  led us to conclude that nitrogen containing functional groups form during the oxidation of UDT by  $\text{NO}_3$ , but decompose during XPS measurements.

Again, as with ODT, NO<sub>3</sub> exposed UDT SAMs showed peaks from SO<sub>3</sub><sup>-</sup> and SO<sub>4</sub><sup>-</sup>. This is consistent with the appearance of a S(2p) peak from oxidized sulfur in XPS spectra of UDT exposed to  $\geq 9.1 \times 10^{-6}$  atm sec.

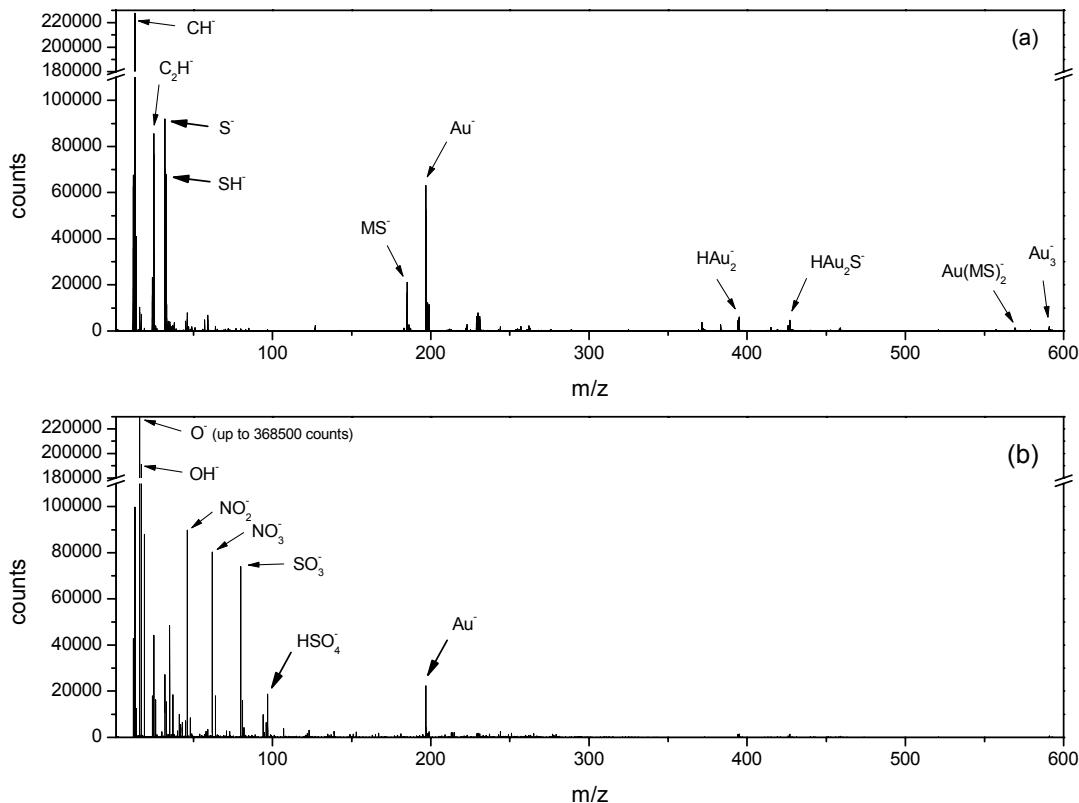


**Figure 9.5: Negative ion ToF-SIMS spectra of UDT on gold in the m/z 1 – 600 region. Spectrum (a) was obtained on a UDT sample without NO<sub>3</sub> exposure, spectrum (b) was obtained after an NO<sub>3</sub> exposure of  $9.1 \times 10^{-6}$  atm sec (equivalent to 50 ppt for 50 h).**

### 9.3.6 Contact Angle Measurements

The initial contact angle determined before NO<sub>3</sub> exposure was  $92^\circ \pm 5^\circ$  for UDT (number given here is the average value and standard deviation). Literature values for monolayers of terminal alkenes (C<sub>8</sub> – C<sub>19</sub>) were reported at  $89^\circ - 107^\circ$ .<sup>47,65,67,203,211,214,215</sup> The large contact angle observed for the unoxidized monolayers indicate the presence of well ordered SAMs in this study. NO<sub>3</sub> exposure of UDT samples was  $9.06 \times 10^{-5}$  atm sec (equivalent to 50 ppt NO<sub>3</sub> for 3 weeks). After this exposure, the contact angle on UDT decreased to  $59^\circ \pm 6^\circ$  – a change of  $33^\circ$ . Two exemplary images of H<sub>2</sub>O droplets on the UDT monolayers are shown in Figure 9.6. The decrease in contact angle gives further

evidence that the monolayers were oxidized leading to a more hydrophilic surface. Previous studies investigating changes in H<sub>2</sub>O contact angles on hydrocarbon monolayers (C<sub>8</sub> – C<sub>19</sub>) after exposure to gas-phase reactants reported the following data for terminal alkene monolayers: after F radical exposure  $\theta = 75^\circ$ ,<sup>214</sup> and after O<sub>3</sub> exposure  $\theta = 74^\circ$  and  $\sim 70^\circ$ .<sup>47,65</sup>

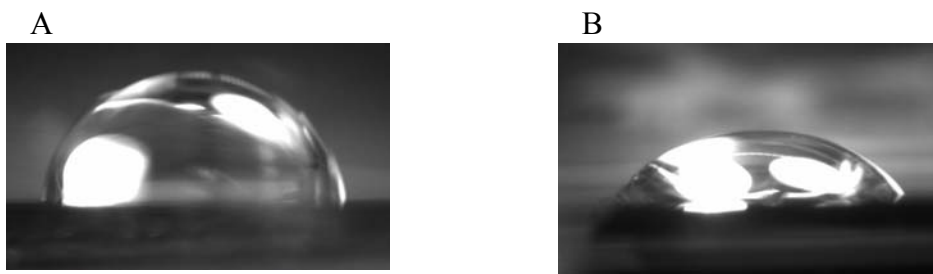


**Figure 9.6: Millipore grade H<sub>2</sub>O droplets on UDT monolayers before (image A) and after NO<sub>3</sub> exposure (equivalent to 50 ppt for 3 weeks, image B).**

### 9.3.7 Proposed Reaction Mechanism

Shown in Figure 9.7 is the proposed mechanism for oxidation of an alkene monolayer by NO<sub>3</sub> radicals in the presence of O<sub>2</sub> and NO<sub>2</sub> based on gas-phase chemistry.<sup>40,41,194,228-232</sup> The gas-phase reaction of NO<sub>3</sub> with alkenes is assumed to proceed via addition of NO<sub>3</sub> to the C-C double bond (Figure 9.7, step 1). This leads to a C-ONO<sub>2</sub> functional group on one of the two C atoms of the double bond and leaves an alkyl radical at the other C atom. This radical compound is expected to react further with O<sub>2</sub> to an alkylperoxy radical (RO<sub>2</sub>, step 2).<sup>1</sup>

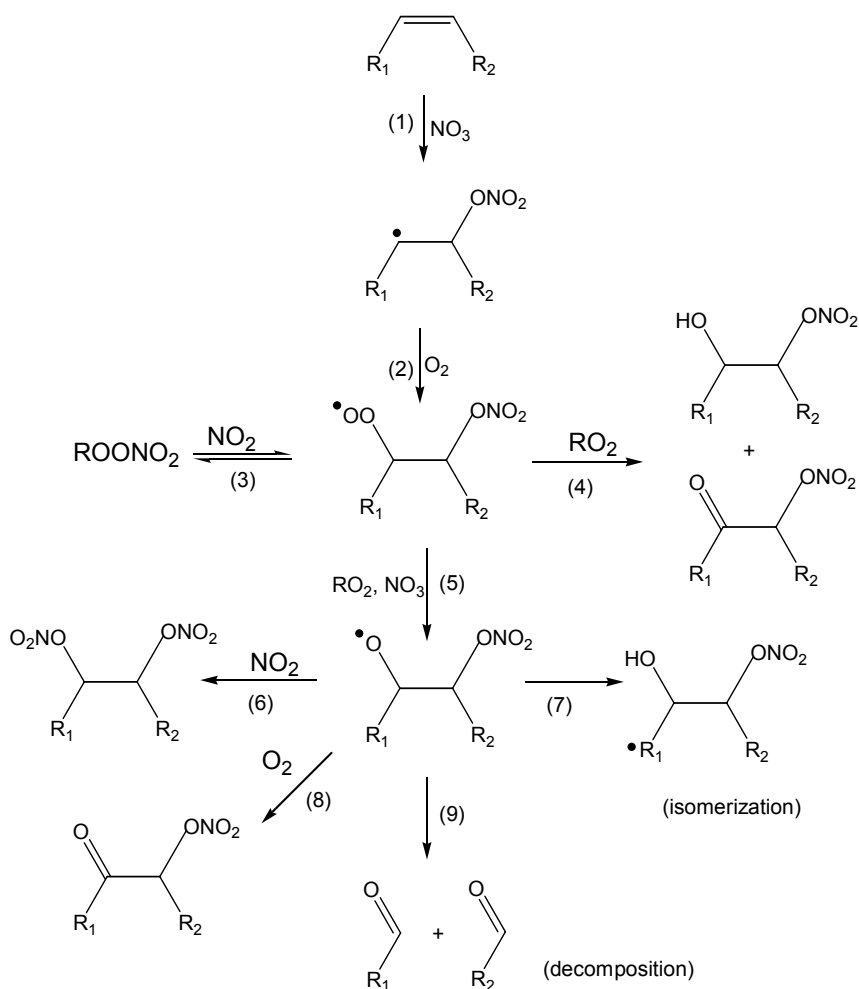


**Figure 9.7: Proposed reaction mechanism for an alkene surface with  $\text{NO}_3$  in the presence of  $\text{NO}_2$  and  $\text{O}_2$  based on gas-phase chemistry.**

Reactions of the  $\text{RO}_2$  radical are believed to occur in the same way as those of the  $\text{RO}_2$  radical in the alkane reaction scheme (Figure 8.6 in the previous chapter), except that the neighbouring C atom contains an  $\text{ONO}_2$  functional group. An additional difference is the fact that the scission channel leads to the elimination of  $\text{NO}_2$  and the formation of two aldehydes (step 9).

Not shown in Figure 9.7 are additional reactions that the alkyl nitrate radical may undergo at low pressures in competition with step 2. When the nitrate radical adds to the double bond, an excited state is formed. If this excited state is not collisionally stabilized, it can decompose to  $\text{NO}_2$  and an aldehyde or ketone or alternatively eliminate  $\text{NO}_2$  and

form an epoxide that reacts further to form a carbonyl.<sup>41,233</sup> However, the importance of these steps on a surface is unclear.

As a reminder, the XPS results are consistent with the formation of C-O, C=O, and C(=O)O functional groups. IR and ToF-SIMS analyses showed the formation of nitrogen-containing species, likely organonitrates. Scission of the carbon chain at the double bond could not be confirmed, but it could not be ruled out either. The formation of C-O and C=O functional groups could be explained by step 4, the Russell mechanism. Formation of C-O could also be explained by step 7, and the formation of C=O could also be explained by steps 8 and 9 in Figure 9.7. Carboxylic functional groups identified using XPS were probably formed in secondary reactions, for example during the oxidation of aldehydes.<sup>70</sup>

Our experiments are the first to investigate heterogeneous reactions between radicals and alkene monolayers in the presence of O<sub>2</sub> and NO<sub>2</sub>. As a result our product analysis should be helpful for understanding this heterogeneous mechanism. D'Andrea et al.<sup>234</sup> investigated the reaction between OH and an alkene monolayer, but in the absence of NO<sub>2</sub> and O<sub>2</sub>, so the results are not directly comparable. In addition, both Hung et al.<sup>66</sup> and Docherty and Ziemann<sup>63</sup> studied the reaction between NO<sub>3</sub> (in the presence of O<sub>2</sub> and NO<sub>2</sub>) and liquid alkenoic acid particles. Hung et al.<sup>66</sup> observed organonitrate, peroxyxynitrate, organonitrite, and carbonyl functional groups using infrared spectroscopy and high molecular weight products were also observed using LC-MS. Docherty and Ziemann<sup>63</sup> identified hydroxyl nitrates, carbonyl nitrates, dinitrates, hydroxydinitrates, and possibly more highly nitrated products using mass spectrometry. It is interesting to note that several of the functional groups identified in these previous liquid reaction studies were also identified in our current monolayer studies. It therefore appears that the reaction pathways for the alkene monolayers are similar to the reaction pathways for the liquid, although the relative importance of the reaction channels may differ.

Also, when studying the reaction between NO<sub>3</sub> and liquid alkenoic acid particles, Docherty and Ziemann<sup>63</sup> observed substantial organonitrate formation after the double bond was completely reacted. This was attributed to either the reaction of N<sub>2</sub>O<sub>5</sub> with a hydroxyl group or H atom abstraction. This latter explanation is consistent with the alkane monolayer results presented above.



## 9.4 Conclusions and Atmospheric Implications

For the terminal alkene SAMs, the  $\gamma$ -value obtained in this study for the terminal alkene UDT is higher than the values that were obtained by Moise et al.<sup>44</sup> using solid alkene bulk films. Using the  $\gamma$ -value determined in our studies, we show that oxidation of an alkene monolayer by  $\text{NO}_3$  can be significantly more important than oxidation by OH, Cl, and Br in the atmosphere. Only  $\text{O}_3$  is of equal importance to  $\text{NO}_3$  due to its much higher tropospheric concentration. We also used our  $\gamma$ -value for the alkene SAM to show that the lifetime of an alkene monolayer in the atmosphere will be short (approximately 23 min) assuming an  $\text{NO}_3$  concentration of 50 ppt.

XPS, IR and ToF-SIMS were used to identify surface functional groups after the oxidation of the alkene monolayers by  $\text{NO}_3$ . The results are consistent with the formation of C-O, aldehyde/ketone, carboxylic groups, and nitrogen-containing species. It is interesting to note that several of the functional groups identified in previous studies of  $\text{NO}_3$  radicals (in the presence of  $\text{O}_2$  and  $\text{NO}_2$ ) with liquid alkene films were also identified in our current monolayer studies.

## 10 CONCLUDING REMARKS

### 10.1 Conclusions

The overall goal of this thesis was to increase scientific understanding of atmospherically important heterogeneous reactions. This was achieved through investigations into the reactions of  $\text{NO}_3$ ,  $\text{N}_2\text{O}_5$ ,  $\text{NO}_2$ ,  $\text{HNO}_3$ , and  $\text{O}_3$  (important tropospheric oxidants) with different organics in the condensed phase. Reactive uptake coefficients were determined to show the relative importance of the different oxidants. Gas-phase products (for PAHs) and condensed-phase products (for alkane and alkene monolayers) were identified for reactions with  $\text{NO}_3$  and made it possible to suggest mechanisms for the heterogeneous reactions of  $\text{NO}_3$  with these classes of organics. In addition, the atmospheric implications of the results obtained in this thesis were discussed with a focus on lifetimes and atmospheric oxidation powers.

In Chapter 6, reactive uptake coefficients were determined for the heterogeneous reactions of  $\text{NO}_3$ ,  $\text{N}_2\text{O}_5$ ,  $\text{NO}_2$ ,  $\text{HNO}_3$ , and  $\text{O}_3$  on three different solid PAH surfaces (pyrene, fluoranthene, and benz[a]anthracene) at 273 K and at 293 – 297 K. This was the first time that the reactive uptake coefficients of  $\text{N}_2\text{O}_5$  and  $\text{NO}_3$  had been measured on PAH surfaces. The reaction of  $\text{NO}_3$  radicals with all three PAHs was observed to be very fast. The measured reactive uptake coefficient ranged from 0.059 (+ 0.11 / - 0.049) for benz[a]anthracene to 0.79 (+ 0.21 / - 0.67) for pyrene. In contrast to the  $\text{NO}_3$  reactions, reactions of the different PAHs with the other gas-phase oxidants were found to be much slower. Uptake coefficients for  $\text{N}_2\text{O}_5$ ,  $\text{NO}_2$ ,  $\text{HNO}_3$ , and  $\text{O}_3$  were at or below the detection limit ( $\gamma \leq 6.6 \times 10^{-5}$ ) in all cases. This showed that these reactions were either very slow or did not occur. The uptake coefficients determined for  $\text{NO}_2$ ,  $\text{HNO}_3$ , and  $\text{O}_3$  showed no discrepancy with values obtained in previous studies. After long  $\text{NO}_3$  exposure times (60 min) the reaction of  $\text{NO}_3$  on all three PAH surfaces slowed down at 263 K. While benz[a]anthracene showed a similar trend at room temperature,  $\gamma_{\text{NO}_3}$  did not decrease on pyrene and fluoranthene after 60 minutes of  $\text{NO}_3$  exposure at 296 K. This difference is

thought to be due to the different volatility of the three different PAHs and their reaction products.

These results have some interesting atmospheric implications. Under certain atmospheric conditions,  $\text{NO}_3$  radicals may be a more important sink for PAHs than  $\text{NO}_2$ ,  $\text{N}_2\text{O}_5$ ,  $\text{HNO}_3$ , or  $\text{O}_3$  and may impact the tropospheric lifetimes of surface-bound PAHs. Based on our data, atmospheric lifetimes of PAH material on aerosol surfaces should be on the order of only seconds to minutes due to heterogeneous reactions with  $\text{NO}_3$  radicals at night.

In Chapter 7 the reactive uptake coefficients of three different organics were determined for  $\text{NO}_3$  and  $\text{N}_2\text{O}_5$ . The organics had different functional groups and were used both as solid and liquid substrates. With  $\text{NO}_3$ , the unsaturated compound (oleic acid, an alkenoic acid) had a much higher  $\gamma$  than the two saturated compounds (an alkanoate and a polyalcohol). All three compounds had higher uptake coefficients with  $\text{NO}_3$  than with  $\text{N}_2\text{O}_5$ . For the alkenoic acid and the alkanoate,  $\gamma$  decreased substantially upon freezing. The alcohol had the highest uptake coefficient with  $\text{N}_2\text{O}_5$ . Comparison with the scarce literature data available showed, in general, good agreement for saturated compounds but our  $\gamma$  obtained for  $\text{NO}_3$  with the alkenoic acid was much higher than  $\gamma$ -values obtained in a previous study.<sup>44</sup> We investigated the atmospheric implications of our data and concluded that  $\text{NO}_3$  may be an important sink for atmospheric organics – both saturated and unsaturated – and that  $\text{N}_2\text{O}_5$  could be important for the loss of atmospheric alcohols. We also showed that heterogeneous reactions need to be considered in laboratory studies investigating the formation of secondary organic aerosols since they can significantly alter the results of these studies.

In Chapters 8 and 9 reactions of self-assembled monolayers with  $\text{NO}_3$  radicals were investigated. For the alkane SAM (Chapter 8), XPS revealed the formation of C-O, C=O, and C(=O)O functional groups upon exposure to  $\text{NO}_3$ . Very little loss of carbon was observed even for long exposures to  $\text{NO}_3$ . IR spectroscopy and ToF-SIMS confirmed the formation of organonitrates ( $\text{RONO}_2$ ). The observation of organonitrates was in contrast to the XPS data which showed very little N(1s) signal. It was shown that the organonitrates decomposed during XPS measurements. The results were used to suggest a reaction mechanism for saturated organic surfaces with  $\text{NO}_3$  radicals. The formation of

organonitrates in our experiments may explain why we did not see significant decomposition of the carbon chains. Formation of organonitrates removes alkyl peroxy ( $\text{RO}_2$ ) and/or alkoxy ( $\text{RO}$ ) species from the system, and hence will reduce the importance of the decomposition channel. This could help explain the differences between our work with  $\text{NO}_3$  and alkane monolayers and some of the recent studies with OH and alkane SAMs where significant decomposition was observed.

In the case of alkene SAMs, the  $\gamma$ -value of the terminal alkene UDT obtained in this study (Chapter 9) was higher than the values obtained by Moise et al.<sup>44</sup> using liquid and solid alkene bulk films. We showed that oxidation of an alkene monolayer by  $\text{NO}_3$  can be significantly more important than oxidation by OH, Cl, and Br in the atmosphere. Only  $\text{O}_3$  is of equal importance to  $\text{NO}_3$  due to its much higher tropospheric concentration. According to our  $\gamma$ -value for the alkene SAM, the lifetime of an alkene monolayer in the atmosphere will be short (approximately 23 minutes assuming an  $\text{NO}_3$  concentration of 50 ppt).

Again, XPS, IR and ToF-SIMS were used to identify surface functional groups after the oxidation of the alkene monolayers by  $\text{NO}_3$ . The results are consistent with the formation of C-O, aldehyde/ketone, carboxylic groups, and nitrogen-containing species. A mechanism was suggested and compared to other studies investigating reactions of unsaturated compounds with  $\text{NO}_3$ .

## 10.2 Considerations for Future Work

All of the studies discussed in this thesis were performed using organic films and monolayers of one organic compound of high purity only. Most likely, there are no surfaces containing only one chemical compound in the atmosphere, but these results are important first outcomes for understanding heterogeneous reactions under controlled laboratory conditions.

Since the reactive behaviour of individual organics is now better understood, the next step would be to increase the complexity of the systems studied. This could be done using mixtures of different organic compounds in order to better mimic atmospheric samples. Another way of increasing the complexity and of moving more toward realistic aerosols would be to use multiphase systems, i.e. solid-liquid mixtures of two or more

organics. These solid-liquid mixtures have been shown to significantly decrease the uptake of ozone on oleic acid<sup>75</sup> and similar behaviour can be expected for other oxidants (e.g. NO<sub>3</sub>). However, this has not been shown to date.

Since organics are thought to form surface coatings on aqueous or solid inorganic aerosol particles, mimicking these surface coatings may also provide valuable insights into atmospheric reactions. As mentioned in Chapter 6, studies on heterogeneous reactions of PAHs on different substrates have resulted in widely different results and this was attributed to differences in the underlying substrate. In addition, experiments on aqueous substrates would be beneficial. Aqueous droplets constitute a large fraction of aerosols in the atmosphere due to the high abundance of water vapour. Surface active organics may coat these droplets and form a surface film. Reactive uptake measurements of NO<sub>3</sub> (and other oxidants) on these substrates would therefore be very interesting. However, these measurements can not be performed in the rotating coated wall flow cell employed in the present work. The rectangular flow cell described in Knopf et al.<sup>235</sup> and Cosman et al.<sup>50,51</sup> allows uptake experiments on a planar aqueous surface and has been shown to be a valuable tool to investigate these types of reactions. Their work has used N<sub>2</sub>O<sub>5</sub> as the gas-phase species. Studies using NO<sub>3</sub>, NO<sub>2</sub>, or O<sub>3</sub> on these surfaces could shed light on the influence of a water subphase.

The work in this thesis investigated the reactions of NO<sub>3</sub> with alkane, alkene, alkanolate, alkenoic acid, alcohol, and aromatic functional groups. In order to increase knowledge about the relative reactivities of different functional groups, systematic studies of uptakes on a variety of different organics would be necessary. For example, only a C<sub>3</sub>-polyalcohol was used to investigate reactive uptakes on hydroxyl groups in Chapter 7. Further work on compounds with only one OH-group on a primary, secondary, and tertiary C atom would allow for more detailed conclusions. Another possibility for future work would be branched carbon chains, as all compounds investigated here were unbranched molecules. Investigations on aldehydes, ketones, or amines would be beneficial as well in order to rank functional groups according to their reactivities in heterogeneous reactions.

Suggested mechanisms for the reactions of NO<sub>3</sub> with different organics were outlined in Chapters 6 through 9. However, these mechanisms are only tentative and

more work is needed to confirm the actual reaction steps and make quantitative statements about the reaction products formed and the branching ratios of different reaction paths. Identification and quantification of gas-phase products in the SAM studies would complement the condensed-phase products observed in Chapters 8 and 9. In contrast, the PAH study (Chapter 6) focused only on the gas-phase products but did not investigate the PAH-derivatives formed in the condensed-phase due to  $\text{NO}_3$  reaction. Quantitative analysis of these products is essential in order to confirm or modify the reaction mechanisms proposed. For several reactions it has been proposed that one or more reaction paths lead to scission in the carbon chain of the organic species. For example, decomposition of alkene chains at the double bond has been suggested, as well as formation of aldehydes from ester functional groups.<sup>154</sup> If scission results in small short chain molecules, these products should be volatile enough to be released into the gas phase. Therefore, investigations on organic gas-phase products in addition to inorganic gas-phase and organic condensed-phase products could increase understanding of the volatilization of organic surfaces.

Experiments throughout this thesis were performed using concentrations of the gas-phase species that were higher than under most natural conditions in the troposphere due to detection limitations of the CIMS. It is assumed that these elevated concentrations did not impact the results observed. However, additional validation of this assumption would be beneficial.

The work presented here uses flat surfaces of more than  $1 \text{ cm}^2$  as proxies for aerosol particles. This is most likely valid as the surface curvature of aerosols should not affect their reactivity for the majority of aerosol particles. However, it would still be interesting to investigate the same reactions on organic aerosols using an aerosol mass spectrometer. This would be especially interesting in the liquid phase. In the experiments presented in this thesis, liquid surfaces were able to replenish themselves during rotation of the glass cylinder. In aerosol particles, liquid organic aerosols are expected to age through heterogeneous reactions and change in composition and reactivity.

## REFERENCES

- (1) Finlayson-Pitts, B. J.; Pitts, J. N. *Chemistry of the upper and lower atmosphere*; Academic Press: San Diego, 2000.
- (2) Wallace, J. M.; Hobbs, P. V. *Atmospheric science*, 2nd ed.; Elsevier: Amsterdam, 2006.
- (3) Pandis, S. N.; Wexler, A. S.; Seinfeld, J. H. *Journal of Physical Chemistry* **1995**, 99, 9646.
- (4) Whitby, K. T.; Clark, W. E.; Marple, V. A.; Sverdrup, G. M.; Sem, G. J.; Willeke, K.; Liu, B. Y. H.; Pui, D. Y. H. *Atmospheric Environment* **1975**, 9, 463.
- (5) Fitzgerald, J. W. *Atmospheric Environment Part a - General Topics* **1991**, 25, 533.
- (6) Stanhill, G.; Cohen, S. *Agricultural and Forest Meteorology* **2001**, 107, 255.
- (7) Andreae, M. O.; Rosenfeld, D. *Earth-Science Reviews* **2008**, 89, 13.
- (8) *Fourth Assessment Report of the Intergovernmental Panel on Climate Change*; Cambridge University Press: Cambridge, 2007.
- (9) Hyslop, N. P. *Atmospheric Environment* **2009**, 43, 182.
- (10) Oberdörster, G. *International Archives of Occupational and Environmental Health* **2001**, 74, 1.
- (11) Bamford, H. A.; Baker, J. E. *Atmospheric Environment* **2003**, 37, 2077.
- (12) Kelly, T. J.; Mukund, R.; Spicer, C. W.; Pollack, A. J. *Environmental Science & Technology* **1994**, 28, A378.
- (13) Andreae, M. O.; Crutzen, P. J. *Science* **1997**, 276, 1052.
- (14) Elbert, W.; Taylor, P. E.; Andreae, M. O.; Pöschl, U. *Atmospheric Chemistry and Physics* **2007**, 7, 4569.
- (15) Rogge, W. F.; Hildemann, L. M.; Mazurek, M. A.; Cass, G. R.; Simoneit, B. R. T. *Environmental Science & Technology* **1991**, 25, 1112.
- (16) Rogge, W. F.; Hildemann, L. M.; Mazurek, M. A.; Cass, G. R. *Environmental Science & Technology* **1994**, 28, 1375.

- (17) Donahue, N. M.; Robinson, A. L.; Pandis, S. N. *Atmospheric Environment* **2009**, *43*, 94.
- (18) Rogge, W. F.; Mazurek, M. A.; Hildemann, L. M.; Cass, G. R.; Simoneit, B. R. T. *Atmospheric Environment Part a-General Topics* **1993**, *27*, 1309.
- (19) Krivacsy, Z.; Hoffer, A.; Sarvari, Z.; Temesi, D.; Baltensperger, U.; Nyeki, S.; Weingartner, E.; Kleefeld, S.; Jennings, S. G. *Atmospheric Environment* **2001**, *35*, 6231.
- (20) Gill, P. S.; Graedel, T. E.; Weschler, C. J. *Reviews of Geophysics* **1983**, *21*, 903.
- (21) Tervahattu, H.; Juhanoja, J.; Kupiainen, K. *Journal of Geophysical Research-Atmospheres* **2002**, *107*, 4319.
- (22) Tervahattu, H.; Hartonen, K.; Kerminen, V. M.; Kupiainen, K.; Aarnio, P.; Koskentalo, T.; Tuck, A. F.; Vaida, V. *Journal of Geophysical Research-Atmospheres* **2002**, *107*, 4053.
- (23) Ellison, G. B.; Tuck, A. F.; Vaida, V. *Journal of Geophysical Research-Atmospheres* **1999**, *104*, 11633.
- (24) Usher, C. R.; Michel, A. E.; Grassian, V. H. *Chemical Reviews* **2003**, *103*, 4883.
- (25) Usher, C. R.; Michel, A. E.; Stec, D.; Grassian, V. H. *Atmospheric Environment* **2003**, *37*, 5337.
- (26) Ketseridis, G.; Hahn, J.; Jaenicke, R.; Junge, C. *Atmospheric Environment* **1976**, *10*, 603.
- (27) Mazurek, M.; Masonjones, M. C.; Masonjones, H. D.; Salmon, L. G.; Cass, G. R.; Hallock, K. A.; Leach, M. *Journal of Geophysical Research-Atmospheres* **1997**, *102*, 3779.
- (28) Pöschl, U. *Angewandte Chemie-International Edition* **2005**, *44*, 7520.
- (29) Decesari, S.; Facchini, M. C.; Fuzzi, S.; Tagliavini, E. *Journal of Geophysical Research-Atmospheres* **2000**, *105*, 1481.
- (30) Pfrang, C.; Martin, R. S.; Canosa-Mas, C. E.; Wayne, R. P. *Physical Chemistry Chemical Physics* **2006**, *8*, 354.



- (31) Pozzoli, L.; Gilardoni, S.; Perrone, M. G.; De Gennaro, G.; De Rienzo, M.; Vione, D. *Annali Di Chimica* **2004**, *94*, 17.
- (32) Arey, J.; Atkinson, R.; Zielinska, B.; McElroy, P. A. *Environmental Science & Technology* **1989**, *23*, 321.
- (33) Marr, L. C.; Dzepina, K.; Jimenez, J. L.; Reisen, F.; Bethel, H. L.; Arey, J.; Gaffney, J. S.; Marley, N. A.; Molina, L. T.; Molina, M. J. *Atmospheric Chemistry and Physics* **2006**, *6*, 1733.
- (34) Reisen, F.; Arey, J. *Environmental Science & Technology* **2005**, *39*, 64.
- (35) Ishii, S.; Hisamatsu, Y.; Inazu, K.; Kadoi, M.; Aika, K. I. *Environmental Science & Technology* **2000**, *34*, 1893.
- (36) Lewis, A. C.; Bartle, K. D.; Pilling, M. J. *Polycyclic Aromatic Compounds* **2002**, *22*, 175.
- (37) Yang, H. H.; Tsai, C. H.; Chao, M. R.; Su, Y. L.; Chien, S. M. *Atmospheric Environment* **2006**, *40*, 1266.
- (38) Ammann, M.; Pöschl, U.; Rudich, Y. *Physical Chemistry Chemical Physics* **2003**, *5*, 351.
- (39) Wayne, R. P.; Barnes, I.; Biggs, P.; Burrows, J. P.; Canosamas, C. E.; Hjorth, J.; Lebras, G.; Moortgat, G. K.; Perner, D.; Poulet, G.; Restelli, G.; Sidebottom, H. *Atmospheric Environment Part a-General Topics* **1991**, *25*, 1.
- (40) Atkinson, R. *Journal of Physical and Chemical Reference Data* **1997**, *26*, 215.
- (41) Atkinson, R. *Journal of Physical and Chemical Reference Data* **1991**, *20*, 459.
- (42) Aschmann, S. M.; Atkinson, R. *Atmospheric Environment* **1995**, *29*, 2311.
- (43) Robinson, A. L.; Donahue, N. M.; Rogge, W. F. *Journal of Geophysical Research-Atmospheres* **2006**, *111*, D03302.
- (44) Moise, T.; Talukdar, R. K.; Frost, G. J.; Fox, R. W.; Rudich, Y. *Journal of Geophysical Research-Atmospheres* **2002**, *107*, 4014.
- (45) Molina, M. J.; Rowland, F. S. *Nature* **1974**, *249*, 810.
- (46) Moise, T.; Rudich, Y. *Geophysical Research Letters* **2001**, *28*, 4083.

- (47) Dubowski, Y.; Vieceli, J.; Tobias, D. J.; Gomez, A.; Lin, A.; Nizkorodov, S. A.; McIntire, T. M.; Finlayson-Pitts, B. J. *Journal of Physical Chemistry A* **2004**, *108*, 10473.
- (48) Vieceli, J.; Ma, O. L.; Tobias, D. J. *Journal of Physical Chemistry A* **2004**, *108*, 5806.
- (49) Seinfeld, J. H.; Pandis, S. N. *Atmospheric chemistry and physics: from air pollution to climate change*, 2nd ed.; John Wiley & Sons, Inc.: Hoboken, 2006.
- (50) Cosman, L. M.; Bertram, A. K. *Journal of Physical Chemistry A* **2008**, *112*, 4625.
- (51) Cosman, L. M.; Knopf, D. A.; Bertram, A. K. *Journal of Physical Chemistry A* **2008**, *112*, 2386.
- (52) Donaldson, D. J.; Vaida, V. *Chemical Reviews* **2006**, *106*, 1445.
- (53) Thornton, J. A.; Abbatt, J. P. D. *Journal of Physical Chemistry A* **2005**, *109*, 10004.
- (54) Park, S. C.; Burden, D. K.; Nathanson, G. M. *Journal of Physical Chemistry A* **2007**, *111*, 2921.
- (55) Atkins, P.; de Paula, J. *Physical Chemistry*, 7th ed.; W.H. Freeman and Company: New York, 2002.
- (56) Molina, M. J.; Ivanov, A. V.; Trakhtenberg, S.; Molina, L. T. *Geophysical Research Letters* **2004**, *31*, L22104.
- (57) Kwan, A. J.; Crounse, J. D.; Clarke, A. D.; Shinozuka, Y.; Anderson, B. E.; Crawford, J. H.; Avery, M. A.; McNaughton, C. S.; Brune, W. H.; Singh, H. B.; Wennberg, P. O. *Geophysical Research Letters* **2006**, *33*, L15815.
- (58) de Gouw, J. A.; Lovejoy, E. R. *Geophysical Research Letters* **1998**, *25*, 931.
- (59) Wadia, Y.; Tobias, D. J.; Stafford, R.; Finlayson-Pitts, B. J. *Langmuir* **2000**, *16*, 9321.
- (60) Smith, G. D.; Woods, E.; DeForest, C. L.; Baer, T.; Miller, R. E. *Journal of Physical Chemistry A* **2002**, *106*, 8085.
- (61) Thornberry, T.; Abbatt, J. P. D. *Physical Chemistry Chemical Physics* **2004**, *6*, 84.

- (62) Eliason, T. L.; Aloisio, S.; Donaldson, D. J.; Cziezo, D. J.; Vaida, V. *Atmospheric Environment* **2003**, *37*, 2207.
- (63) Docherty, K. S.; Ziemann, P. J. *Journal of Physical Chemistry A* **2006**, *110*, 3567.
- (64) Moise, T.; Rudich, Y. *Journal of Geophysical Research-Atmospheres* **2000**, *105*, 14667.
- (65) Thomas, E. R.; Frost, G. J.; Rudich, Y. *Journal of Geophysical Research-Atmospheres* **2001**, *106*, 3045.
- (66) Hung, H. M.; Katrib, Y.; Martin, S. T. *Journal of Physical Chemistry A* **2005**, *109*, 4517.
- (67) Bertram, A. K.; Ivanov, A. V.; Hunter, M.; Molina, L. T.; Molina, M. J. *Journal of Physical Chemistry A* **2001**, *105*, 9415.
- (68) Hearn, J. D.; Smith, G. D. *Geophysical Research Letters* **2006**, *33*, L17805.
- (69) Hearn, J. D.; Renbaum, L. H.; Wang, X.; Smith, G. D. *Physical Chemistry Chemical Physics* **2007**, *9*, 4803.
- (70) George, I. J.; Vlasenko, A.; Slowik, J. G.; Broekhuizen, K.; Abbatt, J. P. D. *Atmospheric Chemistry and Physics* **2007**, *7*, 4187.
- (71) Ziemann, P. J. *Faraday Discussions* **2005**, *130*, 469.
- (72) Esteve, W.; Budzinski, H.; Villenave, E. *Atmospheric Environment* **2004**, *38*, 6063.
- (73) McNeill, V. F.; Wolfe, G. M.; Thornton, J. A. *Journal of Physical Chemistry A* **2007**, *111*, 1073.
- (74) George, I. J.; Slowik, J.; Abbatt, J. P. D. *Geophysical Research Letters* **2008**, *35*, L13811.
- (75) Knopf, D. A.; Anthony, L. M.; Bertram, A. K. *Journal of Physical Chemistry A* **2005**, *109*, 5579.
- (76) Imamura, T.; Rudich, Y.; Talukdar, R. K.; Fox, R. W.; Ravishankara, A. R. *Journal of Physical Chemistry A* **1997**, *101*, 2316.
- (77) Karagulian, F.; Rossi, M. J. *Physical Chemistry Chemical Physics* **2005**, *7*, 3150.

- (78) Karagulian, F.; Rossi, M. J. *Journal of Physical Chemistry A* **2007**, *111*, 1914.
- (79) Schütze, M.; Herrmann, H. *Journal of Atmospheric Chemistry* **2005**, *52*, 1.
- (80) Rudich, Y. *Chemical Reviews* **2003**, *103*, 5097.
- (81) Gross, S.; Bertram, A. K. *Journal of Physical Chemistry A* **2008**, *112*, 3104.
- (82) Mak, J.; Gross, S.; Bertram, A. K. *Geophysical Research Letters* **2007**, *34*, L10804.
- (83) Knopf, D. A.; Mak, J.; Gross, S.; Bertram, A. K. *Geophysical Research Letters* **2006**, *33*, L17816.
- (84) Gross, S.; Bertram, A. K. *Journal of Geophysical Research-Atmospheres* **2009**, *114*, D02307.
- (85) Platt, U.; Perner, D.; Winer, A. M.; Harris, G. W.; Pitts, J. N. *Geophysical Research Letters* **1980**, *7*, 89.
- (86) Aldener, M.; Brown, S. S.; Stark, H.; Williams, E. J.; Lerner, B. M.; Kuster, W. C.; Goldan, P. D.; Quinn, P. K.; Bates, T. S.; Fehsenfeld, F. C.; Ravishankara, A. R. *Journal of Geophysical Research-Atmospheres* **2006**, *111*, D23S73.
- (87) Kamens, R. M.; Guo, J.; Guo, Z.; McDow, S. R. *Atmospheric Environment Part a-General Topics* **1990**, *24*, 1161.
- (88) Hammer, P. D.; Dlugokencky, E. J.; Howard, C. J. *Journal of Physical Chemistry* **1986**, *90*, 2491.
- (89) Tyndall, G. S.; Orlando, J. J.; Cantrell, C. A.; Shetter, R. E.; Calvert, J. G. *Journal of Physical Chemistry* **1991**, *95*, 4381.
- (90) Allan, B. J.; McFiggans, G.; Plane, J. M. C.; Coe, H.; McFadyen, G. G. *Journal of Geophysical Research-Atmospheres* **2000**, *105*, 24191.
- (91) Mentel, T. F.; Bleilebens, D.; Wahner, A. *Atmospheric Environment* **1996**, *30*, 4007.
- (92) *Handbook of Chemistry and Physics*; 82nd ed.; Lide, D. R., Ed.; CRC Press: Boca Raton, 2001.
- (93) Smith, N.; Plane, J. M. C.; Nien, C. F.; Solomon, P. A. *Atmospheric Environment* **1995**, *29*, 2887.

- (94) Dunlea, E. J.; Herndon, S. C.; Nelson, D. D.; Volkamer, R. M.; San Martini, F.; Sheehy, P. M.; Zahniser, M. S.; Shorter, J. H.; Wormhoudt, J. C.; Lamb, B. K.; Allwine, E. J.; Gaffney, J. S.; Marley, N. A.; Grutter, M.; Marquez, C.; Blanco, S.; Cardenas, B.; Retama, A.; Villegas, C. R. R.; Kolb, C. E.; Molina, L. T.; Molina, M. J. *Atmospheric Chemistry and Physics* **2007**, 7, 2691.
- (95) Fleming, Z. L.; Monks, P. S.; Rickard, A. R.; Bandy, B. J.; Brough, N.; Green, T. J.; Reeves, C. E.; Penkett, S. A. *Atmospheric Chemistry and Physics* **2006**, 6, 5415.
- (96) Kunhikrishnan, T.; Lawrence, M. G.; von Kuhlmann, R.; Richter, A.; Ladstatter-Weissenmayer, A.; Burrows, J. P. *Atmospheric Environment* **2004**, 38, 581.
- (97) Brown, S. S.; Stark, H.; Ryerson, T. B.; Williams, E. J.; Nicks, D. K.; Trainer, M.; Fehsenfeld, F. C.; Ravishankara, A. R. *Journal of Geophysical Research-Atmospheres* **2003**, 108, 4299.
- (98) Pitts, J. N.; Zielinska, B.; Sweetman, J. A.; Atkinson, R.; Winer, A. M. *Atmospheric Environment* **1985**, 19, 911.
- (99) McLaren, R.; Salmon, R. A.; Liggio, J.; Hayden, K. L.; Anlauf, K. G.; Leaitch, W. R. *Atmospheric Environment* **2004**, 38, 5837.
- (100) Ayers, J. D.; Simpson, W. R. *Journal of Geophysical Research-Atmospheres* **2006**, 111, D14309.
- (101) Wood, E. C.; Bertram, T. H.; Wooldridge, P. J.; Cohen, R. C. *Atmospheric Chemistry and Physics* **2005**, 5, 483.
- (102) Likens, G. E.; Bormann, F. H. *Science* **1974**, 184, 1171.
- (103) Hanson, D. R. *Geophysical Research Letters* **1990**, 17, 421.
- (104) Heck, W. W.; Taylor, O. C.; Adams, R.; Bingham, G.; Miller, J.; Preston, E.; Weinstein, L. *Journal of the Air Pollution Control Association* **1982**, 32, 353.
- (105) Logan, J. A. *Journal of Geophysical Research-Atmospheres* **1985**, 90, 10463.
- (106) Harrison, A. G. *Chemical Ionization Mass Spectrometry*, 2nd ed.; CRC Press: Boca Raton, 1992.
- (107) Huey, L. G.; Hanson, D. R.; Howard, C. J. *Journal of Physical Chemistry* **1995**, 99, 5001.

- (108) Brown, R. L. *Journal of Research of the National Bureau of Standards* **1978**, 83, 1.
- (109) Rudich, Y.; Talukdar, R. K.; Imamura, T.; Fox, R. W.; Ravishankara, A. R. *Chemical Physics Letters* **1996**, 261, 467.
- (110) Attard, G.; Barnes, C. *Surfaces*; Oxford University Press: New York, 1998.
- (111) *Advances in surface science*; Nalwa, H. S., Ed.; Academic Press: San Diego, 2001.
- (112) *Practical surface analysis*; Briggs, D.; Seah, M. P., Eds.; Salle and Sauerländer: Chichester, 1990.
- (113) Somorjai, G. A. *Introduction to Surface Chemistry and Catalysis*; Wiley-Interscience: New York, 1993.
- (114) Wallart, X.; de Villeneuve, C. H.; Allongue, P. *Journal of the American Chemical Society* **2005**, 127, 7871.
- (115) Hutton, B. M.; Williams, D. E. *Analyst* **2000**, 125, 1703.
- (116) Ulman, A. *Characterization of organic thin films*; Butterworth-Heinemann: Boston, 1995.
- (117) Benninghoven, A.; Rüdenauer, F. G.; Werner, H. W. *Secondary ion mass spectrometry: basic concepts, instrumental aspects, applications, and trends*; J. Wiley: New York, 1987.
- (118) Wilson, R. G.; Stevie, F. A.; Magee, C. W. *Secondary ion mass spectrometry: a practical handbook for depth profiling and bulk impurity analysis*; Wiley: New York, 1989.
- (119) Harris, D. C. *Quantitative Chemical Analysis*, 5th ed.; W.H. Freeman and Company: New York, 1999.
- (120) Lam, B.; Diamond, M. L.; Simpson, A. J.; Makar, P. A.; Truong, J.; Hernandez-Martinez, N. A. *Atmospheric Environment* **2005**, 39, 6578.
- (121) Simpson, A. J.; Lam, B.; Diamond, M. L.; Donaldson, D. J.; Lefebvre, B. A.; Moser, A. Q.; Williams, A. J.; Larin, N. I.; Kvasha, M. P. *Chemosphere* **2006**, 63, 142.

- (122) Kahan, T. F.; Kwamena, N. O. A.; Donaldson, D. J. *Atmospheric Environment* **2006**, *40*, 3448.
- (123) Mmereki, B. T.; Donaldson, D. J.; Gilman, J. B.; Eliason, T. L.; Vaida, V. *Atmospheric Environment* **2004**, *38*, 6091.
- (124) Esteve, W.; Budzinski, H.; Villenave, E. *Atmospheric Environment* **2006**, *40*, 201.
- (125) Arens, F.; Gutzwiller, L.; Gaggeler, H. W.; Ammann, M. *Physical Chemistry Chemical Physics* **2002**, *4*, 3684.
- (126) Ishii, S.; Hisamatsu, Y.; Inazu, K.; Kobayashi, T.; Aika, K. *Chemosphere* **2000**, *41*, 1809.
- (127) Inazu, K.; Kobayashi, T.; Hisamatsu, Y. *Chemosphere* **1997**, *35*, 607.
- (128) Inazu, K.; Tsutsumi, N.; Aika, K. I.; Hisamatsu, Y. *Polycyclic Aromatic Compounds* **2000**, *20*, 191.
- (129) Pöschl, U.; Letzel, T.; Schauer, C.; Niessner, R. *Journal of Physical Chemistry A* **2001**, *105*, 4029.
- (130) Kwamena, N. O. A.; Thornton, J. A.; Abbatt, J. P. D. *Journal of Physical Chemistry A* **2004**, *108*, 11626.
- (131) Mmereki, B. T.; Donaldson, D. J. *Journal of Physical Chemistry A* **2003**, *107*, 11038.
- (132) Alebic-Juretic, A.; Cvitas, T.; Klasinc, L. *Environmental Science & Technology* **1990**, *24*, 62.
- (133) Pitts, J. N.; Paur, H. R.; Zielinska, B.; Arey, J.; Winer, A. M.; Ramdahl, T.; Mejia, V. *Chemosphere* **1986**, *15*, 675.
- (134) Van Vaeck, L.; Van Cauwenberghe, K. *Atmospheric Environment* **1984**, *18*, 323.
- (135) Vione, D.; Barra, S.; De Gennaro, G.; De Rienzo, M.; Gilardoni, S.; Perrone, M. G.; Pozzoli, L. *Annali Di Chimica* **2004**, *94*, 257.
- (136) Aubin, D. G.; Abbatt, J. P. *Journal of Physical Chemistry A* **2003**, *107*, 11030.
- (137) Schott, G.; Davidson, N. *J. Am. Chem. Soc.* **1958**, *80*, 1841.

- (138) Paz, Y.; Trakhtenberg, S.; Naaman, R. *Journal of Physical Chemistry* **1992**, *96*, 10964.
- (139) Paz, Y.; Trakhtenberg, S.; Naaman, R. *Journal of Physical Chemistry* **1994**, *98*, 13517.
- (140) Schauer, C.; Niessner, R.; Pöschl, U. *Environmental Science & Technology* **2003**, *37*, 2861.
- (141) Longfellow, C. A.; Ravishankara, A. R.; Hanson, D. R. *Journal of Geophysical Research-Atmospheres* **2000**, *105*, 24345.
- (142) Nielsen, T. *Environmental Science & Technology* **1984**, *18*, 157.
- (143) Vione, D.; Maurino, V.; Minero, C.; Pelizzetti, E. *Environmental Science & Technology* **2005**, *39*, 1101.
- (144) Sasaki, J.; Aschmann, S. M.; Kwok, E. S. C.; Atkinson, R.; Arey, J. *Environmental Science & Technology* **1997**, *31*, 3173.
- (145) Calvert, J. G.; Atkinson, R.; Becker, K. H.; Kamens, R. M.; Seinfeld, J. H.; Wallington, T. J.; Yarwood, G. *The mechanisms of atmospheric oxidation of aromatic hydrocarbons*; Oxford University Press: New York, 2002.
- (146) Atkinson, R.; Arey, J. *Environmental Health Perspectives* **1994**, *102*, 117.
- (147) Kwok, E. S. C.; Harger, W. P.; Arey, J.; Atkinson, R. *Environmental Science & Technology* **1994**, *28*, 521.
- (148) Kamens, R. M.; Rives, G. D.; Perry, J. M.; Bell, D. A.; Paylor, R. F.; Goodman, R. G.; Claxton, L. D. *Environmental Science & Technology* **1984**, *18*, 523.
- (149) Mazurek, M. A.; Cass, G. R.; Simoneit, B. R. T. *Environmental Science & Technology* **1991**, *25*, 684.
- (150) Hildemann, L. M.; Mazurek, M. A.; Cass, G. R.; Simoneit, B. R. T. *Environmental Science & Technology* **1991**, *25*, 1311.
- (151) Fuzzi, S.; Facchini, M. C.; Decesari, S.; Matta, E.; Mircea, M. *Atmospheric Research* **2002**, *64*, 89.
- (152) Thornton, J. A.; Braban, C. F.; Abbatt, J. P. D. *Physical Chemistry Chemical Physics* **2003**, *5*, 4593.
- (153) Lai, C. C.; Finlayson-Pitts, B. J. *Lipids* **1991**, *26*, 306.



- (154) Vlasenko, A.; George, I. J.; Abbatt, J. P. D. *Journal of Physical Chemistry A* **2008**, *112*, 1552.
- (155) Hearn, J. D.; Lovett, A. J.; Smith, G. D. *Physical Chemistry Chemical Physics* **2005**, *7*, 501.
- (156) Langer, S.; Ljungström, E. *Journal of the Chemical Society-Faraday Transactions* **1995**, *91*, 405.
- (157) Chew, A. A.; Atkinson, R.; Aschmann, S. M. *Journal of the Chemical Society-Faraday Transactions* **1998**, *94*, 1083.
- (158) Langer, S.; Ljungström, E.; Wängberg, I. *Journal of the Chemical Society-Faraday Transactions* **1993**, *89*, 425.
- (159) Atkinson, R.; Baulch, D. L.; Cox, R. A.; Crowley, J. N.; Hampson, R. F.; Hynes, R. G.; Jenkin, M. E.; Rossi, M. J.; Troe, J. *Atmospheric Chemistry and Physics* **2006**, *6*, 3625.
- (160) Davidovits, P.; Kolb, C. E.; Williams, L. R.; Jayne, J. T.; Worsnop, D. R. *Chemical Reviews*. **2006**, *106*, 1323
- (161) Shi, D. Q.; Gao, G. L.; Li, D. Y.; Dong, J. W.; Wang, L. H. *Fluid Phase Equilibria* **2008**, *273*, 87.
- (162) Lopez-Lopez, M. T.; de Vicente, J.; Gonzalez-Caballero, F.; Duran, J. D. G. *Colloids and Surfaces a-Physicochemical and Engineering Aspects* **2005**, *264*, 75.
- (163) de Lorenzi, L.; Fermeglia, M.; Torriano, G. *Journal of Chemical and Engineering Data* **1997**, *42*, 919.
- (164) Kames, J.; Schurath, U.; Flocke, F.; Volzthomas, A. *Journal of Atmospheric Chemistry* **1993**, *16*, 349.
- (165) Stevens, T. E.; Emmons, W. D. *Journal of the American Chemical Society* **1957**, *79*, 6008.
- (166) Warneck, P. *Chemosphere* **2007**, *69*, 347.
- (167) Pfrang, C.; Romero, M. T. B.; Cabanas, B.; Canosa-Mas, C. E.; Villanueva, F.; Wayne, R. P. *Atmospheric Environment* **2007**, *41*, 1652.
- (168) Penkett, S. A.; Burgess, R. A.; Coe, H.; Coll, I.; Hov, O.; Lindskog, A.; Schmidbauer, N.; Solberg, S.; Roemer, M.; Thijssse, T.; Beck, J.; Reeves, C. E. *Atmospheric Environment* **2007**, *41*, 3465.

- (169) Brown, S. S.; Dube, W. P.; Osthoff, H. D.; Stutz, J.; Ryerson, T. B.; Wollny, A. G.; Brock, C. A.; Warneke, C.; De Gouw, J. A.; Atlas, E.; Neuman, J. A.; Holloway, J. S.; Lerner, B. M.; Williams, E. J.; Kuster, W. C.; Goldan, P. D.; Angevine, W. M.; Trainer, M.; Fehsenfeld, F. C.; Ravishankara, A. R. *Journal of Geophysical Research-Atmospheres* **2007**, *112*, D22304.
- (170) Brown, S. S.; Ryerson, T. B.; Wollny, A. G.; Brock, C. A.; Peltier, R.; Sullivan, A. P.; Weber, R. J.; Dube, W. P.; Trainer, M.; Meagher, J. F.; Fehsenfeld, F. C.; Ravishankara, A. R. *Science* **2006**, *311*, 67.
- (171) Cabada, J. C.; Rees, S.; Takahama, S.; Khlystov, A.; Pandis, S. N.; Davidson, C. I.; Robinson, A. L. *Atmospheric Environment* **2004**, *38*, 3127.
- (172) Balkanski, Y. J.; Jacob, D. J.; Gardner, G. M.; Graustein, W. C.; Turekian, K. K. *Journal of Geophysical Research-Atmospheres* **1993**, *98*, 20573.
- (173) Liousse, C.; Penner, J. E.; Chuang, C.; Walton, J. J.; Eddleman, H.; Cachier, H. *Journal of Geophysical Research-Atmospheres* **1996**, *101*, 19411.
- (174) Gaffney, J. S.; Marley, N. A.; Cunningham, M. M. *Atmospheric Environment* **2004**, *38*, 3191.
- (175) Morris, J. W.; Davidovits, P.; Jayne, J. T.; Jimenez, J. L.; Shi, Q.; Kolb, C. E.; Worsnop, D. R.; Barney, W. S.; Cass, G. *Geophysical Research Letters* **2002**, *29*, 1357.
- (176) Weitkamp, E. A.; Hartz, K. E. H.; Sage, A. M.; Donahue, N. M.; Robinson, A. L. *Environmental Science & Technology* **2008**, *42*, 5177.
- (177) Hearn, J. D.; Smith, G. D. *International Journal of Mass Spectrometry* **2006**, *258*, 95.
- (178) Katrib, Y.; Biskos, G.; Buseck, P. R.; Davidovits, P.; Jayne, J. T.; Mochida, M.; Wise, M. E.; Worsnop, D. R.; Martin, S. T. *Journal of Physical Chemistry A* **2005**, *109*, 10910.
- (179) Nash, D. G.; Tolocka, M. P.; Baer, T. *Physical Chemistry Chemical Physics* **2006**, *8*, 4468.
- (180) Zahardis, J.; Petrucci, G. A. *Atmospheric Chemistry and Physics* **2007**, *7*, 1237.

- (181) Hartz, K. E. H.; Weitkamp, E. A.; Sage, A. M.; Donahue, N. M.; Robinson, A. L. *Journal of Geophysical Research-Atmospheres* **2007**, *112*, D04204.
- (182) Marcolli, C.; Luo, B. P.; Peter, T.; Wienhold, F. G. *Atmospheric Chemistry and Physics* **2004**, *4*, 2593.
- (183) Ng, N. L.; Kwan, A. J.; Surratt, J. D.; Chan, A. W. H.; Chhabra, P. S.; Sorooshian, A.; Pye, H. O. T.; Crounse, J. D.; Wennberg, P. O.; Flagan, R. C.; Seinfeld, J. H. *Atmospheric Chemistry and Physics* **2008**, *8*, 4117.
- (184) Yang, Y. W.; Fan, L. J. *Langmuir* **2002**, *18*, 1157.
- (185) Bain, C. D.; Whitesides, G. M. *Journal of Physical Chemistry* **1989**, *93*, 1670.
- (186) Ulman, A. *Chemical Reviews* **1996**, *96*, 1533.
- (187) Ishida, T.; Nishida, N.; Tsuneda, S.; Hara, M.; Sasabe, H.; Knoll, W. *Japanese Journal of Applied Physics Part 2-Letters* **1996**, *35*, L1710.
- (188) Diamond, M. L.; Gingrich, S. E.; Fertuck, K.; McCarry, B. E.; Stern, G. A.; Billeck, B.; Grift, B.; Brooker, D.; Yager, T. D. *Environmental Science & Technology* **2000**, *34*, 2900.
- (189) Donaldson, D. J.; Mmereki, B. T.; Chaudhuri, S. R.; Handley, S.; Oh, M. *Faraday Discussions* **2005**, *130*, 227.
- (190) McNeill, V. F.; Yatavelli, R. L. N.; Thornton, J. A.; Stipe, C. B.; Landgrebe, O. *Atmospheric Chemistry and Physics* **2008**, *8*, 5465.
- (191) Ishida, T.; Tsuneda, S.; Nishida, N.; Hara, M.; Sasabe, H.; Knoll, W. *Langmuir* **1997**, *13*, 4638.
- (192) Allen, D. T.; Palen, E. J.; Haimov, M. I.; Hering, S. V.; Young, J. R. *Aerosol Science and Technology* **1994**, *21*, 325.
- (193) Jang, M. S.; Kamens, R. M. *Environmental Science & Technology* **2001**, *35*, 3626.
- (194) Tuazon, E. C.; Alvarado, A.; Aschmann, S. M.; Atkinson, R.; Arey, J. *Environmental Science & Technology* **1999**, *33*, 3586.
- (195) Williams, D. H.; Fleming, J. *Spectroscopic methods in organic chemistry*, 4th ed.; McGraw-Hill: London, 1989.

- (196) Alvarado, A.; Tuazon, E. C.; Aschmann, S. M.; Arey, J.; Atkinson, R. *Atmospheric Environment* **1999**, *33*, 2893.
- (197) Atkinson, R.; Tuazon, E. C.; Aschmann, S. M. *International Journal of Chemical Kinetics* **1998**, *30*, 577.
- (198) Hallquist, M.; Wängberg, I.; Ljungström, E.; Barnes, I.; Becker, K. H. *Environmental Science & Technology* **1999**, *33*, 553.
- (199) Palen, E. J.; Allen, D. T.; Pandis, S. N.; Paulson, S. E.; Seinfeld, J. H.; Flagan, R. C. *Atmospheric Environment Part a-General Topics* **1992**, *26*, 1239.
- (200) Cassanelli, P.; Cox, R. A.; Orlando, J. J.; Tyndall, G. S. *Journal of Photochemistry and Photobiology a-Chemistry* **2006**, *177*, 109.
- (201) Allen, G.; Remedios, J. J.; Smith, K. M. *Atmospheric Chemistry and Physics* **2005**, *5*, 3153.
- (202) Laibinis, P. E.; Graham, R. L.; Biebuyck, H. A.; Whitesides, G. M. *Science* **1991**, *254*, 981.
- (203) Wasserman, S. R.; Tao, Y. T.; Whitesides, G. M. *Langmuir* **1989**, *5*, 1074.
- (204) Ebbing, D. D. *General Chemistry*, 4th ed.; Houghton Mifflin: Boston, 1993.
- (205) Briggs, D.; Beamson, G. *Analytical Chemistry* **1992**, *64*, 1729.
- (206) Dicke, C.; Morstein, M.; Hahner, G. *Langmuir* **2002**, *18*, 336.
- (207) Wang, H.; Chen, S. F.; Li, L. Y.; Jiang, S. Y. *Langmuir* **2005**, *21*, 2633.
- (208) Offord, D. A.; John, C. M.; Linford, M. R.; Griffin, J. H. *Langmuir* **1994**, *10*, 883.
- (209) Sun, L. M.; Gardella, J. A. *Langmuir* **2002**, *18*, 9289.
- (210) Sohn, S.; Schröder, M.; Lipinsky, D.; Arlinghaus, H. F. *Surface and Interface Analysis* **2004**, *36*, 1222.
- (211) Bain, C. D.; Troughton, E. B.; Tao, Y. T.; Evall, J.; Whitesides, G. M.; Nuzzo, R. G. *Journal of the American Chemical Society* **1989**, *111*, 321.
- (212) Inman, C. E.; Reed, S. M.; Hutchison, J. E. *Langmuir* **2004**, *20*, 9144.
- (213) Owens, T. M.; Ludwig, B. J.; Schneider, K. S.; Fosnacht, D. R.; Orr, B. G.; Holl, M. M. B. *Langmuir* **2004**, *20*, 9636.
- (214) Robinson, G. N.; Freedman, A.; Graham, R. L. *Langmuir* **1995**, *11*, 2600.

- (215) Rudich, Y.; Benjamin, I.; Naaman, R.; Thomas, E.; Trakhtenberg, S.; Ussyshkin, R. *Journal of Physical Chemistry A* **2000**, *104*, 5238.
- (216) Pruppacher, H. R.; Klett, J. D. *Microphysics of Clouds and Precipitation*; Kluwer Academic Publishers: Dordrecht, 1997.
- (217) Russell, G. A. *J. Am. Chem. Soc.* **1957**, *79*, 3871.
- (218) Karagulian, F.; Dilbeck, C. W.; Finlayson-Pitts, B. J. *Journal of the American Chemical Society* **2008**, *130*, 11272.
- (219) Paulson, S. E.; Chung, M. Y.; Hasson, A. S. *Journal of Physical Chemistry A* **1999**, *103*, 8125.
- (220) Fiegland, L. R.; Saint Fleur, M. M.; Morris, J. R. *Langmuir* **2005**, *21*, 2660.
- (221) McIntire, T. M.; Lea, A. S.; Gaspar, D. J.; Jaitly, N.; Dubowski, Y.; Li, Q. Q.; Finlayson-Pitts, B. J. *Physical Chemistry Chemical Physics* **2005**, *7*, 3605.
- (222) Park, J.; Gomez, A. L.; Walser, M. L.; Lin, A.; Nizkorodov, S. A. *Physical Chemistry Chemical Physics* **2006**, *8*, 2506.
- (223) Peanasky, J. S.; McCarley, R. L. *Langmuir* **1998**, *14*, 113.
- (224) Atkinson, R.; Winer, A. M.; Pitts, J. N. *Atmospheric Environment* **1986**, *20*, 331.
- (225) Geyer, A.; Alicke, B.; Konrad, S.; Schmitz, T.; Stutz, J.; Platt, U. *Journal of Geophysical Research-Atmospheres* **2001**, *106*, 8013.
- (226) Geyer, A.; Ackermann, R.; Dubois, R.; Lohrmann, B.; Müller, T.; Platt, U. *Atmospheric Environment* **2001**, *35*, 3619.
- (227) Ulman, A. *An Introduction to Ultrathin Organic Films from Langmuir-Blodgett to Self-Assembly*; Academic Press: San Diego, 1991.
- (228) Atkinson, R. *Atmospheric Environment* **2000**, *34*, 2063.
- (229) Berndt, T.; Böge, O. *Journal of Atmospheric Chemistry* **1995**, *21*, 275.
- (230) Gong, H. M.; Matsunaga, A.; Ziemann, P. J. *Journal of Physical Chemistry A* **2005**, *109*, 4312.
- (231) Kwok, E. S. C.; Aschmann, S. M.; Arey, J.; Atkinson, R. *International Journal of Chemical Kinetics* **1996**, *28*, 925.

- (232) Noda, J.; Hallquist, M.; Langer, S.; Ljungström, E. *Physical Chemistry Chemical Physics* **2000**, *2*, 2555.
- (233) Dlugokencky, E. J.; Howard, C. J. *Journal of Physical Chemistry* **1989**, *93*, 1091.
- (234) D'Andrea, T. M.; Zhang, X.; Jochnowitz, E. B.; Lindeman, T. G.; Simpson, C. J. S. M.; David, D. E.; Curtiss, T. J.; Morris, J. R.; Ellison, G. B. *Journal of Physical Chemistry B* **2008**, *112*, 535.
- (235) Knopf, D. A.; Cosman, L. M.; Mousavi, P.; Mokamati, S.; Bertram, A. K. *Journal of Physical Chemistry A* **2007**, *111*, 11021.
- (236) Davidovits, P.; Hu, J. H.; Worsnop, D. R.; Zahniser, M. S.; Kolb, C. E. *Faraday Discussions* **1995**, *100*, 65.
- (237) Shi, Q.; Davidovits, P.; Jayne, J. T.; Worsnop, D. R.; Kolb, C. E. *Journal of Physical Chemistry A* **1999**, *103*, 8812.
- (238) Hanson, D. R. *Journal of Physical Chemistry B* **1997**, *101*, 4998.

## APPENDIX

The different stages of gas-particle interactions in the atmosphere have been shown in Figure 2.1 for a spherical particle. Figure A.1 gives an equivalent illustration for a flat liquid surface as used throughout this thesis.

A gas-phase molecule diffuses through the air, collides with the surface, and either adsorbs or bounces off. An adsorbed molecule can either desorb, react at the surface, or be taken up into the bulk. If it diffuses through the bulk, it either reacts or evaporates again into the gas-phase.

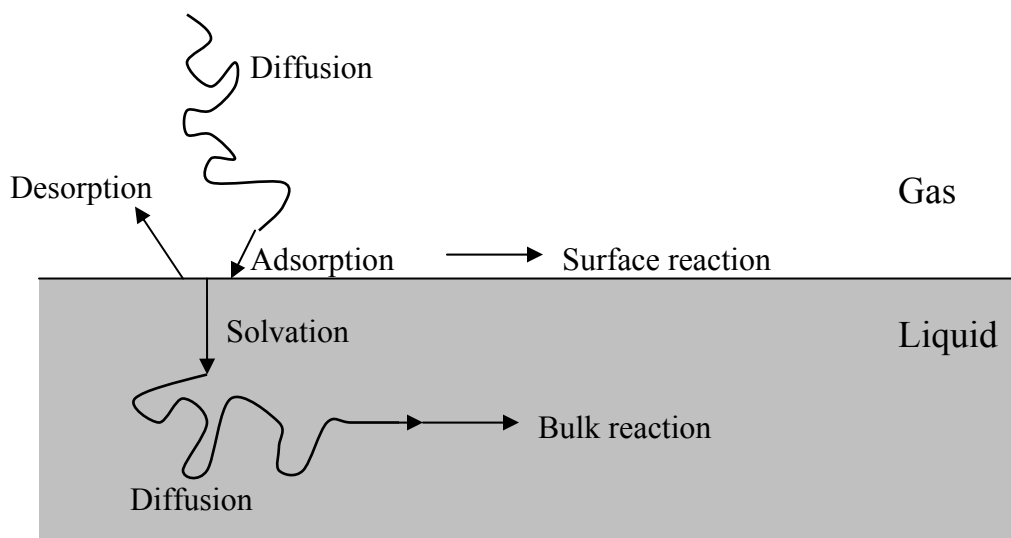


**Figure A.1: Schematic illustration of diffusion, uptake, and reaction of gas-phase species on and in a liquid film, adapted from Finlayson-Pitts and Pitts<sup>1</sup> and Davidovits et al.<sup>160</sup>**

The uptake coefficient  $\gamma$  used throughout this thesis is defined as the fraction of collisions between the gas-phase species and the surface that leads to irreversible uptake. Therefore  $\gamma$  describes the overall process without consideration of the individual steps involved.  $\gamma$  stands for the net uptake as re-evaporation of adsorbed molecules is included.<sup>1</sup>

The uptake, with its individual steps, can be described by a series of coupled differential equations. However, they are not solvable exactly for many cases. A way to

describe the uptake of gas-phase species with all the steps involved is the so called “resistance model”.<sup>1,160</sup> The different processes are treated as if they were not coupled and as if they were components of an electrical circuit.<sup>236</sup> Each physical or chemical process has a specific “speed” – the “conductance  $\Gamma$ ”. The “resistance” of each step is therefore  $(\text{conductance})^{-1}$ , as is the case for electrical circuits.

The different parts of this “circuit” are combined in series and in parallel, as shown in Figure A.2, where  $\Gamma_{\text{diff}}$  is associated with gas-phase diffusion,  $S$  is the surface adsorption coefficient,  $k_{\text{sol}}$  is the rate coefficient for the transfer of molecules from the surface into the liquid,  $k_{\text{des}}$  is the rate coefficient for the transfer of molecules from the surface into the gas, and  $\Gamma_{\text{rxn}}$ ,  $\Gamma_{\text{sat}}$ , and  $\Gamma_{\text{surf}}$  represent the rate of bulk reaction, solubility (saturation) and diffusion, and the rate of surface reaction, respectively.  $S$  is defined as the fraction of collisions that results in thermal accommodation of the gas to the surface.

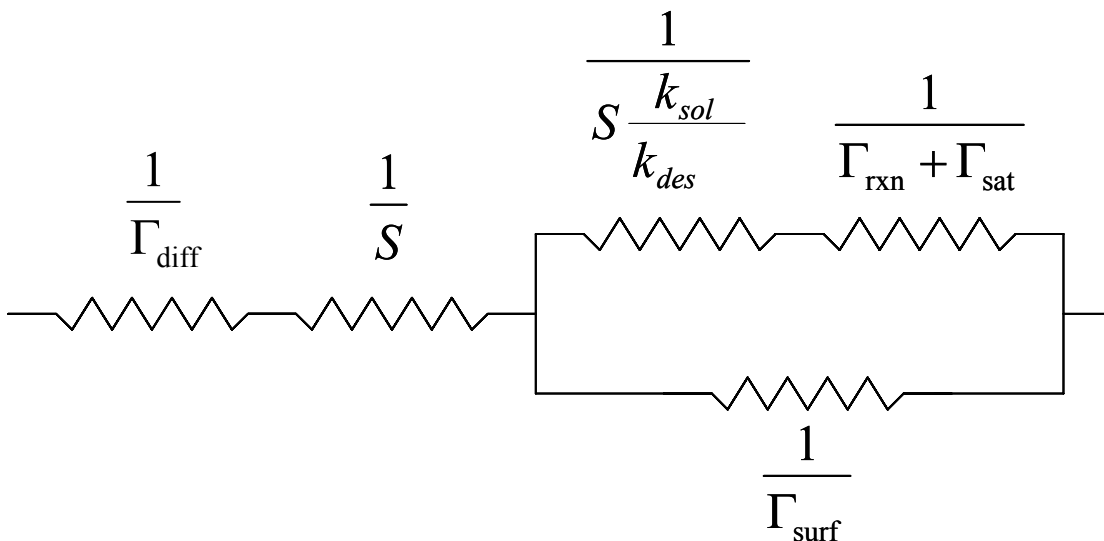


**Figure A.2:** Schematic of the resistance model treating individual chemical and physical processes involved in the uptake of a gas-phase species into a liquid as resistances in an electrical circuit. Processes considered are gas-phase diffusion  $\Gamma_{\text{diff}}$ , surface accommodation  $S$ , rates of solvation and desorption ( $k_{\text{sol}}$  and  $k_{\text{des}}$ ), solubility (liquid phase saturation) and diffusion  $\Gamma_{\text{sat}}$ , reaction in the bulk  $\Gamma_{\text{rxn}}$ , and reaction at the surface  $\Gamma_{\text{surf}}$ , adapted from Davidovits et al.<sup>160</sup>



These steps in series and in parallel lead to the following equation for  $\gamma$ :<sup>160,237,238</sup>

$$\text{A.1} \quad \frac{1}{\gamma} = \frac{1}{\Gamma_{diff}} + \frac{1}{S} + \frac{1}{\frac{1}{\frac{1}{\Gamma_{rxn} + \Gamma_{sat}} + \frac{1}{S \frac{k_{sol}}{k_{des}}}} + \Gamma_{surf}}$$

Equation A.1 reduces to equation A.2, if reaction occurs at the interface only:

$$\text{A.2} \quad \frac{1}{\gamma} = \frac{1}{\Gamma_{diff}} + \frac{1}{S} + \frac{1}{\Gamma_{surf}}$$

and to equation A.3, if surface reaction is irrelevant and bulk reaction only is considered.

$$\text{A.3} \quad \frac{1}{\gamma} = \frac{1}{\Gamma_{diff}} + \frac{1}{S} + \frac{1}{S \frac{k_{sol}}{k_{des}}} + \frac{1}{\Gamma_{sat} + \Gamma_{rxn}}$$

In many cases gas-phase diffusion is fast and the term  $(\Gamma_{diff})^{-1}$  can be ignored.

All of the parameters (S and  $\Gamma$ ) are normalized by the number of collisions of the gas-phase species per  $\text{cm}^2$  per second. This is achieved by dividing the different rates by the number of collisions per area per time, which is given by<sup>1</sup>

$$\text{A.4} \quad \frac{N_g c_{avg}}{4}$$

where  $N_g$  is the gas concentration ( $\text{molecule cm}^{-3}$ ) and  $c_{avg}$  is the average molecular speed in the gas-phase ( $\text{cm s}^{-1}$ ).

Equations for  $\Gamma_{sat}$  and  $\Gamma_{rxn}$  can be derived from the rates of these processes and the normalization given in eq A.4:

The rate of diffusion in the aerosol particle is given by<sup>1</sup>

$$\text{A.5} \quad Rate = N_i \sqrt{\frac{D}{\pi t}}$$

where  $N_i$  is the concentration of the gas-phase species in the liquid in the interface region and equals  $N_g H R T$  (H is Henry's law constant, R is the gas constant), D is the diffusion coefficient of the gas-phase species in the particle, and t is time. Normalizing by the number of collisions gives the expression for  $\Gamma_{sat}$ <sup>1,160</sup>

$$\mathbf{A.6} \quad \Gamma_{sat} = \frac{4HRT}{c_{avg}} \sqrt{\frac{D}{\pi t}}$$

The rate of bulk reaction is<sup>1</sup>

$$\mathbf{A.7} \quad Rate = N_l \sqrt{Dk_{rxn}}$$

where  $k_{rxn}$  is the pseudo-first order rate constant of the reaction between the gas-phase species and the aerosol in the bulk of the particle. Normalizing by the number of collisions (eq A.4) gives<sup>1,160</sup>

$$\mathbf{A.8} \quad \Gamma_{rxn} = \frac{4HRT}{c_{avg}} \sqrt{Dk_{rxn}}$$

The combined expression for diffusion and reaction in the bulk is therefore given by

$$\mathbf{A.9} \quad \Gamma_{sat} + \Gamma_{rxn} = \frac{4HRT}{c_{avg}} \left[ \sqrt{\frac{D}{\pi t}} + \sqrt{Dk_{rxn}} \right]$$